Beyond the Standard Cosmology: Anisotropic Inflation and Baryophilic Dark Matter

Thesis by

Timothy R. Dulaney

In Partial Fulfillment of the Requirements

for the Degree of

Doctor of Philosophy

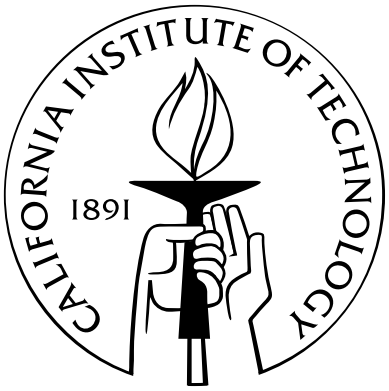

California Institute of Technology

Pasadena, California

2011

(Defended May 12, 2011)

Acknowledgments

I would like to begin by thanking my advisor Mark Wise. I have been very lucky to have an advisor with great physical intuition who was also willing to take the time to develop my talents. I would also like to thank my unofficial advisor, Sean Carroll, for his patience, honesty and understanding throughout my graduate career. It was a great honor to work with you both for this brief period.

In addition to my advisors, I am grateful to my other collaborators Moira Gresham, Heywood Tam, and Pavel Perez. In particular, I thank Moira Gresham for her insightful contributions to our work, for her assistance in the preparation of this thesis and job applications, and for the many lively discussions we had as officemates over the years; I truly enjoyed our collaboration. I also benefitted greatly from the conversations with Matt Johnson, Matt Buckley and Lotty Ackermann during my time at Caltech, and because of this I thank each of you for your time.

I also want to thank Marc Kamionkowski and Sunil Golwala, as well as my advisors Mark Wise and Sean Carroll, for serving on my candidacy and defense committees. I am very grateful for the time Mark Wise, Sean Carroll and Pavel Perez took from their schedule to write letters of recommendation on my behalf. I am grateful to Carol Silberstein for sending out the letters of recommendation as well as all of the logistical assistance she provided throughout my graduate career. I am also grateful to Helen Ticehurst and Donna Driscoll for their support and assistance throughout my time at Caltech.

My graduate work at Caltech was supported by a National Science Foundation graduate research fellowship, as well as the DOE grant that supports the Wise research group.

I am greatly indebted to my parents, Gil and Gina and to my sister, Tara, for their moral support. I know this would have been much more difficult without the support of my family.

Finally, I thank my wife, confidant, partner and teammate, Jamie. I thank her for staying by my side during this often stressful period in our lives and for moving across the country to allow me to follow my dreams. Her support and encouragement was in the end what made this dissertation possible. It is because of her honest and thoughtful advice that I am the man I am today.

Abstract

This thesis discusses two topics in cosmology that resulted in two independent publications. The first topic concerns persistent anisotropy during inflation [1] and the second topic concerns a model of baryophillic dark matter [2].

The motivation for the project contained within chapter 1 came from indications in the cosmic microwave background data that seemed to suggest that there may be a cosmologically preferred direction. Moira Gresham and I derived quantitative predictions about the signals one would observe in Cosmic Microwave Background data if isotropy is not assumed during inflation. We considered a particular example of a dynamical theory of anisotropic inflation that is characterized by a scalar field which is nonminimally coupled to an isotropy breaking abelian gauge field, thereby slowing the decay of the gauge field energy density.

The motivation for the project contained within chapter 2 came from the observation that the global symmetries B (baryon number) and L (lepton number) of the standard model Lagrangian must be broken by higher-dimensional operators at a very high scale. Pavel F. Perez, Mark B. Wise and I analyzed a model that explained the protection of these accidental global symmetries by promoting B and L to gauge symmetries. This model has a natural dark matter, candidate and we discuss the experimental constraints on the parameters in the theory.

Unexpected results are found in each chapter. For example, in chapter 2, we find that the anisotropic contribution to the tensor power spectrum is suppressed with respect to that of the scalar power spectrum and, in chapter 3, we show that a baryon asymmetry can be generated even within a model that has baryon number as a gauge symmetry.

Contents

List of Figures

List of Tables

Chapter 1

Introduction

1.1 This Thesis within a Larger Context

As cosmologists, we study the origin and evolution of our Universe (or universes in general). General relativity teaches us that it is the matter content of our Universe that tells us not only the structure and geometry of the space-time, but also how that space-time is evolving. This is concisely stated mathematically through the Einstein field equations,

$$G_{\mu\nu} = \left(\frac{8\pi G_N}{c^4}\right) T_{\mu\nu}, \tag{1.1}$$

where $G_{\mu\nu}$ is the Einstein tensor (describing the dynamical structure of space-time) and $T_{\mu\nu}$ is the stress-energy tensor (which encodes the matter content of our Universe).[1]

Consistent with other scientists, cosmologists rely on observations and experiments to make headway in our quest to uncover the details of our cosmic history. On the other hand, most other scientists can perform experiments in terrestrial laboratories. Since we have only one Universe, it is not possible for cosmologists to conduct such experiments since the phenomena we are studying is inherently non-local. Cosmologists look out into our Universe to observe signatures of important events in

[1] G_N is Newton's constant and c is the speed of light (the latter will be set to unity for the remainder of this thesis).

our Universe's distant past. By compiling a diverse set of observables, we can have confidence in our understanding of the origin and evolution of our Universe.

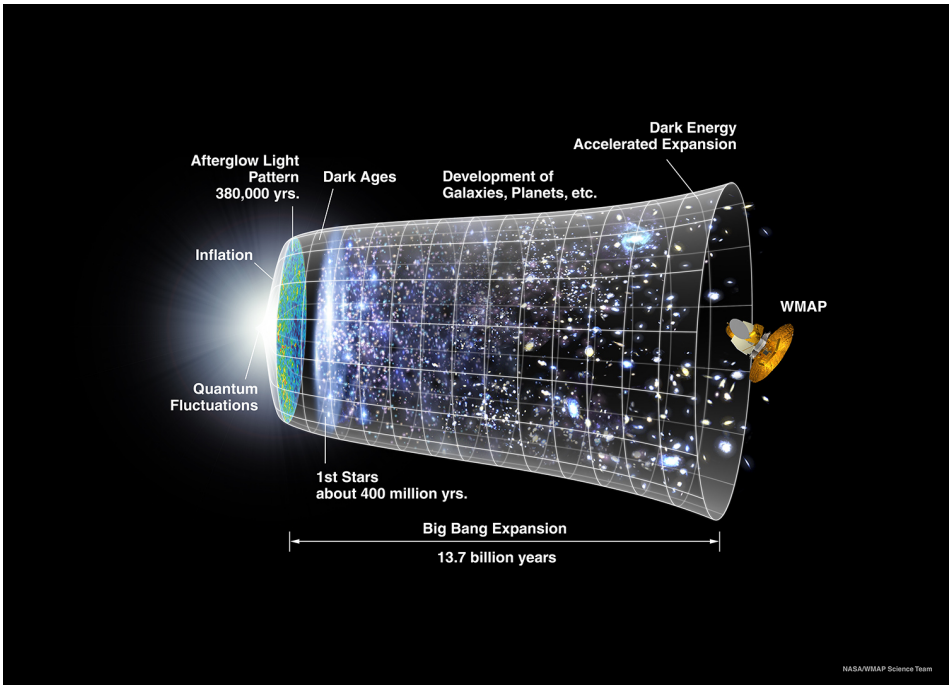

Figure 1.1: An artist's conception of the history of our Universe (Credit: NASA/WMAP Science Team).

The most commonly accepted view by cosmologists of our cosmic history is the following (a cartoon picture can be found in figure 1.1). A cosmic event[2] occurred of which we have little understanding. We know the temperature was very high $T > 10^{27}$ eV and the density was high[3]. Immediately following this event, the Universe experienced a period of rapid exponential expansion, known as inflation. After inflation, the field responsible for the exponential expansion decays and fills the Universe with electromagnetic radiation. As the Universe cools, quarks become confined into nuclei,

[2] This is commonly known as the big bang, but more exotic theories proliferate the literature.

[3] Throughout this thesis, temperature will be stated in units of energy and can be converted back into the more familiar Kelvin (K) by using Boltzmann's constant $k_B = 8.62 \times 10^{-5}$ eV/K.

these nuclei begin to form atoms synthesizing the elements (this is commonly known as nucleosynthesis). Once $T \approx 1$ eV, the atoms could no longer absorb the thermal radiation and the Universe became transparent. The photons freely streamed from this recombination event. Over the next thirteen billion years or so, the temperature continues to cool and local overdensities begin to coalesce into large scale structure (like galaxies and cosmologists).

Today we live in a Universe that is fairly cool $T \approx 2.3 \times 10^{-4}$ eV. Photons (quanta of electromagnetic radiation) from the recombination event approach us from all directions and make up what is known as the Cosmic Microwave Background (CMB) radiation. From our point of view, these photons were emitted from a spherical surface (called the surface of last-scattering) with us at the center. These photons, to a first approximation, have streamed freely to us only changing their wavelength through gravitational redshift[4] due to the continued expansion of our Universe. Cosmologists use these photons to look into our distant past and make observations about the evolution of our Universe.

It is through analysis of CMB data in conjunction with data from galaxy surveys that tell us a great deal about our Universe. For example, we know the energy density of the Universe today comprises approximately 4.6% ordinary matter (like electrons, protons, etc.), 23% dark matter and 72% dark energy. We do not know a great deal about the latter two contributions to the energy density, except that the dark matter is nonluminous, electrically neutral and nonbaryonic matter that interacts mainly gravitationally. It is likely that the dark energy is simply a cosmological constant whose value would naturally arise from a more complete theory of nature.

The second chapter, immediately following this introductory chapter, will focus on a particular issue in inflationary cosmology. The third chapter focuses on a particular explanation of dark matter that naturally arrises in a model that solves some technical issues with the Standard Model of particle physics. In what remains of this introduction, I intend to give some background on the standard approach to the

[4]Redshift is a term used to describe the increase in a photon's wavelength.

topics of inflation and dark matter. These sections are to serve as introduction to the technical aspects of the standard approach as well as an introduction to the notation that will be used throughout the thesis.

While writing this introduction, I consulted many textbooks about cosmology and the early Universe. I most heavily relied on Weinberg's cosmology text [3] and Kolb and Turner's classic text on the early Universe [4]. I consulted my colleague Moira Gresham's thesis on ideas to implement the inflation portion of this chapter.

1.2 Inflation

1.2.1 CMB Observations

In 1965 the radio astronomers Robert Wilson and Arno Penzias observed a faint background glow, almost exactly the same in all directions. This glow was identified to be the CMB radiation and the two scientists were awarded the 1978 Nobel Prize for their discovery. Ground-based experiments during the 1980s put limits on the anisotropy that can exist in the CMB radiation, but it was not until the 1992 NASA mission COBE (COsmic Background Explorer) were the theoretically predicted 10^{-5} deviations from isotropy observed. The COBE team was awarded the 2006 Nobel Prize in Physics for their work on the precision measurement of the CMB radiation.

The COBE team observed a nearly uniform temperature across the sky and measured the spectrum of CMB radiation across the sky. They showed that the CMB radiation has a thermal black body spectrum at a temperature of 2.73K as shown in figure 1.2. COBE was also the first to observe the theoretically predicted deviations from isotropy.

Today, the state of the art data is given by the Wilkinson Microwave Anisotropy Probe (WMAP). This experiment has produced very precise sky-maps such as the one in figure 1.3.

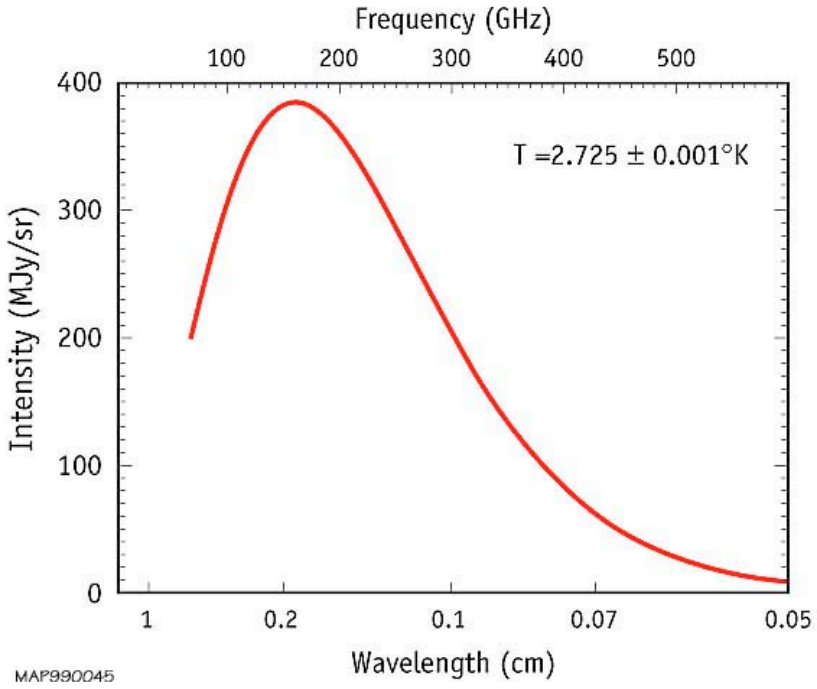

Figure 1.2: COBE observation the CMB radiation thermal spectrum with a temperature of approximately 2.73K.

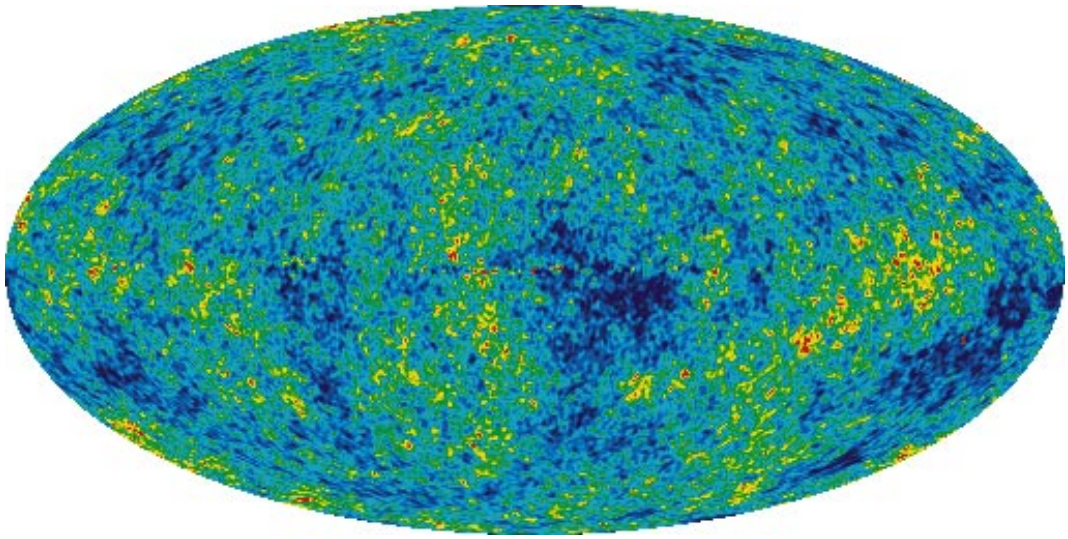

Figure 1.3: WMAP observation of the CMB radiation. The average temperature is 2.725K, and the colors represent the tiny temperature fluctuations, as in a weather map. Red regions are warmer and blue regions are colder by about 0.0002K. Credit: NASA/WMAP Science Team.

1.2.2 CMB Temperature Correlations

The main observable from the early Universe is the Cosmic Microwave Background (CMB). The sky that we see is one particular realization of a statistical ensemble

of possible observations (if we could travel to a distant place in our Universe, we would observe a different realization of the CMB). Since the realizations are position dependent (and we cannot readily change our position on cosmological scales), we study the statistical observables from our particular realization.

We cannot average over different vantage points (cosmic mean), but we can average over realizations (or histories). The difference between these two averaging procedures is known as cosmic variance and is a principle source of uncertainty at the largest of angular scales.[5]

The main observable in CMB physics is the correlation between the deviation of the temperature from the average at different points on our CMB sky (labelled by angles $\theta \in [0, \pi]$ and $\phi \in [0, 2\pi]$). Note that the average temperature, $\bar{T}$, is defined formally as

$$T_0 \equiv \frac{1}{4\pi} \int T(\theta, \phi) d\Omega. \tag{1.2}$$

Since the CMB comes to us from all directions, it is beneficial to expand the temperature difference in spherical harmonics,

$$\frac{\Delta T(\theta, \phi)}{\bar{T}} = \frac{T(\theta, \phi) - \bar{T}}{\bar{T}} = \sum_{l=0}^{\infty} \sum_{m=-l}^{l} a_{lm} Y_l^m(\theta, \phi). \tag{1.3}$$

Since the deviation of the temperature from the average is real, the coefficients (a_{lm}) must satisfy condition $a^*_{l,m} = a_{l,-m}$. The two-point temperature correlation function is defined by

$$C_{ll',mm'} \equiv \langle a^*_{l'm'} a_{lm} \rangle = \left(\frac{2l'+1}{4\pi} \right) \left(\frac{2l+1}{4\pi} \right) \times \int d\Omega' \int d\Omega Y_{l'}^{m'*}(\theta', \phi') Y_l^m(\theta, \phi) \left\langle \frac{\Delta T(\theta', \phi')}{\bar{T}} \frac{\Delta T(\theta, \phi)}{\bar{T}} \right\rangle, \tag{1.4}$$

where the numerical factors in front are due to the normalization of the spherical

[5] One can show that this accuracy limit decreases as $2/(2l+1)$ if the temperature deviations are are governed by a Gaussian distribution.

harmonics. If the fluctuations at the surface of last-scattering were Gaussian, then all statistical properties about the CMB could be written in terms of this two-point correlation function. The average in this equation refers to the cosmic mean.

A statistically isotropic power spectrum has the addition feature that the correlations take the following form,

$$C_{ll',mm'} = C_l \delta_{ll'} \delta_{mm'}. \tag{1.5}$$

The quantity we observe in CMB experiments is,

$$C_l^{\rm obs} \equiv \frac{\bar{T}^2}{2l+1} \sum_m a_{lm} a_{l,m}^* = \frac{1}{4\pi} \int d^2\hat{n} d^2\hat{n}' \; P_l(\hat{n} \cdot \hat{n}') \Delta T(\hat{n}) \Delta T(\hat{n}'). \tag{1.6}$$

In figure 1.4, we show the angular power spectrum observed by the WMAP satellite (normalized by $l(l+1)/2\pi$) in units of μK^2. There is a great deal of information contained within this measurement. From analysis of this data, one can determine vir-

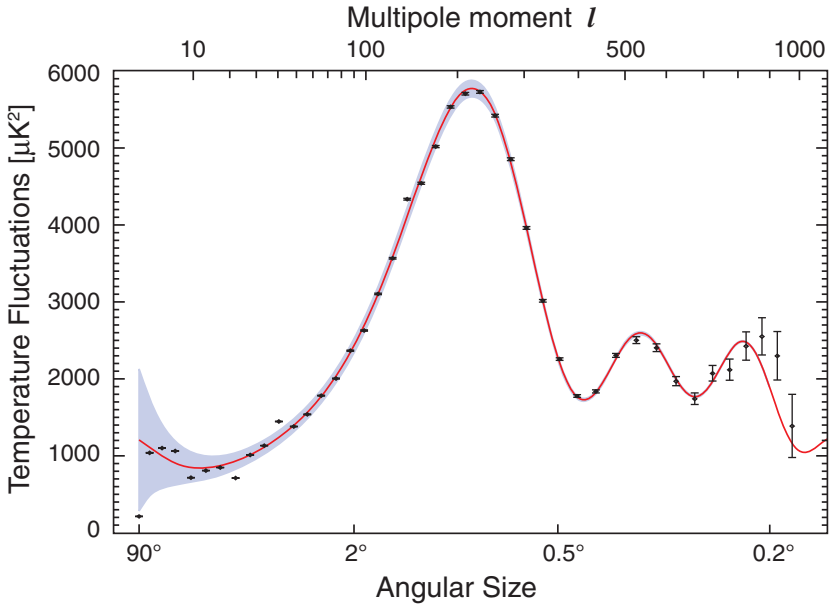

Figure 1.4: This graph illustrates how much the temperature fluctuates on different angular sizes in the map (from larger angles to smaller angular scales). WMAP was the first experiment to clearly show the presence of the second and third acoustic peaks (the harmonic overtones of the first peak). Credit: NASA/WMAP Science Team.

tually all the significant cosmological parameters (age of the Universe, energy density of normal matter, energy density of dark matter and dark energy, etc.).

1.2.3 Primordial Perturbations

The purpose of this section is to connect the statistical observables of the previous section with the predictions of theories of the very early Universe. The main prediction of theories of inflation are power spectra (either of curvature fluctuations or of gravitational wave fluctuations). Fluctuations in the energy density in the early Universe led to patterns of the photons emanating from the surface of last scattering and eventually to the CMB we observe today.

In particular, the deviation from the mean CMB temperature in our sky is

$$\frac{\Delta T(\theta,\phi)}{\bar{T}} = \int d^3k \sum_l \left(\frac{2l+1}{4\pi}\right) (-i)^l \delta_\epsilon(\vec{k}) P_l(\hat{k}\cdot\hat{e})\Theta_l(k), \tag{1.7}$$

where P_l are Legendre polynomials and $\hat{e} = \hat{e}(\theta,\phi)$ is a unit-vector pointing in the direction specified by the angular coordinates (θ,ϕ). In this equation, Θ_l is the transfer function that encapsulates all of the physical effects (assumed to be statistically isotropic) on the photons from the very Universe until today. Further details about the transfer function are beyond the scope of this introduction. Finally, $\delta_\epsilon(\vec{k})$ is the Fourier transform of the fractional deviation of the energy density from the average in the early Universe.

Given this form of the deviation from the mean CMB temperature (in terms of transfer functions, etc.), we can work through the implications for Eq. (1.4). We

have

$$
\begin{aligned}
C_{ll',mm'} &= \left(\frac{2l+1}{4\pi}\right)\left(\frac{2l'+1}{4\pi}\right)\int d^3k d^3k' \sum_{l_1}\sum_{l_2}\left(\frac{2l_1+1}{4\pi}\right)\left(\frac{2l_2+1}{4\pi}\right)(-i)^{l_1+l_2} \\
&\times \left\langle \delta_\epsilon(\vec{k})\delta_\epsilon(\vec{k}')\right\rangle \Theta_{l_1}(k)\Theta_{l_2}(k')\int d\Omega \int d\Omega' Y_l^{m*}(\theta,\phi)Y_{l'}^{m'}(\theta',\phi')P_{l_1}(\hat{k}\cdot\hat{e})P_{l_2}(\hat{k}\cdot\hat{e}') \\
&= \left(\frac{2l+1}{4\pi}\right)\left(\frac{2l'+1}{4\pi}\right)\int d^3k d^3k' \sum_{l_1,m_1}\sum_{l_2,m_2}(-i)^{l_1+l_2}\left\langle \delta_\epsilon(\vec{k})\delta_\epsilon(\vec{k}')\right\rangle \Theta_{l_1}(k)\Theta_{l_2}(k') \\
&\times \left(\int d\Omega Y_l^{m*}(\theta,\phi)Y_{l_1}^{m_1}(\theta,\phi)\right)\left(\int d\Omega' Y_{l'}^{m'}(\theta',\phi')Y_{l_2}^{m_2*}(\theta',\phi')\right)Y_{l_1}^{m_1*}(\hat{k})Y_{l_2}^{m_2}(\hat{k}') \\
&= \left(\frac{2l+1}{4\pi}\right)\left(\frac{2l'+1}{4\pi}\right)\int d^3k d^3k' \sum_{l_1,m_1}\sum_{l_2,m_2}(-i)^{l_1+l_2}\left\langle \delta_\epsilon(\vec{k})\delta_\epsilon(\vec{k}')\right\rangle \Theta_{l_1}(k)\Theta_{l_2}(k') \\
&\qquad \times \left(\frac{4\pi}{2l+1}\delta_{l,l_1}\delta_{m,m1}\right)\left(\frac{4\pi}{2l'+1}\delta_{l',l_2}\delta_{m',m_2}\right)Y_{l_1}^{m_1*}(\hat{k})Y_{l_2}^{m_2}(\hat{k}') \\
&\qquad = \int d^3k d^3k'(-i)^{l+l'}\left\langle \delta_\epsilon(\vec{k})\delta_\epsilon(\vec{k}')\right\rangle \Theta_l(k)\Theta_{l'}(k')Y_l^{m*}(\hat{k})Y_{l'}^{m'}(\hat{k}'). \quad (1.8)
\end{aligned}
$$

During the simplification of this expression, we have used the normalization condition of the spherical harmonics as well as the relationship between spherical harmonics and the Legendre polynomials. In calculations of primordial perturbations, we calculate the average $\left\langle \delta_\epsilon(\vec{k})\delta_\epsilon(\vec{k}')\right\rangle$ as a quantum mechanical expectation value. We then use the ergodic theorem to posit the equivalence of this averaging procedure with that of the cosmic mean.

Throughout this thesis, we will assume that the expectation value in Eq. (1.8) is translationally invariant. This means that there is no special position in the Universe and therefore the expectation value can only depend on differences in positions.

Explicitly, if we have $\langle \delta_\epsilon(\vec{x})\delta_\epsilon(\vec{y})\rangle = f(\vec{x}-\vec{y})$, then the Fourier transform is simplified,

$$\begin{aligned}\left\langle \delta_\epsilon(\vec{k})\delta_\epsilon(\vec{k}')\right\rangle &= \int d^3x \int d^3y f(\vec{x}-\vec{y}) e^{i(\vec{x}\cdot\vec{k}+\vec{y}\cdot\vec{k}')} \\ &= \int d^3x \int d^3y f(\vec{x}-\vec{y}) e^{\frac{i}{2}((\vec{x}+\vec{y})\cdot(\vec{k}+\vec{k}')+(\vec{x}-\vec{y})\cdot(\vec{k}-\vec{k}'))} \\ &= \left(\int d^3x_- f(\vec{x}_-) e^{i\vec{x}_-\cdot(\vec{k}-\vec{k}')}\right)\left(\int d^3x_+ e^{i\vec{x}_+\cdot(\vec{k}+\vec{k}')}\right) \\ &= (2\pi)^3\delta^{(3)}(\vec{k}+\vec{k}')\int d^3x_- f(\vec{x}_-) e^{i\vec{x}_-\cdot(\vec{k}-\vec{k}')} = (2\pi)^3\delta^{(3)}(\vec{k}+\vec{k}')P(\vec{k}), \quad (1.9)\end{aligned}$$

where we defined $\vec{x}_\pm = 1/2(\vec{x}\pm\vec{y})$ in order to simplify the above expressions. This serves to define the power spectrum of primordial energy density fluctuations, $P(\vec{k})$. Plugging this expression into Eq. (1.8) we derive

$$\begin{aligned}C_{ll',mm'} &= \int d^3k(-i)^{l+l'}\Theta_l(k)\Theta_{l'}(k)(2\pi)^3 P(\vec{k}) Y_l^{m*}(\hat{k}) Y_{l'}^{m'}(-\hat{k}) \\ &= \int d^3k(-i)^{l+l'}(-i)^{-2l'}\Theta_l(k)\Theta_{l'}(k)(2\pi)^3 P(\vec{k}) Y_l^{m*}(\hat{k}) Y_{l'}^{m'}(\hat{k}) \\ &= \int d^3k(-i)^{l-l'}\Theta_l(k)\Theta_{l'}(k)(2\pi)^3 P(\vec{k}) Y_l^{m*}(\hat{k}) Y_{l'}^{m'}(\hat{k}). \quad (1.10)\end{aligned}$$

If the power spectrum is rotationally invariant, then $P(\vec{k})$ can only depend on the magnitude of the photon's momentum. In this case,

$$\begin{aligned}C_{ll',mm'} &= \int d^3k(-i)^{l-l'}\Theta_l(k)\Theta_{l'}(k)(2\pi)^3 P(k) Y_l^{m*}(\hat{k}) Y_{l'}^{m'}(\hat{k}) \\ &= \int dk k^2(-i)^{l-l'}\Theta_l(k)\Theta_{l'}(k)(2\pi)^3 P(k)\left(\int d\Omega_k Y_l^{m*}(\hat{k}) Y_{l'}^{m'}(\hat{k})\right) \\ &= \int dk k^2(-i)^{l-l'}\Theta_l(k)\Theta_{l'}(k)(2\pi)^3 P(k)\left(\frac{4\pi}{2l+1}\delta_{l,l'}\delta_{m,m'}\right) \\ &= \delta_{l,l'}\delta_{m,m'}\left(\frac{1}{2l+1}\int dk(4\pi k^2)\Theta_l(k)^2(2\pi)^3 P(k)\right). \quad (1.11)\end{aligned}$$

Note that this result has the diagonal form mentioned in Eq. (1.5).

One can work out what implications a small departure from statistical isotropy during inflation would have on the measured correlation functions by considering a

power spectrum of the form

$$P(\vec{k}) = P_0(k)\left(1 + g(k)(\hat{n}\cdot\hat{k})^2\right) \tag{1.12}$$

and then expanding to first non-trivial order in $g(k)$. Here $\hat{n}$ indicates the preferred direction which must be extracted from the data. Sean Carroll, Mark Wise and Lotty Ackerman proposed this form of the power spectrum and completed this calculation. For the detailed form that the correlations take, consult their paper [5]. The authors of this paper also gave physical arguments for the scale dependence of $g(k)$ (the quadrapolar modulation effect).

The next section of this chapter goes through the standard calculation of primordial power spectra in the case of isotropic inflation, sourced by a potential energy dominated scalar field. In the next chapter of this thesis, Moira Gresham and I calculate the primordial power spectrum in a dynamical theory of anisotropic inflation. This is the first time a complete calculation of primordial power spectra was conducted in an anisotropic background. In particular, we calculate the leading order effects of the anisotropy on the curvature power spectrum as well as the gravitational wave power spectrum and show the logarithmic scale dependence of this quadrapolar modulation effect.

1.2.4 Standard Slow-Roll Inflation

When studying standard slow-roll inflation, one typically considers a scalar field minimally coupled to gravity with the following action[6]

$$S = \int d^4x\sqrt{-g}\left(\frac{R}{2\kappa^2} - \frac{1}{2}(\nabla_\mu\phi)(\nabla^\mu\phi) - V(\phi)\right), \tag{1.13}$$

where R is the Ricci scalar, $\kappa^2 = 8\pi G_N$, $V(\phi)$ is the potential for the scalar field ϕ and g is the determinant of the metric. By examining the background equations of motions, we will show in the following sections that if the scalar field has a potential

[6]If an index is repeated, summation is implied. A greek index implies a summation $\mu \in \{0,1,2,3\}$ using the metric and a latin index implies a summation $i \in \{1,2,3\}$ using the Kronecker-delta.

dominated energy density then the Universe will begin to expand. Furthermore, we will give criteria for the expansion to be exponential and nearly exponential. Finally, we will give a detailed derivation of the primordial power spectrum of scalar and tensor perturbations predicted by standard slow-roll inflation.

1.2.4.1 Background Equations

As in all cases in general relativity, we must begin by choosing a metric parameterization that respects all of the (at least approximate) symmetries of the space-time we are describing. Since we are describing the Universe at large scales (which we observe to be approximately flat, isotropic and homogeneous) we use the following parameterization

$$ds^2 = -dt^2 + a(t)^2 \left(dx^2 + dy^2 + dz^2\right). \tag{1.14}$$

The matter that gives rise to this metric must also exhibit these approximate symmetries and therefore the stress-energy tensor must take the form,

$$T^{\mu}_{\nu} = \begin{pmatrix} -\rho(t) & 0 & 0 & 0 \\ 0 & p(t) & 0 & 0 \\ 0 & 0 & p(t) & 0 \\ 0 & 0 & 0 & p(t) \end{pmatrix}, \tag{1.15}$$

where $\rho(t)$ is the energy density and $p(t)$ is the pressure of the matter.

The background scalar field configuration is homogeneous and isotropic ($\phi = \phi(t)$) and leads to a stress-energy tensor of this form with

$$\rho_\phi(t) = \frac{1}{2}\left(\frac{d\phi(t)}{dt}\right)^2 + V(\phi(t)), \quad \text{and} \quad p_\phi(t) = \frac{1}{2}\left(\frac{d\phi(t)}{dt}\right)^2 - V(\phi(t)). \tag{1.16}$$

Here we consider the equations derived from Einstein's field equations in Eq. (1.1). The time-time Einstein equation ($G^0_0 = \kappa^2 T^0_0$) gives an equation for the Hubble

parameter ($H(t) = \dot{a}(t)/a(t)$),[7]

$$3H^2 = \kappa^2 \left(\frac{1}{2}\dot{\phi}(t)^2 + V(\phi(t)) \right). \tag{1.17}$$

An equation for the second derivative of the scale factor ($\ddot{a}(t)/a(t)$) is found by taking a linear combination of the space-space and time-time Einstein equations,

$$\left(\frac{\ddot{a}(t)}{a(t)} \right) = \dot{H} + H^2 = -\frac{\kappa^2}{3} \left(\dot{\phi}(t)^2 - V(\phi(t)) \right). \tag{1.18}$$

For completeness, we should also include the scalar field equation of motion that results from varying the action in Eq. (1.13) with respect to ϕ,[8]

$$\ddot{\phi} = -3H\dot{\phi} - \kappa^2 a(t)^2 V'(\phi). \tag{1.19}$$

One should also note that the content of this equation is not independent from Eq. (1.17) and Eq. (1.18) and is just a statement of the conservation of stress-energy.

From Eq. (1.18), we can see that accelerated expansion occurs if $V(\phi(t)) > \dot{\phi}(t)^2$ since this will make the second derivative of the scale factor greater than zero. This requirement demands that the energy density of the scalar field is potential dominated for accelerated expansion to occur.

For nearly exponential expansion, we require the derivatives of the Hubble parameter to be small in order to approximate the scale factor with $a(t) \approx \exp(H\ t)$. To quantitatively analyze deviations from exponential expansion, we define the slow-roll parameters,

$$\epsilon = -\frac{\dot{H}}{H^2}, \quad \text{and} \quad \delta = \frac{\ddot{H}}{2H\dot{H}}. \tag{1.20}$$

Although there are actually an infinite set of slow-roll parameters (involving higher derivatives of H), it is sufficient for our purposes to define these two. Note that the

[7]Here, and throughout this chapter, we will use the notation d/dt and $\dot{}$ interchangeably.

[8]Unless otherwise stated, a $'$ indicated a derivative with respect to ϕ.

following identity holds:

$$\dot{\epsilon} = -\frac{\ddot{H}}{H^2} + 2\frac{\dot{H}^2}{H^3} = H\left(-\frac{\dot{H}}{H^2}\right)\left(\frac{\ddot{H}}{H\dot{H}} - 2\frac{\dot{H}}{H^2}\right) = 2H\epsilon(\delta + \epsilon). \tag{1.21}$$

We now endeavor to write the background quantities in terms of these slow-roll parameters, the Hubble parameter and κ^2. Rearranging Eq. (1.17) and Eq. (1.18) we have

$$H^2 = \frac{\kappa^2}{3}\left(\frac{1}{2}\dot{\phi}(t)^2 + V(\phi(t))\right) \quad \text{and} \quad H^2(1-\epsilon) = \frac{\kappa^2}{3}\left(V(\phi(t)) - \dot{\phi}(t)^2\right). \tag{1.22}$$

These are two independent equations that allow us to determine $\dot{\phi}$ and $V(\phi)$ in terms of H, κ and slow-roll parameters. Using this procedure, one derives

$$\dot{\phi}^2 = H^2\left(\frac{2\epsilon}{\kappa^2}\right), \quad \text{and} \quad V(\phi) = \frac{H^2}{\kappa^2}(3-\epsilon). \tag{1.23}$$

We see that the scalar field has a vanishing first derivative in the limit $\{\epsilon, \delta\} \to 0$ (exponential expansion). Taking the first derivative of the former equation, one derives

$$\begin{aligned} 2\ddot{\phi}\dot{\phi} &= 2H\dot{H}\left(\frac{2\epsilon}{\kappa^2}\right) + H^2\left(\frac{2\dot{\epsilon}}{\kappa^2}\right) = H^3\left[-2\epsilon + 2\epsilon + 2\delta\right]\left(\frac{2\epsilon}{\kappa^2}\right) \\ \Rightarrow \quad \frac{\ddot{\phi}}{\dot{\phi}H} &= \left(\frac{\ddot{\phi}\dot{\phi}}{\dot{\phi}^2 H}\right) = \delta. \end{aligned} \tag{1.24}$$

We see what one means by "slow-roll" inflation since the first and second derivative of the scalar field must be small in order for the expansion to be nearly exponential.

One often states the conditions for slow-roll inflation in terms of flatness conditions on the inflaton potential.[9] For example, taking a derivative of the potential equation

[9]The field responsible for the exponential expansion is usually called the inflaton.

gives

$$V'(\phi) = -(3+\delta)H\dot{\phi} \quad \Rightarrow \left(\frac{V'(\phi)}{V(\phi)}\right)^2 = \left(\frac{\kappa^4\dot{\phi}^2}{H^2}\right)\left(\frac{3+\delta}{3-\epsilon}\right)^2$$
$$= 2\kappa^2\epsilon\left(\frac{3+\delta}{3-\epsilon}\right)^2. \tag{1.25}$$

So the potential must be moderately flat in order for the expansion to be nearly exponential.

Taking a derivative of the last equation leads to the following condition,

$$\left[\left(\frac{V''(\phi)}{V(\phi)}\right) - \left(\frac{V'(\phi)}{V(\phi}\right)^2\right]\left(2\frac{V'(\phi)}{V(\phi)}\dot{\phi}\right) \approx 2\kappa^2\dot{\epsilon}$$
$$\Rightarrow \left[\left(\frac{V''(\phi)}{V(\phi)}\right) - 2\kappa^2\epsilon\right](-4H\epsilon) \approx 4\kappa^2 H\epsilon(\epsilon+\delta)$$
$$\Rightarrow \left(\frac{V''(\phi)}{V(\phi)}\right) \approx \kappa^2\left(\epsilon-\delta\right). \tag{1.26}$$

We see that the inflaton potential must be quite flat in order to seed nearly exponential expansion. Now that we have determined the background dynamics in terms of H, κ^2 and slow-roll parameters, we have the necessary information to move forward and talk quantitatively about predictions of power spectra resulting from slow-roll inflation.

1.2.4.2 Power Spectra from Single-Field Slow-Roll Inflation

We begin our discussion by considering a universe that is expanding approximately exponentially due to the dynamics of a scalar field in its potential as described in the previous section. Dynamical fields are in their respective quantum mechanical ground state. We will be computing the variance of quantum mechanical fluctuations about this vacuum configuration to derive power spectra.

The standard approach is to canonically normalize the amplitude of these quantum-mechanical fluctuations when physical wavelengths[10] are too small to resolve space-time curvature. As expansion continues, physically wavelengths increase and gravita-

[10]The physical wavelength is related to the wavelength of a mode by $\lambda_{phys} = a(t)\lambda$.

tional dynamics become important. Once the fluctuations have physical wavelength larger than the Hubble radius, the modes become essentially non-dynamical and their statistics are frozen into curvature or gravitational wave perturbations. It is therefore the combination of the initial quantum nature of the fluctuations and the gravitational interactions during inflation that lead to the pattern of temperature correlations in the CMB.

In the previous section, we defined the quantities in the background and derived relationships of between these quantities and slow-roll parameters. It turns out to be convenient for our purposes to work in conformal time.,

$$dt^2 = a(\eta)^2 d\eta^2. \tag{1.27}$$

In this section, we denote all background quantities with an overbar (e.g. the background scalar field is $\phi(\eta) = \bar{\phi}$).

We begin by defining the inhomogeneous fluctuations about the homogeneous background. We define

$$\phi(x^\mu) = \bar{\phi}(\eta) + \delta\phi(x^\mu), \quad \text{and} \quad g_{\alpha\beta}(x^\mu) = \bar{g}_{\alpha\beta}(\eta) + \delta g_{\alpha\beta}(x^\mu), \tag{1.28}$$

where $\bar{g}_{\mu\nu} = a(\eta)^2\eta_{\mu\nu}$ where $\eta_{\mu\nu}$ is the usual Minkowski metric. In other words, all departures from homogeneity are encapsulated in the perturbed fields $\delta\phi$ and $\delta g_{\alpha\beta}$.

Since we are expanding about a spatially homogeneous background, and we will be deriving a power spectrum, it is convenient to work in Fourier space (Φ is just some linear combination of metric and scalar field perturbations):

$$\delta\Phi(x^\mu) = \int \frac{d^3k}{(2\pi)^3}\delta\Phi(\vec{k},\eta)e^{i\vec{k}\cdot\vec{x}}. \tag{1.29}$$

At very early times, we treat the perturbations as quantum excitations. The Fourier transformed fields are written as Fourier amplitudes multiplied by creation ($\hat{a}^\dagger$) and

annihilation ($\hat{a}$) operators as in

$$\delta\Phi(\vec{k},\eta) = f(\vec{k},\eta)\hat{a}_{\vec{k}} + f^*(\vec{k},\eta)\hat{a}^\dagger_{-\vec{k}}. \tag{1.30}$$

Note that the above relationship between the amplitudes for the creation and annihilation operators is guaranteed by the fact that we are dealing with real fields in position space.

The creation and annihilation operators satisfy the canonical commutation[11] relations,

$$\left[\hat{a}_{\vec{k}}, \hat{a}^\dagger_{\vec{q}}\right] = (2\pi)^3\delta^3(\vec{k}-\vec{q}) \quad \text{and } \left[\hat{a}_{\vec{k}}, \hat{a}_{\vec{q}}\right] = 0. \tag{1.31}$$

One finds the appropriate normalization of the amplitudes of the creation and annihilation operators by expanding the action in Eq. (1.13) to second order in perturbations. One must remove constrained variables and construct an action of the form

$$S^{(2)} = \int \frac{d^3k}{(2\pi)^3}\int d\eta \sum_i \Big(\frac{1}{2}\delta\Phi_i'(\eta,\vec{k})\delta\Phi_i'(\eta,-\vec{k}) \\ - \frac{1}{2}\left(\vec{k}\cdot\vec{k} - f_i(\eta)\right)\delta\Phi_i(\eta,\vec{k})\delta\Phi_i(\eta,-\vec{k})\Big). \tag{1.32}$$

This process is straightforward (for the most part) and tedious.

The power spectrum is related to the two-point correlation function by the following definition,

$$\langle\delta\Phi(\eta,\vec{x})\delta\Phi(\eta,\vec{y})\rangle = \int\frac{d^3k}{(2\pi)^3}\int\frac{d^3k'}{(2\pi)^3}\delta\Phi(\eta,\vec{k})\delta\Phi^*(\eta,\vec{k'})e^{i(\vec{k}\cdot\vec{x}-\vec{k'}\cdot\vec{y})}\left[a_{\vec{k}}, a^\dagger_{\vec{k'}}\right] \\ = \int\frac{d^3k}{(2\pi)^3}\left|\delta\Phi(\eta,\vec{k})\right|^2 e^{i\vec{k}\cdot(\vec{x}-\vec{y})} \equiv \int\frac{d^3k}{(2\pi)^3}P_{\delta\Phi}(\eta,\vec{k})e^{i\vec{k}\cdot(\vec{x}-\vec{y})}. \tag{1.33}$$

[11] A commutator of two quantum operators $\hat{A}$ and $\hat{B}$ is defined to be $\left[\hat{A},\hat{B}\right] \equiv \hat{A}\hat{B} - \hat{B}\hat{A}$.

We see that all we need to find a power spectrum is the properly normalized solutions to the differential equations for the dynamical variables in the quadratic action. The power spectrum is then just the absolute square of the mode function.

The most general way to parameterize metric perturbations is the following,

$$ds^2 = a(\eta)^2 \left[-(1+2A)d\eta^2 + 2B_i dx^i d\eta + (\delta_{ij} + h_{ij})dx^i dx^j\right], \tag{1.34}$$

where

$$B_i = ik_i B + \bar{B}_i, \quad \text{and} \quad h_{ij} = 2C - 2k_i k_j E + 2ik_{(i}E_{j)} + 2E_{ij}. \tag{1.35}$$

In order to not over-parameterize the perturbations, E_{ij}, $\bar{B}_i$ and E_j must be transverse[12] and E_{ij} must be traceless.[13]

Under a local coordinate (gauge) transformation, the metric variables mix into one another, and in this new coordinate system one can redefine the perturbations in terms of the fluctuations defined above. Since physical measurements should have no dependence on the particular coordinate system used, the variables we should consider should be invariant under such transformations. These perturbations are usually called gauge-invariant variables.

One can show that the following combinations of metric and scalar variables are gauge invariant,

$$\Phi(k) = A + \frac{1}{a}\left[a\left(B - E'\right)\right]', \tag{1.36}$$

$$\Psi(k) = -C - \frac{a'}{a}\left[B - E'\right], \tag{1.37}$$

$$\Phi^i(k) = \bar{B}^i - (E^i)', \tag{1.38}$$

$$\chi(k) = \delta\phi + \bar{\phi}'\left[B - E'\right], \tag{1.39}$$

[12] For example, $ik_i E_i = 0$.

[13] $E_{ii} = 0$.

as well as the transverse, traceless perturbation E_{ij}. Here we have used $'$ to denote derivatives with respect to conformal time.

One derives the quadratic action by simply plugging in the above perturbed variables, then using constraint equations and integrating by parts. After this process has taken place, the quadratic action takes the form

$$S^{(2)} = \int \frac{d^3k}{(2\pi)^3} \int d\eta \Big(\frac{1}{2} r'(\eta, \vec{k}) r'(\eta, -\vec{k}) - \frac{1}{2} \left(k^2 - \frac{z''}{z} \right) r(\eta, \vec{k}) r(\eta, -\vec{k}) \\ \sum_{s=+,\times} \frac{1}{2} \hat{h}'_s(\eta, \vec{k}) \hat{h}'_s(\eta, -\vec{k}) - \frac{1}{2} \left(k^2 - \frac{a''}{a} \right) \hat{h}_s(\eta, \vec{k}) \hat{h}_s(\eta, -\vec{k}) \Big), \quad (1.40)$$

where $z = a^2 \bar{\phi}'/a'$ and the dynamical variables are the following linear combination of the gauge-invariant variables listed above,

$$r = a \left(\chi + a \frac{\phi'}{a'} \Psi \right), \quad (1.41)$$

$$\hat{h}_+ = \frac{a}{\kappa} \left(\frac{e_1^i e_1^j - e_2^i e_2^j}{\sqrt{2}} E_{ij} \right), \quad (1.42)$$

$$\hat{h}_\times = \frac{a}{\kappa} \left(\frac{e_1^i e_2^j + e_2^i e_1^j}{\sqrt{2}} E_{ij} \right), \quad (1.43)$$

where $\vec{e}_a \cdot \vec{e}_b = \delta_{ab}$, and $\vec{e}_a \cdot \vec{k} = 0$. This combination of unit vectors spanning the space orthogonal to the wavevector ensures that the dynamical tensor amplitudes correspond to spatial metric perturbations that are transverse and traceless.

To find approximate solutions to the equations of motion for the dynamical variables, it is convenient to use our previous analysis of the background to write the functions of time in the action in terms of the conformal time coordinate η and the slow-roll parameters ϵ and δ. Assuming ϵ and δ are small and almost constant, we have the following,

$$\frac{a''}{a} = \frac{2}{\eta^2} \left(1 + \frac{3}{2} \epsilon \right), \quad \text{and} \quad \frac{z''}{z} = \frac{2}{\eta^2} \left(1 + \frac{3}{2} \delta + 3\epsilon \right). \quad (1.44)$$

The solutions to the differential equations are now simply Henkel Functions (at least in

the approximation that ϵ and δ are approximately constant). Explicitly, the solutions take the form

$$\hat{h}_{+,\times} \approx \sqrt{\frac{\pi}{4a\bar{H}}}\mathcal{H}^{(1)}_{\frac{3}{2}+\epsilon}\left(\frac{k}{a\bar{H}}\right), \tag{1.45}$$

$$r \approx \sqrt{\frac{\pi}{4a\bar{H}}}\mathcal{H}^{(1)}_{\frac{3}{2}+\delta+2\epsilon}\left(\frac{k}{a\bar{H}}\right), \tag{1.46}$$

where normalization of the mode functions was determined canonically,

$$\Phi'\Phi^* - \Phi(\Phi')^* = -i. \tag{1.47}$$

The physical gravitational wave amplitudes in Eq. (1.45) are related to these normalized variables through

$$h_s = 2\kappa\left(\frac{\hat{h}_s}{a}\right). \tag{1.48}$$

Similarly, the curvature perturbation, ζ, is related to the normalized scalar variable in Eq. (1.46) through

$$\zeta = -\frac{r}{z}. \tag{1.49}$$

In the long-wavelength limit ($k \ll a\bar{H}$), the quantities $\hat{h}_{+,\times}/a$ and r/z are approximately conserved outside the horizon (meaning that these quantities are approximately non-dynamical when $k \ll a\bar{H}$). Consider the solutions we have derived in the long-wavelength limit,

$$\hat{h}_{+,\times} \approx \sqrt{\frac{\pi}{a\bar{H}}}\left(\frac{\Gamma\left(\frac{3}{2}+\epsilon\right)}{\pi}\right)\left(\frac{2a\bar{H}}{k}\right)^{3/2+\epsilon} \approx \sqrt{\frac{1}{4a\bar{H}}}\left(\frac{2a\bar{H}}{k}\right)^{3/2+\epsilon}, \tag{1.50}$$

$$r \approx \sqrt{\frac{\pi}{a\bar{H}}}\left(\frac{\Gamma\left(\frac{3}{2}+\delta+2\epsilon\right)}{\pi}\right)\left(\frac{2a\bar{H}}{k}\right)^{\frac{3}{2}+\delta+2\epsilon} \approx \sqrt{\frac{1}{4a\bar{H}}}\left(\frac{2a\bar{H}}{k}\right)^{3/2+\delta+2\epsilon}. \tag{1.51}$$

At this point, it is important to note that $z = \sqrt{2\epsilon}(a/\kappa)$. Computing the curvature

power spectrum first (in the long-wavelength limit),

$$\begin{aligned} P_\zeta(k) &= \frac{P_r(k)}{z^2} \approx \frac{\kappa^2}{\epsilon a^2}\left(\frac{1}{16a\bar{H}}\right)\left(\frac{2a\bar{H}}{k}\right)^3\left(\frac{k}{2a\bar{H}}\right)^{-2\epsilon} \\ &= \frac{\kappa^2}{2\epsilon}\left(\frac{\bar{H}^2}{2k^3}\right)\left(\frac{k}{a\bar{H}}\right)^{-2\epsilon}. \end{aligned} \tag{1.52}$$

Similarly, the gravitational wave power spectrum is given by

$$\begin{aligned} P_h(k) &= 4\kappa^2\frac{P_{\dot{h}}(k)}{a^2} \approx \frac{4\kappa^2}{a^2}\left(\frac{1}{4a\bar{H}}\right)\left(\frac{2a\bar{H}}{k}\right)^3\left(\frac{k}{2a\bar{H}}\right)^{-2\delta-4\epsilon} \\ &= 4\kappa^2\left(\frac{\bar{H}^2}{2k^3}\right)\left(\frac{k}{a\bar{H}}\right)^{-2\delta-4\epsilon}. \end{aligned} \tag{1.53}$$

Ignoring the scale dependence[14] at present, we see that the tensor to scalar ratio is

$$\frac{P_{h_+} + P_{h_\times}}{P_\zeta} = 16\epsilon. \tag{1.54}$$

We also see that in single-field inflation the scale dependence of the curvature and gravitational-wave power spectra is approximately that of the tensor to scalar ratio. This is an important consistency relation of single-field inflation and is a prediction that will be tested by future experiments. In chapter 2, we will derive a similar consistency relation for the model of anisotropic inflation that we will introduce in the next section.

1.2.5 A Model of Anisotropic Inflation

The second chapter of this thesis contains a quantitative analysis of the model of anisotropic inflation introduced by Watanabe, Kanno and Soda in [6]. The common lore in early universe cosmology is that the exponential expansion quickly washes out

[14] The curvature and gravitational wave power spectra are approximately scale invariant $P(k) \approx 1/k^3$. The fact that the curvature power spectrum is nearly scale invariant is important since experiments prefer a nearly scale invariant spectrum.

any initial anisotropy or inhomogeneity in the spacetime. Watanabe, Kanno and Soda got around this commonly accepted idea by noticing that nearly exponential expansion can allow for a persistent anisotropy. As we saw in the previous section, realistic models of inflation exhibit expansion that is nearly (but not exactly) exponential.

When building a model of anisotropic inflation, one needs to add a field that can break rotational invariance (another scalar will not work, but any higher-spin field will do). The authors of this paper considered adding a massless vector field to their theory of inflation. The last ingredient needed to make this a potentially workable theory of anisotropic inflation is that one must engineer the anisotropic source of energy density to persist. Usually vector fields have an energy density that decays due to expansion of the Universe as a^{-4}, where a is the scale factor. Watanabe, Kanno and Soda altered this energy density decay rate by adding a coupling of the scalar field to the vector field.

The action for their theory of anisotropic inflation takes the form,

$$S = \int d^4x\sqrt{-g}\left(\frac{R}{2\kappa^2} - \frac{1}{2}(\nabla_\mu\phi)(\nabla^\mu\phi) - V(\phi) - \frac{f(\phi)^2}{4}F_{\mu\nu}F^{\mu\nu}\right), \tag{1.55}$$

where $F_{\mu\nu} = \partial_\mu A_\nu - \partial_\nu A_\mu$ and A_μ is the vector field. In [6], the authors showed that if the coupling function $f(\phi)$ took a particular form then the energy density in the vector field would remain approximately constant during inflation (rather than quickly decaying). In chapter 2 we analyze the background of the model in complete generality and then we derive evolution equations for cosmological perturbations in this anisotropic background. We finally derive the power spectra of curvature and gravitational wave fluctuations.

1.3 Dark Matter

1.3.1 Introduction

The first evidence for dark matter (DM) came from Zwicky's work at Caltech in 1933. He observed the Coma cluster of galaxies and estimated the cluster's total mass based

on the motions of galaxies near its edge. Zwicky then compared that estimate to one based on the number of galaxies within the cluster. The gravity of the visible galaxies in the cluster would be far too small to support the fast orbits he observed at large radii. Zwicky realized that there must be some non-luminous form of matter that is providing the mass needed to hold the cluster together.

Based on observations of galactic rotation curves, gravitational lensing, precision analysis of CMB data and supernova Type 1a distance measurements (to name a few) dark matter has established a strong experimental footing. As mentioned previously, dark matter makes up roughly 23% of the energy density of the Universe while ordinary matter makes up only about 4.6% of the energy density. Currently we do not know much about DM except that it is non-luminous, electrically-neutral, non-baryonic and that it interacts mainly gravitationally.

We will see in the next section that a theoretically well-motivated scenario for dark matter is that it consists of weakly interacting massive particles (WIMPs). Theoretically, we expect new physics particles to appear around the mass-scale of a TeV (roughly 1000 times the proton mass). It turns out that if we have a dark matter mass around this scale and the dark matter interacts with ordinary matter with a strength comparable to our weak interactions, then the dark matter will naturally have approximately the correct abundance.[15] This is commonly known as the "WIMP Miracle."

If the particle interpretation of dark matter is correct, then a large number of dark matter particles are constantly passing through the Earth. Although these particles must interact weakly with ordinary matter, there are experiments today that are hoping to find evidence of these particles. Direct detection experiments (CDMS, XENON, etc.) hope to observe dark matter interacting with atomic nuclei in their detector. Indirect detection experiments (DAMA, EGRET, PAMELA, etc.) hope

[15] Meaning that the amount of dark matter predicted in this scenario is roughly the amount we observe today.

to observe the products of dark matter annihilations that take place inside their detectors. Finally, collider experiments (LHC, etc.) hope to produce dark matter particles by scattering ordinary particles at high-enough energies. Each of these experiments attack the same dark matter interaction from different angles and in the next several years they will collectively rule out a large region of theoretically motivated dark matter models.

1.3.2 Dark Matter as a Thermal Relic

In the early Universe, most of the particles species were in thermal equilibrium. This basically means that particle interactions were rapid enough to evenly distribute the energy density. As the Universe cools and expands, some interactions become inefficient. For example, if the temperature drops below a certain particle's mass, it is unlikely that two other particles in thermal equilibrium will have enough energy to annihilate into those particles. This section will go through the standard calculation of relic abundances of particles species, following them from thermal equilibrium and through "freeze-out" when their abundance has been fixed within a comoving volume. For much of this section, I follow Kolb and Turner's approach to thermodynamics in the expanding Universe [4].

In order to properly treat the transition from thermal equilibrium to decoupling, we must work with Boltzmann equations. A Boltzmann equation is an integral partial differential equation for the microscopic evolution of a particle's phase space distribution function $f_i(x^\mu, p^\mu)$. The covariant, relativisitic Boltzmann equation is

$$\hat{L}[f] = \left(p^\alpha \frac{\partial}{\partial x^\alpha} - \Gamma^\alpha_{\beta\gamma} p^\beta p^\gamma \frac{\partial}{\partial p^\alpha} \right) f_i(x^\mu, p^\mu) = \hat{C}[f], \tag{1.56}$$

where $\hat{C}$ is the collision operator, $\hat{L}$ is the Liouville operator and Γ is the affine connection. To a first approximation, the Universe is spatially homogeneous (and flat) as well as isotropic. Therefore the metric takes the form,

$$ds^2 = -dt^2 + a(t)^2(dx^2 + dy^2 + dz^2), \tag{1.57}$$

and $f_i = f_i(E,t)$. In this case, the Liouville operator takes the simplified form,

$$\hat{L}[f(E,t)] = E\frac{\partial f}{\partial t} - \frac{\dot{a}}{a}|\vec{p}|^2\frac{\partial f}{\partial E}, \tag{1.58}$$

where $\dot{}$ denotes a derivative with respect to the time coordinate in the Robertson-Walker metric.

One usually has more physical intuition for the number density, which is defined in terms of the phase space density as

$$n(t) = \frac{g}{(2\pi)^3}\int d^3p f(E,t), \tag{1.59}$$

where g is the number of internal degrees of freedom. From this definition, we have the following equation for the number density as a function of time,[16]

$$\dot{n} + 3Hn = \frac{g}{(2\pi)^3}\int \hat{C}[f]\frac{d^3p}{E}, \tag{1.60}$$

where the second term comes from integrating by parts as follows

$$\begin{aligned}\int \frac{|\vec{p}|^2}{E}\frac{\partial f}{\partial E}d^3p &= \int_{4\pi}\left(\int_0^\infty \frac{|\vec{p}|^4}{E}\frac{\partial f}{\partial E}d|\vec{p}|\right)d\Omega_p = \int_{4\pi}\left(\int_m^\infty (E^2-m^2)^{3/2}\frac{\partial f}{\partial E}dE\right)d\Omega_p \\ &= \int_{4\pi}\left[(E^2-m^2)^{3/2}f(E)\Big|_m^\infty - \int_m^\infty f(E)\frac{\partial}{\partial E}(E^2-m^2)^{3/2}dE\right]d\Omega_p \\ &= -\int_{4\pi}\left(\int_m^\infty f(E)3(E^2-m^2)^{1/2}EdE\right)d\Omega_p = -3n(t), \end{aligned} \tag{1.61}$$

where I twice used the fact that $|\vec{p}|d|\vec{p}| = EdE$ as well as the fact that $f(E)$ falls off exponentially for large E (in both the Fermi-Dirac distribution and Bose-Einstein Distribution).

The last term we need to address is the term on the right side of Eq. (1.60). One can read about more general treatments of collision terms in [4], but for this introduction we specialize to the case most relevant for the remainder of the thesis.

[16]Here I have defined the Hubble parameter $H = \dot{a}/a$.

Suppose we have a dark matter candidate, X, and we want to follow its number density. First we label its four momentum p_X. Suppose further that X has CP (or T) invariant interactions with other particles and that it is stable. The first of these conditions results in the simplification that the matrix-element for the process $X+a+b+\cdots \to i+j+\ldots$ is the same as the matrix element for the inverse process. The second condition implies that the only processes that can change the number of X particles are the processes $\psi\bar{\psi} \leftrightarrow X\bar{X}$. We can write the collision term for this process as

$$\int \hat{C}[f]\left(\frac{g}{(2\pi)^3}\frac{d^3p_X}{E_X}\right) = -\int d\Pi_X d\Pi_{\bar{X}}\Pi_\psi d\Pi_{\bar{\psi}}(2\pi)^4\delta^{(4)}(p_X+p_{\bar{X}}-p_\psi-p_{\bar{\psi}}) \times \overline{|\mathcal{M}|}^2\left(f_X f_{\bar{X}}(1\pm f_\psi)(1\pm f_{\bar{\psi}}) - f_\psi f_{\bar{\psi}}(1\pm f_X)(1\pm f_{\bar{X}})\right), \quad (1.62)$$

where $(+)/(-)$-sign should be taken if the species is bosonic/fermionic and

$$d\Pi_i = \frac{g_i}{(2\pi)^3}\frac{d^3p_i}{E_i}. \quad (1.63)$$

In this equation, $\overline{|\mathcal{M}|}^2$ is the spin-averaged matrix element for the process $\psi\bar{\psi} \leftrightarrow X\bar{X}$. Since we are discussing thermodynamics in the early Universe (where temperatures are high), we can simplify this expression by setting $1 \pm f_i = 1$.[17]

Specializing to our situation, we have the Boltzmann equation

$$\dot{n} + 3Hn = -\int \prod_i d\Pi_i (2\pi)^4\delta^{(4)}(p_X+p_{\bar{X}}-p_\psi-p_{\bar{\psi}})\overline{|\mathcal{M}|}^2\left(f_X f_{\bar{X}} - f_\psi f_{\bar{\psi}}\right). \quad (1.64)$$

In the absence of interactions we would have the solution for the number density

$$\frac{\dot{n}}{n} = -3\frac{\dot{a}}{a} \quad \to \quad n(t) \approx a^{-3}. \quad (1.65)$$

[17] Departures from this simplification are the basis of the low-temperature phenomena known as Bose condensation $(+)$ and Fermi degeneracy $(-)$.

This solution is physically intuitive since, without interactions, we would expect the number density to simply dilute as the Universe expands.

To consider a more physically meaningful quantity, we study the comoving number density. This is defined by $Y = n_X/s$ where s is the entropy density. Since temperature is a much more physical variable then time for our study of comoving number densities, we convert to the dimensionless variable $x = m_X/T$ and use the relationship between time and temperature from the radiation dominated era.[18] One can derive this relationship as follows. During the radiation dominated era, we have the Friedmann equation,

$$H^2 = \frac{8\pi}{3m_{Pl}^2}(\rho_R) = \frac{8\pi}{3m_{Pl}^2}\left(\frac{\pi^2}{30}g_* T^4\right), \tag{1.66}$$

where $g_* = g_*(T)$ is the number of relativistic degrees of freedom at temperature T and $m_{Pl}^2 = 1/G_N$ is the Planck mass. One can show from the Friedmann equations that $a(t) \propto t^{1/2}$ and therefore $H = 1/2t$. Plugging all of this in, we find

$$\begin{aligned} \frac{1}{2t} = \sqrt{\frac{8\pi^3}{90}}\sqrt{g_*}\frac{T^2}{m_{Pl}} \quad &\Rightarrow \quad t = \sqrt{\frac{90}{32\pi^3}}\sqrt{g_*}\frac{m_{Pl}}{T^2} \approx \frac{0.301}{\sqrt{g_*}}\frac{m_{Pl}}{T^2} \\ &\Rightarrow t(x) = \frac{0.301}{\sqrt{g_*}}\frac{m_{Pl}}{m_X^2}x^2, \quad \text{and} \quad H(T) \approx 1.67\sqrt{g_*}T^2/m_{Pl} = \frac{H(m_X)}{x^2}. \end{aligned} \tag{1.67}$$

Changing variables, we have the following Boltzmann equation,

$$\frac{dY}{dx} = -\frac{x}{H(m_X)s}\int \prod_i d\Pi_i (2\pi)^4 \delta^{(4)}(p_X + p_{\bar{X}} - p_\psi - p_{\bar{\psi}}) \overline{|\mathcal{M}|}^2 \left(f_X f_{\bar{X}} - f_\psi f_{\bar{\psi}}\right), \tag{1.68}$$

where ψ represents a particular species into which X can annihilate. Since ψ and $\bar{\psi}$

[18] It turns out that most weak-scale mass particles fall out of thermal equilibrium during the radiation-dominated era.

are in thermal equilibrium, we have

$$f_\psi f_{\bar{\psi}} = \exp\left(-\frac{E_\psi + E_{\bar{\psi}}}{T}\right) = \exp\left(-\frac{E_X + E_{\bar{X}}}{T}\right) = f_X^{\rm EQ} f_{\bar{X}}^{\rm EQ}. \tag{1.69}$$

where we have used the delta function to enforce the condition $E_\psi + E_{\bar{\psi}} = E_X + E_{\bar{X}}$. One can now write Eq. (1.68) in the following form,

$$\frac{dY}{dx} = -\frac{x\left\langle\sigma_{X\bar{X}\to\psi\bar{\psi}}|v|\right\rangle s}{H(m_X)}\left(Y^2 - Y_{\rm EQ}^2\right), \tag{1.70}$$

where the thermally averaged annihilation cross section (times velocity) is defined by

$$\left\langle\sigma_{X\bar{X}\to\psi\bar{\psi}}|v|\right\rangle \equiv \left(n_X^{\rm EQ}\right)^{-2}\int\prod_i d\Pi_i (2\pi)^4\delta^{(4)}(p_X + p_{\bar{X}} - p_\psi - p_{\bar{\psi}}) \times \overline{|\mathcal{M}|}^2 \exp(-E_X/T)\exp(-E_{\bar{X}}/T). \tag{1.71}$$

Above we have defined that actual comoving number density of X particles by $Y = n_X/s$ and the equilibrium comoving number density of particles by $Y_{\rm EQ} = n_X^{\rm EQ}/s$. The final result simply comes from summing over all two-body final states and writing the total annihilation cross section in place of the partial annihilation cross section,

$$\frac{dY}{dx} = -\frac{x\left\langle\sigma_A|v|\right\rangle s}{H(m_X)}\left(Y^2 - Y_{\rm EQ}^2\right). \tag{1.72}$$

One can derive the equilibrium comoving number density in the relativistic regime ($T \gg m_X$) by first calculating the normal number density,

$$n(T) = \frac{g}{(2\pi)^3}\int f(p)(4\pi)p^2dp = \frac{g}{2\pi^2}\int_{m_X}^\infty \frac{\sqrt{E^2 - m_X^2}}{e^{-E/T}\pm 1}EdE = \frac{\zeta(3)}{\pi^2}g_{eff}T^3. \tag{1.73}$$

where $g_{eff} = g$ for bosons, $g_{eff} = 3g/4$ for fermions. The entropy density is dominated by the contribution of relativistic particles, which can be written as

$$s = \frac{2\pi^2}{45}\left(\sum_{i=\rm bosons} g_i\left(\frac{T_i}{T}\right)^3 + \frac{7}{8}\sum_{i=\rm fermions} g_i\left(\frac{T_i}{T}\right)^3\right)T^3 = \frac{2\pi^2}{45}g_{*,S}T^3. \tag{1.74}$$

So in the ultrarelativisitic regime, when temperatures are high compared to the mass of X ($x \ll 3$), we have

$$Y_{\rm EQ}(x) = \frac{45\zeta(3)}{2\pi^4}\frac{g_{eff}}{g_{*,S}}, \quad \text{for } (x \ll 3). \tag{1.75}$$

One can analogously derive the non-relativistic expression for the equilibrium comoving number density of X particles given by

$$Y_{\rm EQ}(x) = \frac{45}{4\pi^4}\left(\frac{\pi}{2}\right)^{1/2}\frac{g}{g_{*,S}}x^{3/2}e^{-x}, \quad \text{for } (x \gg 3). \tag{1.76}$$

Given a thermally averaged annihilation cross section, one can simply numerically integrate Eq. (1.72) to find the late-time abundance of dark matter.

To get a handle on the results that this numerical information would provide, we consider a simplified example. In most cases, the annihilation cross section is dominated by the lowest contributing partial wave so that $\sigma_A|v| \approx v^{2n}$ and therefore $\langle\sigma_A|v|\rangle \approx \sigma_0/x^n$ where $n = 0$ refers to s-wave annihilation, $n = 1$ to p-wave annihilation, etc. One can then show that the late-time comoving number density of X particles is given by the approximate formula,

$$Y_\infty = \frac{3.79\left(g_{*,S}/g_*^{1/2}\right)(n+1)x_f}{m_{Pl}m_X\langle\sigma_A|v|\rangle}, \tag{1.77}$$

where x_f (the freeze-out temperature) can be estimated from $\Gamma(x_f) \approx H(x_f)$ where Γ is the typical rate for the annihilation process.[19] Note that the comoving number density is inversely proportional to the annihilation cross section.

Once Y_∞ is calculated (either numerically or semianalytically as above), one can write the mass density today as

$$\rho_X = m_X s_0 Y_\infty \quad \Rightarrow \quad \Omega_X = \frac{m_X s_0 Y_\infty}{\Omega_c}, \tag{1.78}$$

[19] The freeze-out temperature is usually around $m_X/20$ (or $x_f \approx 20$).

where $s_0 = 2889/\text{cm}^3$ is the present-day entropy density and $\Omega_c = 1.05\times10^{-5}h^2\text{GeV}/\text{cm}^3$ is the critical density. In the approximate formula, this results in

$$\Omega_X h^2 = \frac{8.77\times10^{-11}/\text{GeV}^2}{\langle\sigma_A|v|\rangle}\left(\frac{(n+1)x_f\sqrt{g_*}}{g_{*,S}}\right) \approx \frac{1.05\times10^{-27}\text{cm}^3/s}{\langle\sigma_A|v|\rangle}\left(\frac{(n+1)x_f\sqrt{g_*}}{g_{*,S}}\right). \quad (1.79)$$

The WMAP team recently gave a seven year fit [7] and found the present day dark matter energy density to be $\Omega_{DM}h^2 = 0.1109 \pm 0.0056$. It turns out that a weak scale annihilation cross section[20] results in a dark matter abundance that is this order of magnitude. A weakly interacting massive particle (WIMP) fits the bill. This is known as the "WIMP Miracle."

In chapter 3, we explicitly compute the annihilation cross section for a dark matter candidate in a model with gauged baryon and lepton number. We use both the approximate formula, mentioned above, and the more precise numerical solution of the derived equation. We also compute the numerical solution and show important implications this solution has on the viable parameter space within the model.

[20] By this we mean a thermally averaged total annihilation cross section times velocity of about $3\times10^{-26}\text{cm}^3/\text{s}$.

Chapter 2

Primordial Power Spectra from Anisotropic Inflation

We examine cosmological perturbations in a dynamical theory of inflation in which an Abelian gauge field couples directly to the inflaton, breaking conformal invariance. When the coupling between the gauge field and the inflaton takes a specific form, inflation becomes anisotropic and anisotropy can persist throughout inflation, avoiding Wald's no-hair theorem. After discussing scenarios in which anisotropy can persist during inflation, we calculate the dominant effects of a small persistent anisotropy on the primordial gravitational wave and curvature perturbation power spectra using the "in-in" formalism of perturbation theory. We find that the primordial power spectra of cosmological perturbations gain significant direction dependence and that the fractional direction dependence of the tensor power spectrum is suppressed in comparison to that of the scalar power spectrum.

The contents of this chapter were written in collaboration with Moira Gresham and have been published in [1].

2.1 Introduction

Inflation gives a compelling explanation of the flatness, homogeneity, and isotropy of our Universe on large scales. It also generically predicts a nearly scale-invariant spectrum of density perturbations, which is consistent with our observations of the cosmic microwave background (CMB) and of structure formation. Because of these

successes, the inflationary paradigm has dominated very early Universe cosmology in recent years.

In this paper we focus on the prediction of isotropy from inflation. The no-hair theorem of inflation states, roughly speaking, that an initially expanding, homogeneous universe with positive cosmological constant, Λ, and matter satisfying the dominant energy condition will become indistinguishable from a universe with de Sitter geometry on a timescale of $\sqrt{3/\Lambda}$ [8]. Because of the no-hair theorem, isotropy is generally taken as a prediction of inflation.

But there could be ways around the no-hair theorem. For example, models with spacelike vector fields that get vacuum expectation values can lead to a preferred direction during inflation, evading the no-hair theorem because the vector field stress-energy tensor does not satisfy the dominant (or even the weak) energy condition [5]. However, such "aether" models have been shown to be unstable [9, 10, 11].

Recently, another model has been shown to support a persistent anisotropy during inflation [6]. In this model, there is a nonminimal coupling between a $U(1)$ gauge field and the inflaton, essentially leading to a time-dependent $U(1)$ charge during inflation:

$$S = \int d^4x\sqrt{-g}\left[\frac{R}{2\kappa^2} - \frac{1}{2}(\partial_\mu\phi)(\partial^\mu\phi) - V(\phi) - \frac{f^2(\phi)}{4}F_{\mu\nu}F^{\mu\nu}\right]. \tag{2.1}$$

Here, the $U(1)$ field strength, $F_{\mu\nu}$, may or may not be the electromagnetic field strength. When the coupling, $f(\phi)$, between the inflaton, ϕ, and the $U(1)$ field takes a particular form and there exists a nonzero homogeneous $U(1)$ seed field, an anisotropy persists throughout inflation even though the space-time is undergoing nearly exponential expansion. More specifically, the "electric" field contributes non-negligible extra negative pressure in the direction in which it points, which causes space-time to expand more slowly in that direction.

The model avoids the no-hair theorem by having (1) expansion that is not purely exponential and (2) a coupling between the inflaton and other matter. The mechanism for evasion of the no-hair theorem shows up in our results in the following ways: (A) all modifications to power spectra associated with the anisotropy go to zero when

slow-roll parameters vanish and (B) isotropic dynamics is quickly restored if the inflaton-dependent coupling that breaks conformal invariance goes to a constant (as is the case at the end of inflation, when the inflaton field relaxes to the minimum of its potential).

All of the standard energy conditions are satisfied in this model, which means it should not be plagued by stability issues as in aether models. The model does, however, suffer from the standard fine-tuning problems of single field inflation. Nevertheless, to our knowledge this model could be the first consistent model of inflation that evades the no-hair theorem and includes anisotropy at a significant level. It is therefore interesting to investigate whether the model is truly consistent and to investigate its potential astrophysical signatures.

To that end, in this chapter we consider gauge-invariant cosmological perturbations in this anisotropic inflation model. We consider and discuss a model generalized from that of [6], and extend their formula for the relation between the anisotropic expansion parameter and the slow-roll parameter to include arbitrary forms of the inflaton potential. We also present the dominant effect of the anisotropy on the power spectra of tensor, vector and scalar perturbation correlations at the end of inflation.

Our main conclusions are

- The power spectra for gravitational wave and curvature perturbations can develop dramatic direction dependence for very small values of the anisotropy parameter[1] if the parameter is nearly constant for a large period of inflation.

- The main cause of direction dependence of the power spectra is a coupling between the $U(1)$ vector degrees of freedom to both tensor and scalar degrees of freedom through the anisotropic background. These interactions significantly affect the power spectra of modes after horizon crossing.

[1] The anisotropy parameter is basically the fractional difference between the rate of expansion in the preferred direction and that of a perpendicular direction.

- The ratio of the fractional direction-dependent change in the gravitational wave power spectrum over that of the curvature perturbation power spectrum is nearly equal to the tensor-to-scalar ratio. In particular, the curvature perturbation power spectrum has much stronger direction dependence than the gravitational wave power spectrum.

- For a given scale, the tensor and scalar power in modes with wave vector perpendicular to the preferred direction is greater than the power in modes with wave vector parallel to the preferred direction.[2]

- There is no indication that the anisotropic inflation model is unstable (e.g. there are no ghosts). This should be unsurprising since the stress-energy tensor for matter in the model satisfies the dominant energy condition.

Many have studied inflationary scenarios with actions similar to (2.1), interpreting $F_{\mu\nu}$ as the standard model electromagnetic field strength, in the context of explaining the existence of large-scale magnetic fields in the Universe. Initially Parker [12] and then Turner and Widrow [13] showed that magnetic fields produced in an inflationary Universe are "uninterestingly small" (i.e., too small to possibly account for the observed large-scale magnetic fields in the Universe) unless the conformal invariance of the electromagnetic field is broken. The generation of seed magnetic fields starting from the action in (2.1) and a particular $f(\phi)$ was considered in [14] and more recently in [15]. Generic predictions for magnetic fields in a large class of models, of which the model we consider here is an example, were presented by Bamba, et. al. [16]; the particular realization of the model we consider in this paper is what these authors refer to as the "weak coupling case." Magnetogenesis, including the backreaction due to electromagnetic fields, in the inflationary scenario we consider here was considered in [17]. For a review of the generation of magnetic fields during inflation in a more

[2] I.e., the parameter g_* (see equation (2.39)), as defined in [5], that characterizes the direction-dependence of the power spectrum due to a preferred direction is *negative*.

general context see, for example, [18].

More recently, the effect of vector fields during inflation has been studied in the context of their effects on the curvature perturbation power spectrum. A "vector curvaton" scenario, in which a vector field with time-varying mass and Maxwell-type kinetic coupling term contributes to the curvature power spectrum, was found in [19] to allow significant anisotropic contributions to the curvature spectrum and bispectrum if the vector field remains light until the end of inflation. A similar massless vector curvaton scenario was considered in [20], and again the possibility of significant anisotropic contributions was found.[3] The anisotropic contribution of vector field perturbations to primordial curvature perturbation correlations in various inflationary scenarios was also considered in [21, 22, 23, 24, 25, 26]. Perturbations of what correspond to our cross polarization gravitational wave degree of freedom were studied in [27], but in a scenario in which a second scalar field, uncoupled to the $U(1)$ field and the scalar field that couples to the $U(1)$ field, causes a transition back to isotropic expansion before the end of inflation.

This chapter is organized as follows. In section 2.2, we introduce the model. In section 2.3, we discuss our philosophy and methods for calculating and analyzing primordial perturbation spectra. Finally, in sections 2.4 and 2.5 we calculate the primordial perturbation spectra and briefly discuss stability. We summarize our conclusions in section 2.6.

2.2 Model and Background Solution

We consider a space-time governed by the following action [6]:

$$S = \int d^4x\sqrt{-g}\left[\frac{R}{2\kappa^2} - \frac{1}{2}(\partial_\mu\phi)(\partial^\mu\phi) - V(\phi) - \frac{f^2(\phi)}{4}F_{\mu\nu}F^{\mu\nu}\right], \tag{2.2}$$

[3] Both studies employed the δN formalism in calculating the curvature perturbation power spectra.

where $g = \det(g_{\mu\nu})$, R is the Ricci scalar, ϕ is the inflaton, and $F_{\mu\nu} = \partial_\mu A_\nu - \partial_\nu A_\mu$ is a $U(1)$ gauge field strength. For convenience, we will refer to the $U(1)$ field as the "electromagnetic" (EM) field, even though it need not be the standard model EM field. Here we have defined

$$\kappa^2 \equiv 8\pi G = 1/M^2_{\text{Planck}}. \tag{2.3}$$

We assume that the background is homogeneous, and that there is a nonzero homogeneous electric field.[4] We orient coordinates such that $F_{ij} = F_{\eta y} = F_{\eta z} = 0$ and $F_{\eta x \neq 0}$. One could just as easily have chosen to consider a homogeneous magnetic field. This choice does not change the form of the background stress tensor, and we expect the results of this chapter to apply in the magnetic field case as well. However, allowing for both electric and magnetic fields of arbitrary relative alignment is beyond the scope of this chapter.

The background space-time is Bianchi I, and the metric can be written in the following form by appropriate choice of coordinate axes:[5]

$$ds^2 = a(\eta)^2 \left(-d\eta^2 + \gamma_{ij}(\eta) dx^i dx^j\right), \tag{2.4}$$

where[6]

$$\gamma_{xx} = e^{-4\beta(\eta)}, \quad \gamma_{yy} = \gamma_{zz} = e^{2\beta(\eta)}, \quad \text{and} \qquad \gamma_{ij} = 0 \quad \text{for all} \quad i \neq j. \tag{2.5}$$

[4] At least we assume that the "electric" field was aligned in our causal patch. We will not consider the effects of regions with differing directions of alignment of the electric field.

[5] The form is chosen so that the spatial metric has unit determinant (and therefore scaling or translating $\beta(\eta)$ does not affect the spatial volume element).

[6] An equivalent ansatz would have been $ds^2 = -dt^2 + a_\parallel(t)^2 dx^2 + a_\perp(t)^2(dy^2 + dz^2)$.

Since g is independent of β, the scale factor, a, completely characterizes the space-time volume. For convenience we define α to be the logarithm of the scale factor, so

$$a = e^{\alpha}. \tag{2.6}$$

In parametrizing the metric, we have used the conventions of [28]. The solution to the background electromagnetic field equation of motion is then [6],

$$F_{\eta x} = p_A \frac{e^{-4\beta(\eta)}}{f^2(\bar{\phi})}, \tag{2.7}$$

where p_A is an integration constant of mass dimension two and a prime indicates a derivative with respect to conformal time η. In these coordinates, Einstein's equations take the form [6],

$$\alpha'^2 = \beta'^2 + \frac{\kappa^2}{3}\left[\frac{\phi'^2}{2} + e^{2\alpha}V(\bar{\phi}) + \frac{p_A^2 e^{-2\alpha-4\beta}}{2f^2(\bar{\phi})}\right], \tag{2.8}$$

$$\alpha'' = -2\alpha'^2 + \kappa^2 e^{2\alpha}V(\bar{\phi}) + \frac{p_A^2\kappa^2 e^{-2\alpha-4\beta}}{6f^2(\bar{\phi})}, \tag{2.9}$$

$$\beta'' = -2\alpha'\beta' + \frac{p_A^2\kappa^2 e^{-2\alpha-4\beta}}{3f^2(\bar{\phi})}. \tag{2.10}$$

Given Einstein's equations above, the equation of motion for ϕ is redundant.[7]

It was shown that inflation can occur for suitable initial conditions such that the Universe is initially expanding, and that the energy density of the vector field will remain almost constant with respect to the inflaton energy density if $f(\phi) \propto e^{-2\alpha}$ [6]. Recall that if there is no inflaton-electromagnetic coupling, the ratio of electromagnetic energy density to inflaton energy density decays as a^{-4}. Let us briefly show how this can occur.

If expansion is nearly exponential (in cosmic time), then the "slow-roll" parame-

[7] Recall that Einstein's equations and the matter-field equations are related through the conservation equation, $\nabla_\mu T^\mu_\nu = 0$, where T^μ_ν is the matter stress-energy tensor.

ters,

$$\epsilon \equiv -\frac{\partial_t H}{H^2} = \frac{\alpha'^2 - \alpha''}{\alpha'^2}, \tag{2.11}$$

$$\delta \equiv \frac{\partial_t^2 H}{2H\partial_t H}, \tag{2.12}$$

are very small compared to one and as usual, $H \equiv \frac{\partial_t a}{a}$.[8] Higher derivatives of H must, of course, also be small if expansion is nearly exponential.

The field equations (2.8), (2.9) and (2.10), can be cast in the following form:

$$\hat{\rho}_A \equiv \frac{\kappa^2 p_A^2 e^{-4\beta}}{2a^2 f^2(\bar{\phi})\alpha'^2} = \frac{3}{2}\left(3\Sigma - \epsilon\Sigma + \frac{\Sigma'}{\alpha'}\right), \tag{2.14}$$

$$\hat{\rho}_\phi \equiv \frac{a^2\kappa^2 V(\bar{\phi})}{\alpha'^2} = 3 - \epsilon - \frac{3}{2}\Sigma + \frac{\epsilon}{2}\Sigma - \frac{\Sigma'}{2\alpha'} = 3 - \epsilon - \frac{1}{3}\hat{\rho}_A, \tag{2.15}$$

$$\frac{\kappa^2\bar{\phi}'^2}{\alpha'^2} = 2\epsilon - 6\Sigma + 2\epsilon\Sigma - 6\Sigma^2 - 2\frac{\Sigma'}{\alpha'} = 2\epsilon - \frac{4}{3}\hat{\rho}_A - 6\Sigma^2, \tag{2.16}$$

$$\text{where} \quad \Sigma \equiv \beta'/\alpha'. \tag{2.17}$$

The quantities $\hat{\rho}_\phi$ and $\hat{\rho}_A$ are dimensionless energy densities, normalized by the Hubble scale squared times the Planck mass squared.

In standard single field inflation with an inflaton potential V, for example, one finds from the field equations that $\frac{\kappa\phi'}{\alpha'} \sim \sqrt{\epsilon}$, so that if expansion is nearly exponential, then the inflaton must be slowly rolling. Taking derivatives of the above equations in the isotropic case, one can find expressions for derivatives of V in terms of slow-roll parameters—thus yielding requirements of a potential that can give rise to inflation.

[8] Note that

$$\frac{\epsilon'}{\alpha'} = 2\epsilon(\epsilon + \delta). \tag{2.13}$$

From (2.15) and (2.14) one finds

$$\frac{\hat{\rho}'_\phi}{\hat{\rho}_\phi \alpha'} = \frac{\partial_\phi V}{\kappa V}\frac{\kappa\bar{\phi}'}{\alpha'} + 2\epsilon = \frac{-\frac{\epsilon'}{\alpha'} - \frac{1}{3}\frac{\hat{\rho}'_A}{\alpha'}}{3 - \epsilon - \frac{1}{3}\hat{\rho}_A}, \tag{2.18}$$

$$\frac{\hat{\rho}'_A}{\hat{\rho}_A \alpha'} = -4 - 2\frac{\partial_\phi f}{\kappa f}\frac{\kappa\bar{\phi}'}{\alpha'} + 2\epsilon - 4\Sigma = \frac{2\frac{\Sigma'}{\alpha'} + \ldots}{3\Sigma - \epsilon\Sigma + \frac{\Sigma'}{\alpha'}}, \tag{2.19}$$

where $\ldots \sim \mathcal{O}(\Sigma\frac{\epsilon'}{\alpha'}, \epsilon\frac{\Sigma'}{\alpha'}, \frac{\Sigma''}{\alpha'^2})$.

We can glean a fair bit of information from equations (2.14) through (2.19) without much effort. First, what if expansion were purely exponential so that $\delta = \epsilon = 0$? From (2.16) we can immediately see that $\hat{\rho}_A$ and Σ had better then also be zero based simply on the fact that $\frac{\kappa^2\bar{\phi}'^2}{\alpha'^2}$, $\hat{\rho}_A$, and Σ^2 are positive. This could be seen as confirmation of the no-hair theorem; anisotropy can exist only if expansion is *not* purely exponential.[9] Similarly, if ϵ is small, then $\hat{\rho}_A$ and Σ had also better be small. In particular, even in small field models of inflation where typically $\epsilon \ll \delta \ll 1$, the anisotropy parameters Σ and $\hat{\rho}_A$ must be order ϵ or smaller. Second, from (2.18) we see that $\hat{\rho}_\phi$ is nearly constant with respect to the Hubble parameter if ϵ and Σ are small. Also from (2.18) we see that

$$\frac{\partial_\phi V}{\kappa V}\frac{\kappa\bar{\phi}'}{\alpha'} = -2\epsilon + \mathcal{O}(\epsilon'/\alpha') + \ldots \tag{2.21}$$

Third, from (2.19), if ϵ and Σ are small, we see that $\hat{\rho}_A$ decreases rapidly with respect

[9] A more direct confirmation of the no-hair theorem comes from supposing $\phi' = 0$ (and, for simplicity, $\epsilon << 1$) so that $V(\phi)$ functions as a cosmological constant. Then from (2.16) and (2.15)

$$\frac{d\log\hat{\rho}_A}{dt} \approx -4\frac{d}{dt}\alpha \approx -4\kappa\sqrt{\frac{V(\phi)}{3}}. \tag{2.20}$$

So $\hat{\rho}_A$, and thus by (2.14) also ϵ and Σ, go to zero on the time scale promised by the no-hair theorem.

to the Hubble parameter *unless*

$$\frac{f'}{f\alpha'} \lesssim -2, \tag{2.22}$$

or equivalently unless

$$\frac{\partial_\phi f}{\kappa f} \lesssim -2/\left(\frac{\kappa\bar{\phi}'}{\alpha'}\right). \tag{2.23}$$

Now since

$$\left(\frac{\partial_\phi V}{\kappa V}\right)^{-1} \sim \pm\sqrt{1/2\epsilon}\sqrt{1-3\Sigma/\epsilon+\ldots} \sim -\left(\frac{\kappa\bar{\phi}'}{\alpha'}\right)^{-1}, \tag{2.24}$$

a ready choice for the coupling function, f, if one wants the energy density of the electromagnetic field (and thus the anisotropy) not to decay rapidly with respect to the inflaton energy density, is thus

$$f(\phi) = \exp\left\{2c\kappa\int\left(\frac{\partial_\phi V}{\kappa V}\right)^{-1} d\phi\right\}, \tag{2.25}$$

where c is an order one constant. This is the coupling function motivated and examined in [6]. Let us suppose the coupling function is of this exact form, so

$$\frac{\hat{\rho}'_A}{\hat{\rho}_A\alpha'} = -4 - 4c\left(\frac{\kappa\bar{\phi}'}{\alpha'}\right)^2\left(\frac{\partial_\phi V}{\kappa V}\frac{\kappa\bar{\phi}'}{\alpha'}\right)^{-1} + 2\epsilon - 4\Sigma \tag{2.26}$$

$$= -4 - 4c(2\epsilon - 6\Sigma + \ldots)(-2\epsilon + \mathcal{O}(\epsilon'/\alpha') + \ldots)^{-1} + 2\epsilon - 4\Sigma \tag{2.27}$$

$$= (c-1)4 - 4(3c)\frac{\Sigma}{\epsilon} + \ldots \tag{2.28}$$

Suppose initially that $\Sigma \ll \epsilon$. If $c < 1$ then $\hat{\rho}_A$ decreases along with Σ as long as ϵ is small. Anisotropy is wiped out (albeit much more slowly than in the case where $f(\phi) = 1$). If $c > 1$, then $\hat{\rho}_A$ initially increases, as does Σ (see (2.14)). The derivative of the electromagnetic field energy density will thus approach zero, $\frac{\hat{\rho}'_A}{\hat{\rho}_A\alpha'} \longrightarrow 0$, and so $\hat{\rho}_A$ and Σ will become nearly constant for a time. If Σ is initially greater than $\frac{(c-1)}{3c}\epsilon$, then $\hat{\rho}_A$ and Σ will initially decrease, ϕ will climb its potential, and then it will fall back down (slowly) after Σ has approached a constant [6].

From (2.14) one can see that if Σ is approximately constant then Σ must be

positive. So when the space-time undergoes anisotropic expansion in this model (and Σ is nearly constant) the preferred direction expands more slowly than the perpendicular directions.

When (2.25) holds, we can find an expression for Σ in terms of the slow-roll parameter during the period in which it is nearly constant. Assuming

$$\begin{aligned} &\mathcal{O}(\epsilon) \approx \mathcal{O}(\delta), \qquad c-1 > \mathcal{O}(\epsilon), \qquad \Sigma \lesssim \mathcal{O}(\epsilon), \\ &\frac{\Sigma'}{\alpha'} \lesssim \mathcal{O}(\epsilon\Sigma), \qquad \text{and} \qquad \left(\frac{\Sigma'}{\alpha'}\right)'/\alpha' \lesssim \mathcal{O}(\epsilon^2\Sigma), \end{aligned} \tag{2.29}$$

we can set the two different expressions for $\partial_\phi V/V$ derived from equations (2.18) and (2.19) equal to each other. Using this method we find

$$\Sigma \equiv \frac{\beta'}{\alpha'} = \frac{c-1}{3c}\epsilon + \frac{1+c-4c^2}{18c^2}\epsilon^2 + \frac{1-2c-4c^2}{18c^2}\epsilon\delta + \ldots \tag{2.30}$$

The authors of [6] derived this expression to first order in ϵ for the particular potential $V = \frac{1}{2}m^2\phi^2$ and argued that Σ generically tracks the slow-roll parameter for general potentials. We find that the expression (2.30) actually holds for any potential V in a slow-roll regime ($\epsilon, \delta \ll 1$).

As $c \to 1$, the story is a bit different. For example, if $c = 1$, looking back to equations (2.26) - (2.28) one finds that $\hat{\rho}_A$, if it is initially greater in magnitude than $\mathcal{O}(\epsilon^2)$, decreases until its on the order of ϵ^2, and then stays nearly constant. From numerical studies it appears that if $\hat{\rho}_A$ is initially much greater in magnitude than $\mathcal{O}(\epsilon^2)$, then it will rapidly settle to a value much smaller than $\mathcal{O}(\epsilon^2)$. If the magnitude of $\hat{\rho}_A$ is initially on the order of ϵ^2 or less, then it will stay very nearly constant until the end of inflation. An example with $c = 1$ is provided in Fig. 2.1.

The trick of this model is to choose $f(\phi)$, given $V(\phi)$, such that the electromagnetic field energy density does not decay rapidly with respect to the inflaton energy density during inflation. We saw above that a choice guaranteed to work is

$$f(\phi) \approx \exp\left\{2\kappa \int \left(\frac{\partial_\phi V}{\kappa V}\right)^{-1} d\phi\right\}. \tag{2.31}$$

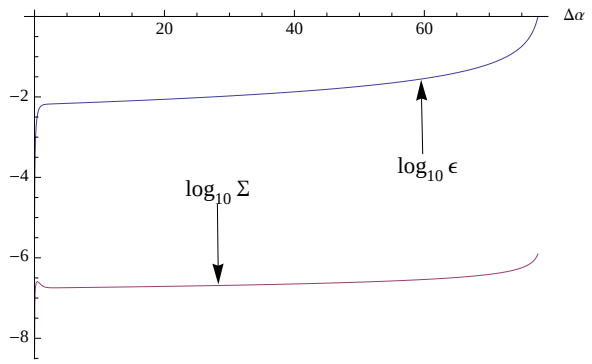

Figure 2.1: Log plot of Σ and ϵ as a function of e-foldings ($\Delta\alpha = \alpha - \alpha_0$) during inflation. The plot was generated with the potential $V = \frac{1}{2}m^2\phi^2$ and coupling function $f(\phi) = \exp\left[\frac{\kappa^2\phi^2}{2}\right]$. The initial conditions were $\phi_0 = 17.5/\kappa$, $\phi_0' = 0$, $\alpha_0 = -75$, $\beta_0 = 0$ and $\beta_0' = 0$. The constants m and p_A were chosen so that initially $\rho_A/\rho_\phi \approx 10^{-6}$. Notice that Σ very quickly settles to a value that is somewhat smaller than the square of the slow-roll parameter ϵ.

For example, if $V(\phi) \propto \phi^n$, then $f(\phi) \approx \exp[\kappa^2\phi^2/n]$. What if we were to choose instead, say, $f(\phi) \approx \exp[\lambda\kappa\phi]$? Then we would have

$$\frac{\hat{\rho}_A'}{\hat{\rho}_A\alpha'} = -4 - 2\lambda\frac{\kappa\bar{\phi}'}{\alpha'} + 2\epsilon - 4\Sigma. \tag{2.32}$$

If λ is order one, then the anisotropy will rapidly decay. However, if λ were large enough in magnitude then the anisotropy could persist for a good portion of inflation.

In our analysis, we will use only the background equations of motion, leaving $f(\phi)$ and $V(\phi)$ generic. We will then be interested in scenarios in which anisotropy can persist over several e-folds—scenarios in which $\frac{f'}{f\alpha'} = -2 + \mathcal{O}(\epsilon)$ and where $\hat{\rho}_A \approx 9\Sigma/2$ is approximately constant. We saw that consistency of the background equations and a slow-roll scenario dictates that $\hat{\rho}_A$ must be order ϵ or smaller. We also discussed specific examples of functions, $f(\phi)$, that can lead to such scenarios (assuming, otherwise, a slow-roll scenario, $\epsilon, \delta \ll 1$). In order to calculate primordial power spectra, we will use the "in-in" formalism of perturbation theory, assuming

- $\epsilon \ll 1$, $\delta \ll 1$,

- $\hat{\rho}_A \approx 9\Sigma/2 \lesssim \mathcal{O}(\epsilon)$,

- $\hat{\rho}'_A/(\hat{\rho}_A \alpha') \lesssim \mathcal{O}(\epsilon)$.

2.3 Perturbations: Setup and Strategy

Our goal is to examine whether the background described in the previous section (slightly generalized from the space-time of [6]) is perturbatively stable, and to examine its signature at the level of primordial perturbation spectra.

We have calculated the quadratic action for dynamical modes in terms of the gauge-invariant variables defined in appendix A.1. We calculated the action to quadratic order in perturbations starting with the form of the second-order Einstein-Hilbert action given in appendix A.2, and a similar expression for the quadratic-order matter action. We worked in Newtonian gauge and used a differential geometry package in *Mathematica* to massage the quadratic action into the (relatively) simple, manifestly gauge-invariant form presented in sections 2.4 and 2.5.

Regarding perturbative stability of the background, we find that there are no ghosts (fields with wrong-sign kinetic terms), and no other indication of instability at the quadratic level. Here, we take "perturbative stability" to mean that dimensionless combinations of fields assumed to be much less than one in the perturbative expansion of the action remain small. We find that such small quantities do indeed stay small.

In the remainder of this section we describe how we set up the calculation and analysis of perturbation spectra; we describe the physical scenario, the expression for expectation values in the "in-in" formalism, the definitions for the relevant degrees of freedom, and, finally, the current bound on a preferred direction during inflation. In sections 2.4 and 2.5 we calculate power spectra and briefly discuss stability.

2.3.1 Physical Scenario

Perturbations from inflation are usually assumed to be generated in the following way [29]:

- Quantum mechanical perturbative modes are in their ground state throughout inflation. So the vacuum expectation value of individual modes is zero, though the variance is generally nonzero.

- The normalization of the ground states is such that when the modes are well within the horizon, the canonically normalized[10] fields, ϕ, obey a simple harmonic oscillator equation and satisfy the canonical commutation relations.[11]

- As modes cross the horizon, their correlations are "frozen in" and translate into classical perturbations that lead to, for example, density perturbations that seed the formation of structure in the Universe and lead to temperature anisotropies of the cosmic microwave background radiation.

We shall assume the same, with one complication. We assume the quantity, $\Sigma \equiv \beta'/\alpha'$, which characterizes the deviation from isotropy, is nonzero so that expansion of the background space-time is slightly anisotropic, and modes that corresponded to scalar, vector, and tensor degrees of freedom in the isotropic background are now coupled. (Several scenarios in which this can occur were discussed in section 2.2.) Because of the coupling of modes, the amplitudes of tensor, vector, and scalar perturbations are not separately conserved outside the horizon. As the inflaton decays at the end of inflation, the dynamics becomes isotropic again, and tensor,

[10] In conformal time, the kinetic term for a canonically normalized field, ϕ, in the quadratic action takes the form $\frac{1}{2}\phi'^2$.

[11] Specifically,

$$[\partial_\eta \phi(\eta, \vec{x}), \phi(\eta, \vec{y})] = -i\hbar\delta^3(\vec{x} - \vec{y}), \tag{2.33}$$

where η is conformal time.

scalar, and vector modes decouple. At this point, superhorizon perturbations should be frozen in. We are therefore interested in the correlations of perturbations at the end of inflation. Especially if the $U(1)$ field in our model were interpreted as the electromagnetic field, the details of the reheating process at the end of inflation could also be important in calculating the direction dependence of CMB power spectra. In this chapter, however, we will only examine the effects of the gauge field on curvature and gravitational wave power spectra until just before reheating.

2.3.2 Correlations Using "In-In" Formalism

Because in the context of cosmological perturbations as described above we know only the quantum "in" states, and we are interested in expectation values evaluated at a particular time, we use the "in-in" formalism of perturbation theory (see e.g. [30]). We separate our Hamiltonian into a free portion H_0 and an interacting portion H_I. The interaction-picture (free) fields' evolution is determined by the free Hamiltonian. The expectation value for a general operator X at (conformal) time η can be written as

$$\begin{aligned} \langle X(\eta)\rangle &= \left\langle X^I(\eta)\right\rangle + i\int^{\eta} d\eta' \left\langle [H_I(\eta'), X^I(\eta)]\right\rangle \\ &+ (i)^2 \int^{\eta} d\eta' \int^{\eta'} d\eta'' \left\langle [H_I(\eta'), [H_I(\eta''), X^I(\eta)]]\right\rangle + \ldots \end{aligned} \tag{2.34}$$

where the ellipsis denotes terms with more powers of H_I and where X^I is the interaction-picture operator.

It should be noted that corrections of quadratic (or higher) order in the interaction Hamiltonian can lead to ambiguities when the details of the contour integration are not carefully considered [31]. We will work only to linear order in H_I, and therefore we need not worry about such ambiguities.

2.3.3 Decomposition of Perturbations

Since the background space-time is homogeneous, we decompose our perturbations into Fourier modes

$$\delta(x^i, \eta) = \int \frac{d^3k}{(2\pi)^3} \, e^{ik_j x^j} \delta(k_i, \eta). \tag{2.35}$$

We analyze perturbations about an anisotropic background. Since the background is anisotropic and thus there is no $SO(3)$ symmetry, perturbations cannot be decomposed into spin-0, spin-1, and spin-2 degrees of freedom and analyzed separately. We instead decompose gauge-invariant perturbations according to their transformation properties in the isotropic limit. (See appendix A.1.)

There are five dynamical degrees of freedom in our model, corresponding to

- one scalar degree of freedom, r (spin-0 in isotropic limit),[12]
- two electromagnetic vector degrees of freedom, δA^+ and δA^- (spin-1 in isotropic limit),
- and two metric tensor degrees of freedom, E^+ and $E^\times$ (spin-2 in isotropic limit).

In order to analyze the relevant dynamical perturbative degrees of freedom in our scenario, we derived the quadratic action in terms of the gauge-invariant variables of appendix A.1. Then we eliminated the nondynamical degrees of freedom by using constraint equations derived from the action. Finally, we canonically normalized the degrees of freedom that correspond to the dynamical "free" fields in the limit as $\beta'/\alpha' \longrightarrow 0$. Within the "in-in" formalism of perturbation theory, we take the interaction-picture fields to be those governed by the dynamics in the $\beta'/\alpha' = 0$ limit.

The quadratic action separates into two uncoupled pieces according to a residual symmetry under parity transformations. (See appendix A.1.) The "odd" sector has two degrees of freedom, $E^\times$ and δA^-. The "even" sector has three degrees of freedom, E^+, δA^+, and r. The fields $E^+, E^\times$, and r correspond to fields that are conserved

[12] See (A.22) in appendix A.1.

outside the horizon during isotropic inflation. Here r is a Mukhanov-Sasaki variable, equal to minus the curvature perturbation, $-\zeta$, as defined in, e.g. [32], in a gauge with spatially flat slicing. We will therefore refer to r as the curvature perturbation.

2.3.4 Canonically Normalized Variables

The canonically normalized fields in each sector ("even" and "odd," respectively) are given by

$$\begin{aligned} \hat{A}^+ &= f(\bar{\phi})\,\delta A^+, \\ \hat{h}^+ &= a(\eta)\,E^+/\kappa, \\ \hat{r} &= z(\eta)\,r, \end{aligned} \qquad \text{and} \qquad \begin{aligned} \hat{A}^- &= f(\bar{\phi})\,\delta A^-, \\ \hat{h}^\times &= a(\eta)\,E^\times/\kappa, \end{aligned} \tag{2.36}$$

where

$$z(\eta) \equiv a(\eta)\frac{\bar{\phi}'}{\alpha'}. \tag{2.37}$$

The fields on the right-hand sides of equations (2.36) are defined in appendix A.1. As mentioned above, in the isotropic limit E^+, E^- and r are conserved outside the horizon. The other important fact about the fields above is that the perturbative expansion of the action is valid when

$$E^+, E^\times, \frac{|\vec{k}|}{\bar{F}_{\eta x}}\delta A^+, \frac{|\vec{k}|}{\bar{F}_{\eta x}}\delta A^-, r \ll 1. \tag{2.38}$$

2.3.5 Comparison with Data

A formalism for finding signatures of a generic primordial preferred direction in the CMB has been developed [5, 27]. In [5] a small direction-dependent contribution to the primordial curvature power spectrum is parametrized by g_*, where

$$P(\vec{k}) = P_0(k)(1 + g_*\,(\hat{n}\cdot\hat{k})^2), \tag{2.39}$$

and where $\hat{n}$ is some preferred direction in the sky.

It is postulated that g_* will be approximately independent of the scale for modes

of astrophysical interest and that parity is still conserved. Parity conservation guarantees the absence of terms with odd powers of $(\hat{n} \cdot \hat{k})$. Contributions proportional to higher powers of $(\hat{n} \cdot \hat{k})^2$ are assumed to be negligible.

Using this formalism, a nonzero value for g_* was found using 5-year WMAP data at the 9 sigma level [33]. The central value found for g_* is 0.29 for a preferred direction very close to the ecliptic pole. Since the WMAP scanning strategy is tied to the ecliptic plane, this strongly suggests that the nonzero value of g_* is due to some systematic effect [34, 33]. Still, we may reasonably take from the analysis in [33] an upper bound for g_* of

$$|g_*| < 0.3. \tag{2.40}$$

In [35] it is estimated that Planck will be sensitive to values of $|g_*|$ as small as 0.02.

Obviously, the gravitational wave power spectrum has not yet been measured, so there is no limit on the analogous parameter, $g_{*\mathrm{grav}}$, for the gravitational wave power spectrum.

2.4 Perturbations: Odd Sector

As described in section 2.3.3, the quadratic action separates into two uncoupled pieces according to a residual symmetry under parity transformations. We'll therefore analyze the two "sectors"—which we refer to as "odd" and "even" for reasons discussed in appendix A.1—in different sections. We start in this section by analyzing the odd sector[13] because it is less complicated than the even sector, having only two coupled degrees of freedom (a tensor and a vector degree of freedom) instead of three degrees of freedom as in the even sector. The even sector, which includes the curvature perturbation, contains the most interesting physics; analyzing the odd sector is valuable for extracting $g_{*\mathrm{grav}}$ and as a warm-up for the analysis of the even sector.

In this section we present the action for the odd sector to quadratic order in gauge-

[13] Our odd sector corresponds to the $2d$-vector sector analyzed numerically in [27].

invariant perturbation variables. Then we argue that the form of the action implies that the background is classically stable. Next we diagonalize the kinetic term in the action by defining new perturbation variables in terms of which the kinetic term in the action is canonically normalized. This diagonalization allows us to identify the fields that should be quantized. The Hamiltonian derived from the diagonal form of the action is then separated into a "free" part and an "interacting" part, and "in-in" perturbation theory is used to find the autocorrelations (power spectra) and cross correlations of the vector and tensor degrees of freedom (see (2.36)) in terms of the preferred direction and the background quantities H and Σ. The most interesting result in this section is the tensor perturbation power spectrum, given in (2.79).

In the odd sector, the action takes the form

$$\begin{aligned} S^{\text{odd}} = \int d\eta \int \frac{d^3k}{(2\pi)^3} \Big(& \frac{1}{2}\hat{h}^{\times *\prime}\hat{h}^{\times\prime} + \frac{1}{2}\hat{A}^{-*\prime}\hat{A}^{-\prime} \\ & - \frac{1}{2}\hat{h}^{\times *}\hat{h}^{\times}\left(k^2 - \frac{a''}{a} - 4\hat{\rho}_A\alpha'^2/3 + \frac{1}{2}\Delta_{\vec{k}}\alpha'^2\left(2\hat{\rho}_A/3 + 6\Sigma^2 - \frac{3}{2}\Delta_{\vec{k}}\Sigma^2\right)\right) \\ & - \frac{1}{2}\hat{A}^{-*}\hat{A}^{-}\left(k^2 - \frac{f''}{f} + 2\Sigma\alpha'\frac{f'}{f} + \alpha'^2(2\hat{\rho}_A - 2\Sigma + 2\Delta_{\vec{k}}\hat{\rho}_A/3 - \Sigma^2)\right) \\ & + \left(i\psi'_{\vec{k}}\hat{h}^{\times *}\hat{A}^{-}\left(\frac{f'}{f} + \alpha'\Sigma + \Delta_{\vec{k}}\alpha'\Sigma\right) - i\psi'_{\vec{k}}\hat{h}^{\times *}\hat{A}^{-\prime} + \text{h.c.}\right)\Big), \end{aligned} \tag{2.41}$$

where

$$k^2 \equiv \gamma^{ij}k_ik_j = k_1^2e^{4\beta} + k_2^2e^{-2\beta}, \tag{2.42}$$

$$\Delta_{\vec{k}} \equiv \frac{k^{2\prime}}{k^2\beta'} = \frac{4\,k_1^2e^{4\beta} - 2\,k_2^2e^{-2\beta}}{k_1^2e^{4\beta} + k_2^2e^{-2\beta}}, \tag{2.43}$$

$$\frac{\psi'_{\vec{k}}}{\alpha'} \equiv \frac{k_2e^{-\beta}}{\sqrt{k^2}}\sqrt{\hat{\rho}_A}, \tag{2.44}$$

and f' denotes the derivative of $f(\bar{\phi}(\eta))$ with respect to conformal time. Without loss of generality we have set $k_3 = 0$ and we have taken the preferred direction (the direction along which the background electric field points) to be $\hat{x}^1$.

By inspection we can see that $\hat{h}^{\times}$ and $\hat{A}^{-}$ decouple when the wave vector is parallel to the preferred direction (so $k_2 = 0$). This decoupling should be expected due to the enhanced rotational symmetry about the wave vector in this case.

2.4.1 Preliminary Look at Stability

By design, the kinetic terms are canonically normalized. And in the short wavelength limit ($k \gg aH$), the action simplifies to that of two uncoupled harmonic oscillators; there is no indication of instability in the short wavelength limit.

Let us consider the case where $k_2 = 0$ so the wave vector corresponding to a mode points in the preferred direction. In this case, $\psi'_{\vec{k}} = 0$ and $\Delta_{\vec{k}} = 4$. By inspection, one sees that the cross-terms vanish. More explicitly,

$$S^{\text{odd}} \longrightarrow_{k_2 \to 0} \int d\eta \int \frac{d^3k}{(2\pi)^3} \Big(\frac{1}{2}\hat{h}^{\times *\prime}\hat{h}^{\times \prime} + \frac{1}{2}\hat{A}^{-*\prime}\hat{A}^{-\prime} - \frac{1}{2}\hat{h}^{\times *}\hat{h}^{\times} \left(k^2 - \frac{a''}{a} \right) - \frac{1}{2}\hat{A}^{-*}\hat{A}^{-} \left(k^2 - \frac{f''}{f} + 2\Sigma\alpha' \frac{f'}{f} + \alpha'^2(14\hat{\rho}_A/3 - 2\Sigma - \Sigma^2) \right) \Big). \quad (2.45)$$

When $k_2 \to 0$ the action for $\hat{h}^{\times}$ takes the same form as in the isotropic case. Though the effective mass for $\hat{h}^{\times}$ is not real for all time (so naively, there is a tachyon), the important point is that $\hat{h}^{\times}/a$, which we assumed to be much less than one in our perturbative expansion of the metric (see (2.38)), oscillates with decaying amplitude before horizon crossing, and then remains constant or decays after horizon crossing. In other words, $\hat{h}^{\times} \sim aE^{\times}$ never increases faster than a, which is consistent with the perturbative expansion. Similarly, given that $2\Sigma\alpha' \frac{f'}{f} + \alpha'^2(14\hat{\rho}_A/3 - 2\Sigma - \Sigma^2) \ll \frac{f''}{f}$, the long wavelength solution for $\hat{A}^{-}$ is approximately, $\hat{A}^{-} \approx C_1 f + C_2 f \int \frac{d\eta}{f^2}$. Now given that $f \approx a^{-2} \approx H^2\eta^2$, one can see that $\frac{|\vec{k}|}{\bar{F}_{\eta x}}\delta A^{-} \sim (C_1 + \frac{C_2}{H}a^3)a^{-4}$ (which is decaying) in the long wavelength limit. So clearly the perturbative expansion of the action remains valid when $k_2 = 0$.

Now let us consider a wave vector that is antiparallel to the preferred direction, so $k_1 = 0$. In this case, $\psi'_{\vec{k}} = \sqrt{\hat{\rho}_A}\,\alpha'$ and $\Delta_{\vec{k}} = -2$. Then the effective mass squared for $\hat{h}^{\times}$ becomes

$$m^2_{\text{eff}} = k^2 - \frac{a''}{a} - \alpha'^2(2\hat{\rho}_A + 9\Sigma^2).$$

Compared to the isotropic case, the effective mass squared for $\hat{h}^{\times}$ receives an additional negative contribution. This suggests that $\hat{h}^{\times}$ will grow slightly faster than a

outside the horizon. The situation is, of course, complicated by the coupling to $\hat{A}^-$, but all extra terms in the action when $k_1 = 0$ compared to the terms present when $k_2 = 0$ are small. This suggests that any possible growth of the perturbative fields in this case will be very moderate and does not represent an instability. This reasoning will be checked by calculating the power spectra of perturbative fields; we can check that the magnitudes of power spectra do not grow rapidly in time.

The same situation occurs in the even sector; perturbations clearly do not grow when $k_2 = 0$ and all extra terms in the action when $k_1 = 0$ compared to the terms present when $k_2 = 0$ are small.

2.4.2 Diagonalized Action

In general, the canonical quantization of a theory can only proceed once the kinetic interactions have been diagonalized. Usually the diagonalization is accomplished by some constant field redefinition. In our case, we need a time-dependent field redefinition because the "coefficients" in the kinetic portions of the action are not constant. (See appendix A.3.)

The kinetic terms can be diagonalized by performing a time-dependent unitary rotation,

$$\begin{pmatrix} \hat{h}^\times \\ \hat{A}^- \end{pmatrix} = \begin{pmatrix} \cos\psi_{\vec{k}}(\eta) & -i\sin\psi_{\vec{k}}(\eta) \\ -i\sin\psi_{\vec{k}}(\eta) & \cos\psi_{\vec{k}}(\eta) \end{pmatrix} \begin{pmatrix} U_1 \\ U_2 \end{pmatrix}. \tag{2.46}$$

In terms of the rotated fields, U_i, the odd-sector action takes the form,

$$S^{\text{odd}} = \int d\eta \int \frac{d^3k}{(2\pi)^3} \left[\frac{1}{2} \begin{pmatrix} U_1' \\ U_2' \end{pmatrix}^\dagger \begin{pmatrix} U_1' \\ U_2' \end{pmatrix} - \frac{1}{2} \begin{pmatrix} U_1 \\ U_2 \end{pmatrix}^\dagger M \begin{pmatrix} U_1 \\ U_2 \end{pmatrix} \right], \tag{2.47}$$

where the Hermitian matrix M is defined

$$\begin{aligned} M &\equiv \left(k^2 - \frac{1}{2}\left(\frac{a''}{a} + \frac{f''}{f}\right) + \Sigma\alpha'^2\left(\frac{f'}{f\alpha'} - 1 - \frac{1}{2}\Sigma + \frac{3}{2}\Sigma\Delta_{\vec{k}} - \frac{3}{8}\Sigma{\Delta_{\vec{k}}}^2\right)\right. \\ &+ \left.\frac{1}{3}\hat{\rho}_A\alpha'^2\left(3 + \Delta_{\vec{k}}\right)\right)\mathbb{I} \\ &+ \left[\sin(2\psi_{\vec{k}})\sigma_3 - \cos(2\psi_{\vec{k}})\sigma_2\right]\left(\frac{\psi'_{\vec{k}}}{\alpha'}\right)\alpha'^2\left(1 - \frac{f'}{f\alpha'} + \Sigma - \frac{3}{2}\Sigma\Delta_{\vec{k}}\right) \\ &+ \left[\cos(2\psi_{\vec{k}})\sigma_3 + \sin(2\psi_{\vec{k}})\sigma_2\right]\left(\frac{1}{2}\left(\frac{f''}{f} - \frac{a''}{a}\right)\right. \\ &- \left.\Sigma\alpha'^2\left(\frac{f'}{f\alpha'} - 1 - \frac{1}{2}\Sigma - \frac{3}{2}\Sigma\Delta_{\vec{k}} + \frac{3}{8}\Sigma{\Delta_{\vec{k}}}^2\right) - \frac{1}{3}\hat{\rho}_A\alpha'^2\left(5 + \frac{1}{2}\Delta_{\vec{k}}\right)\right), \end{aligned} \tag{2.48}$$

and where $\mathbb{I}$ is the 2×2 identity matrix and we have used the following convention for the Pauli matrices

$$\sigma_2 = \begin{pmatrix} 0 & -i \\ i & 0 \end{pmatrix}, \quad \text{and} \quad \sigma_3 = \begin{pmatrix} 1 & 0 \\ 0 & -1 \end{pmatrix}. \tag{2.49}$$

Physical quantities should not depend on the initial value of $\psi_{\vec{k}}$. Indeed, we will see that correlations of $\hat{h}^\times$ and $\hat{A}^-$ at a time, η, calculated using the "in-in" formalism of perturbation theory, depend only on the change in $\psi_{\vec{k}}$ after horizon crossing.

2.4.3 Correlations Using Perturbation Theory

In order to calculate correlations, we use the "in-in" formalism of perturbation theory, taking the small parameters to be ϵ, δ, $\hat{\rho}_A$, and Σ. As discussed at the end of section 2.2 we take

$$\begin{aligned} \epsilon &= \frac{\alpha'^2 - \alpha''}{\alpha'^2} \ll 1, \qquad \delta = \frac{\partial_t^2 H}{2H\partial_t H} \ll 1, \\ \hat{\rho}_A &\approx 9\Sigma/2 \lesssim \mathcal{O}(\epsilon), \qquad \frac{\hat{\rho}'_A}{\hat{\rho}_A\alpha'} \lesssim \mathcal{O}(\epsilon). \end{aligned} \tag{2.50}$$

Given these assumptions and the background field equations (2.8) through (2.10),

$$\frac{f'}{f\alpha'} = -2 + \mathcal{O}(\epsilon), \qquad \frac{f''}{f\alpha'^2} = 2 + \mathcal{O}(\epsilon) = \frac{a''}{a\,\alpha'^2}, \qquad \text{and} \qquad \alpha' \approx -\frac{1}{\eta}. \tag{2.51}$$

We choose as our free Hamiltonian

$$H_0^{\rm odd} \equiv \int \frac{d^3k}{(2\pi)^3} \left[\frac{1}{2} \begin{pmatrix} U_1' \\ U_2' \end{pmatrix}^\dagger \begin{pmatrix} U_1' \\ U_2' \end{pmatrix} + \frac{1}{2} \begin{pmatrix} U_1 \\ U_2 \end{pmatrix}^\dagger M^{(0)} \begin{pmatrix} U_1 \\ U_2 \end{pmatrix} \right], \tag{2.52}$$

where

$$M^{(0)} \equiv \left(\gamma^{ij}(\eta_0) k_i k_j - \frac{2}{\eta^2} \right) \mathbb{I}. \tag{2.53}$$

The interaction-picture fields then obey the following equations:

$$\frac{d^2 U_i^I}{d\eta^2} + \left(\gamma^{ij}(\eta_0) k_i k_j - \frac{2}{\eta^2} \right) U_i^I = 0. \tag{2.54}$$

Each of these fields can be expanded in terms of time-independent creation and annihilation operators as

$$\begin{aligned} U_i^I(\vec{x}, \eta) &= \int \frac{d^3k}{(2\pi)^3} e^{ik_j x^j} U_i^I(\vec{k}, \eta) \\ &= \int \frac{d^3k}{(2\pi)^3} \left(e^{ik_i x^i} \chi^{(0)}(k_{\eta_0}, \eta) \hat{a}_{\vec{k}}^i + e^{-ik_i x^i} \chi^{(0)*}(k_{\eta_0}, \eta) (\hat{a}_{\vec{k}}^i)^\dagger \right), \end{aligned} \tag{2.55}$$

where the canonically normalized mode functions are

$$\chi^{(0)}(k, \eta) = \frac{e^{-ik\eta}}{\sqrt{2k}} \left(1 - \frac{i}{k\eta} \right), \tag{2.56}$$

and where the commutation relations of the creation and annihilation operators are

$$\left[\hat{a}_{\vec{k}}^i, (\hat{a}_{\vec{q}}^j)^\dagger \right] = (2\pi)^3 \delta^{ij} \delta(\vec{k} - \vec{q}) \quad \text{and} \quad \left[\hat{a}_{\vec{k}}^i, \hat{a}_{\vec{q}}^j \right] = 0. \tag{2.57}$$

Here,

$$k_{\eta_0} \equiv \sqrt{\gamma^{ij}(\eta_0) k_i k_j}. \tag{2.58}$$

If we choose $\beta_0 = 0$ then $\gamma^{ij}(\eta_0) = \delta^{ij}$. But then if β changes during inflation, the coordinates at the end of inflation will not be isotropic. On the other hand, if we choose β_0 so that $\beta = 0$ at the end of inflation (when the dynamics returns to being

isotropic), then the coordinates at the end of inflation will be isotropic. The latter choice is more convenient.

Using the results of the previous section and the form of the matrix M in (2.48), the interaction-picture Hamiltonian takes the form

$$H_I(\eta) = \int \frac{d^3k}{(2\pi)^3} \left(\frac{1}{2} \begin{pmatrix} U_1^I \\ U_2^I \end{pmatrix}^\dagger M^{(1)} \begin{pmatrix} U_1^I \\ U_2^I \end{pmatrix} \right), \tag{2.59}$$

where,

$$\begin{aligned} M^{(1)} = M - M^{(0)} &= f_1(\eta, \vec{k})\mathbb{I} + \left[\sin(2\psi_{\vec{k}})\sigma_3 - \cos(2\psi_{\vec{k}})\sigma_2\right] f_2(\eta, \hat{k}) \\ &+ \left[\cos(2\psi_{\vec{k}})\sigma_3 + \sin(2\psi_{\vec{k}})\sigma_2\right] f_3(\eta, \hat{k}) \end{aligned} \tag{2.60}$$

and we have defined

$$\begin{aligned} f_1(\eta, \vec{k}) &\equiv (\gamma^{ij}(\eta) - \gamma^{ij}(\eta_0))k_i k_j - \frac{1}{2}\left(\frac{a''}{a} + \frac{f''}{f} - \frac{4}{\eta^2}\right) \\ &+ \Sigma\alpha'^2\left(\frac{f'}{f\alpha'} - 1 - \frac{1}{2}\Sigma + \frac{3}{2}\Sigma\Delta_{\vec{k}} - \frac{3}{8}\Sigma{\Delta_{\vec{k}}}^2\right) + \frac{1}{3}\hat{\rho}_A\alpha'^2\left(3 + \Delta_{\vec{k}}\right) \end{aligned} \tag{2.61}$$

$$f_2(\eta, \hat{k}) \equiv \left(\frac{\psi'_{\vec{k}}}{\alpha'}\right)\alpha'^2\left(1 - \frac{f'}{f\alpha'} + \Sigma - \frac{3}{2}\Sigma\Delta_{\vec{k}}\right) \tag{2.62}$$

$$\begin{aligned} f_3(\eta, \hat{k}) &\equiv \frac{1}{2}\left(\frac{f''}{f} - \frac{a''}{a}\right) - \Sigma\alpha'^2\left(\frac{f'}{f\alpha'} - 1 - \frac{1}{2}\Sigma - \frac{3}{2}\Sigma\Delta_{\vec{k}} + \frac{3}{8}\Sigma{\Delta_{\vec{k}}}^2\right) \\ &- \frac{1}{3}\hat{\rho}_A\alpha'^2\left(5 + \frac{1}{2}\Delta_{\vec{k}}\right). \end{aligned} \tag{2.63}$$

Our convention for the correlations of the fields will be

$$\left\langle U_i(\vec{k}, \eta)U_j(\vec{q}, \eta)\right\rangle = C_{ij}(\vec{k}, \eta)(2\pi)^3\delta(\vec{k} + \vec{q}), \tag{2.64}$$

where the power spectra are the diagonal entries of the matrix C_{ij}. Using (2.34), the

correlations can be written as

$$\langle U_i(\vec{p},\eta)\, U_j(\vec{q},\eta)\rangle = \langle U_i^I(\vec{p},\eta) U_j^I(\vec{q},\eta)\rangle + i\int^\eta d\eta' \langle [H_I(\eta'), U_i^I(\vec{p},\eta) U_j^I(\vec{q},\eta)]\rangle + \ldots \tag{2.65}$$

More explicitly, the correlations take the form,

$$C_{ij}(\vec{p},\eta) = |\chi^{(0)}(p_{\eta_0},\eta)|^2\delta_{ij} + i\int^\eta d\eta' M_{ij}^{(1)}(\vec{p},\eta') I_{p_{\eta_0}}(\eta',\eta) + \ldots, \tag{2.66}$$

where

$$I_p(\eta',\eta) = \left((\chi^{(0)}(p,\eta')\chi^{(0)*}(p,\eta))^2 - (\chi^{(0)*}(p,\eta')\chi^{(0)}(p,\eta))^2\right). \tag{2.67}$$

It is clear from this formula that the zeroth-order power spectra of the fields U_i are isotropic and scale invariant and that the cross-correlation vanishes. Here it is convenient to define the function

$$\tilde{I}(p\eta', p\eta) \equiv ip^2 I_p(\eta',\eta) \tag{2.68}$$

where,

$$\begin{aligned}\tilde{I}(x,y) &= \left(\frac{1}{2x^2y^2} - \frac{1}{2x^2} + \frac{2}{xy} - \frac{1}{2y^2} + \frac{1}{2}\right)\sin(2x-2y) \\ &+ \left(\frac{1}{x^2y} - \frac{1}{xy^2} + \frac{1}{x} - \frac{1}{y}\right)\cos(2x-2y).\end{aligned} \tag{2.69}$$

Solving for the correlations of the variables $\hat{h}^\times$ and $\hat{A}^-$ in terms of the correlations of the rotated variables U_i, we find

$$P_{\hat{h}^\times}(\vec{p}) = \cos^2\psi_{\vec{p}}\, C_{11}(\vec{p}) + \sin^2\psi_{\vec{p}}\, C_{22}(\vec{p}) + \frac{i}{2}\sin(2\psi_{\vec{p}})(C_{12}(\vec{p}) - C_{21}(\vec{p})), \tag{2.70}$$

$$P_{\hat{A}^-}(\vec{p}) = \sin^2\psi_{\vec{p}}\, C_{11}(\vec{p}) + \cos^2\psi_{\vec{p}}\, C_{22}(\vec{p}) - \frac{i}{2}\sin(2\psi_{\vec{p}})(C_{12}(\vec{p}) - C_{21}(\vec{p})), \tag{2.71}$$

$$\begin{aligned}C_{\hat{h}^\times\hat{A}^-}(\vec{p}) &= \cos^2\psi_{\vec{p}}\, C_{12}(\vec{p}) + \sin^2\psi_{\vec{p}}\, C_{21}(\vec{p}) + \frac{i}{2}\sin(2\psi_{\vec{p}})(C_{11}(\vec{p}) - C_{22}(\vec{p})) \\ &= -C_{\hat{A}^-\hat{h}^\times}(\vec{p}),\end{aligned} \tag{2.72}$$

where we have used the fact that $\psi_{-\vec{k}} = -\psi_{\vec{k}}$. All of the above correlations, and $\psi_{\vec{p}}$, are functions of time. It is understood that these expressions are evaluated at the end of inflation.

From here on, we will use the shorthand notation

$$p = p_{\eta_0}. \tag{2.73}$$

Using (2.66) and the expression for $M^{(1)}$, the power spectra and correlations are given more explicitly by

$$\begin{aligned} P_{\hat{h}^\times}(\vec{p},\eta) = |\chi^{(0)}(p,\eta)|^2 + p^{-2}\Bigg\{ & \int^\eta f_1(\eta',\vec{p})\,\tilde{I}(p\eta',p\eta)d\eta' \\ & + \left(\int^\eta \sin\left(2\psi_{\vec{p}}(\eta') - 2\psi_{\vec{p}}(\eta)\right)\ f_2(\eta',\hat{p})\,\tilde{I}(p\eta',p\eta)d\eta'\right) \\ & + \left(\int^\eta \cos\left(2\psi_{\vec{p}}(\eta') - 2\psi_{\vec{p}}(\eta)\right)\ f_3(\eta',\hat{p})\,\tilde{I}(p\eta',p\eta)d\eta'\right)\Bigg\} + \ldots, \end{aligned} \tag{2.74}$$

$$\begin{aligned} P_{\hat{A}^-}(\vec{p},\eta) = |\chi^{(0)}(p,\eta)|^2 + p^{-2}\Bigg\{ & \int^\eta f_1(\eta',\vec{p})\,\tilde{I}(p\eta',p\eta)d\eta' \\ & - \left(\int^\eta \sin\left(2\psi_{\vec{p}}(\eta') - 2\psi_{\vec{p}}(\eta)\right)\ f_2(\eta',\hat{p})\,\tilde{I}(p\eta',p\eta)d\eta'\right) \\ & - \left(\int^\eta \cos\left(2\psi_{\vec{p}}(\eta') - 2\psi_{\vec{p}}(\eta)\right)\ f_3(\eta',\hat{p})\,\tilde{I}(p\eta',p\eta)d\eta'\right)\Bigg\} + \ldots, \end{aligned} \tag{2.75}$$

$$\begin{aligned} C_{\hat{h}^\times\hat{A}^-}(\vec{p},\eta) = ip^{-2}\Bigg\{ & \int^\eta \cos\left(2\psi_{\vec{p}}(\eta') - 2\psi_{\vec{p}}(\eta)\right)\ f_2(\eta',\hat{p})\,\tilde{I}(p\eta',p\eta)d\eta' \\ & - \int^\eta \sin\left(2\psi_{\vec{p}}(\eta') - 2\psi_{\vec{p}}(\eta)\right)\ f_3(\eta',\hat{p})\,\tilde{I}(p\eta',p\eta)d\eta'\Bigg\} + \ldots. \end{aligned} \tag{2.76}$$

It is clear from the expression above that the correlations are functions only of the change in the angle $\psi_{\vec{p}}$.

2.4.4 Discussion

We are interested primarily in *direction-dependent* modifications to the power spectra—i.e., modifications of the power spectra that depend on the direction of the wave vector, not just its magnitude. Non-direction-dependent effects will modify spectral

indices, but such effects cannot be disentangled experimentally as due to primordial anisotropy. In principle, one could use our method to calculate spectral indices and, for example, relate them to the size of the direction-dependent effects.

The largest direction-dependent contribution comes from the piece involving f_2. The contribution is given by

$$p^{-2}\left(\int^{\eta}\sin\left(2\psi_{\vec{p}}(\eta')-2\psi_{\vec{p}}(\eta)\right)\ f_2(\eta',\hat{p})\,\tilde{I}(p\eta',p\eta)d\eta'\right)$$
$$\approx -\frac{(aH)^2}{p^3}\left(\cos[2\frac{\psi'_{\vec{p}}}{\alpha'}\log(aH/p)]-1\right) \tag{2.77}$$

assuming $\frac{\psi'_{\vec{p}}}{\alpha'}$ is approximately constant throughout inflation, where we have used the fact that $\left(1-\frac{f'}{f\alpha'}\right)\approx 3$ and the relevant integral is calculated in appendix A.4. Modes of astrophysical interest crossed the horizon about sixty e-folds before the end of inflation, so for such modes, $\log(aH/p)\approx 60$.

When

$$f(\phi)=\exp\left\{2c\kappa\int\left(\frac{\partial_\phi V}{\kappa V}\right)^{-1}d\phi\right\}, \tag{2.78}$$

for $c-1\sim\mathcal{O}(1)$ we found that $\hat{\rho}_A\approx\frac{3(c-1)}{2c}\epsilon$ during the anisotropic period of expansion. If the anisotropic period of expansion were to last all sixty e-folds before the end of inflation, then we should expect order one direction-dependent corrections to the gravitational wave power spectrum for inflationary scenarios in which $\sqrt{\epsilon}\gtrsim\frac{1}{60}$. Such values of ϵ can easily be realized in large-field inflationary models. This analytic result seems to confirm the numerical findings in [27].

Demanding the direction-dependent effect on the gravitational wave power spectrum for modes of astrophysical interest is less than, say, about 30% would mean that the argument of the cosine function in (2.77) is small so that the cosine can be expanded in a Taylor series. In this case the power spectrum for $\hat{h}^{\times}$ is approximately

$$\begin{aligned}P_{\hat{h}^{\times}}(\vec{p},\eta) &\approx \frac{(aH)^2}{2p^3}(1+\left(2\frac{\psi'_{\vec{p}}}{\alpha'}\log(aH/p)\right)^2)\\ &\approx \frac{(aH)^2}{2p^3}\left(1+4\hat{\rho}_A(\log(aH/p))^2(1-(\hat{n}\cdot\hat{p})^2)\right).\end{aligned} \tag{2.79}$$

where $\hat{n}$ is the preferred direction. Thus we may identify

$$g_{*\mathrm{grav}} \approx -4\hat{\rho}_A(\log(aH/p))^2 \approx -18\Sigma(\log(aH/p))^2. \tag{2.80}$$

Note that $g_{*\mathrm{grav}}$ is nearly (though not exactly) scale invariant for modes of astrophysical interest.

Imposing a limit like $|g_{*\mathrm{grav}}| < 0.3$ for modes of astrophysical interest corresponds to a limit on $\hat{\rho}_A$ like

$$\hat{\rho}_A|_{\text{average after horizon crossing}} \lesssim 10^{-4}, \qquad \text{when} \qquad |g_{*\mathrm{grav}}| < 0.3. \tag{2.81}$$

2.5 Perturbations: Even Sector

The even-sector action is much more complicated than that of the odd sector. This sector contains three dynamical degrees of freedom that, in the isotropic limit, transform as a scalar, vector and tensor under rotations. This sector is further complicated by additional nondynamical scalar variables.

As in the previous section, we begin in this section by diagonalizing the kinetic part of the quadratic action. This process is more complicated for the three dynamical degrees of freedom in this (even) sector than for the two of the odd sector, and the smallness of certain background quantities must be exploited; we eventually work in the limit $\hat{\rho}_A \ll \epsilon \ll 1$, which is confirmed to be a sensible limit at the end of the calculation. As in the odd-sector calculation, we quantize and use "in-in" perturbation theory to calculate power spectra and cross correlations of the scalar, vector, and tensor degrees of freedom. The most interesting results in this section are the scalar perturbation power spectrum (2.110) and corresponding value for g_* (2.111), and also the ratio of the direction-dependent correction to the scalar power spectrum over that of the tensor power spectrum (2.115).

Instead of presenting the entire quadratic action (as we did in (2.41) for the odd sector), here we present the action to lowest order in δ, ϵ, $\hat{\rho}_A$, and Σ. We expand the

action assuming that $\hat{\rho}_A$, Σ, and $\hat{\rho}'_A/\hat{\rho}_A$ are order ϵ or smaller. For simplicity, we first present the action to lowest order before elimination of the auxiliary fields Φ and Ψ. (See appendix A.1 for the definitions of Φ and Ψ.) The action can be written

$$S^{\text{even}} = \int d\eta \int \frac{d^3k}{(2\pi)^3} \left[\mathbf{H}^\dagger \mathbf{M}_1 \mathbf{H} + \mathbf{\Phi}^\dagger \mathbf{Q} \mathbf{H} + \mathbf{H}^\dagger \mathbf{Q}^\dagger \mathbf{\Phi} + \mathbf{\Phi}^\dagger \mathbf{M}_2 \mathbf{\Phi} \right], \tag{2.82}$$

where the vectors $\mathbf{H}$ and $\mathbf{\Phi}$ are defined by

$$\mathbf{H} = \begin{pmatrix} \hat{h}^{+\prime} \\ \hat{A}^{+\prime} \\ \hat{r}' \\ \hat{h}^{+} \\ \hat{A}^{+} \\ \hat{r} \end{pmatrix}, \qquad \mathbf{\Phi} = \begin{pmatrix} \Phi \\ \Psi \end{pmatrix}, \tag{2.83}$$

and the matrices $\mathbf{M}_1$, $\mathbf{M}_2$, and $\mathbf{Q}$ are given by

$$\begin{aligned} \mathbf{M}_1 \;=\; & \begin{pmatrix} \frac{1}{2} & 0 & 0 & 0 & 0 & 0 \\ 0 & \frac{1}{2} & 0 & 0 & 0 & 0 \\ 0 & 0 & \frac{1}{2} & 0 & 0 & 0 \\ 0 & 0 & 0 & \alpha'^2 - \frac{k^2}{2} & 0 & 0 \\ 0 & 0 & 0 & 0 & \alpha'^2 - \frac{k^2}{2} & 0 \\ 0 & 0 & 0 & 0 & 0 & \frac{1}{2}\frac{z''}{z} - \frac{k^2}{2} \end{pmatrix} \\ + & \begin{pmatrix} 0 & 0 & 0 & 0 & 0 & 0 \\ 0 & 0 & 0 & -i\psi'_{\vec{k}} & 0 & -i2\sqrt{2}\frac{a}{\kappa z}\psi'_{\vec{k}} \\ 0 & 0 & 0 & 0 & 0 & 0 \\ 0 & i\psi'_{\vec{k}} & 0 & 0 & 2i\psi'_{\vec{k}}\alpha' & 2\sqrt{2}\frac{a}{\kappa z}{\psi'_{\vec{k}}}^2 \\ 0 & 0 & 0 & -2i\psi'_{\vec{k}}\alpha' & 0 & -i4\sqrt{2}\frac{a\alpha'}{\kappa z}\psi'_{\vec{k}} \\ 0 & i2\sqrt{2}\frac{a}{\kappa z}\psi'_{\vec{k}} & 0 & 2\sqrt{2}\frac{a}{\kappa z}{\psi'_{\vec{k}}}^2 & i4\sqrt{2}\frac{a\alpha'}{\kappa z}\psi'_{\vec{k}} & 16\frac{a^2}{\kappa^2 z^2}{\psi'_{\vec{k}}}^2 - 8\frac{a^2\alpha'^2}{\kappa^2 z^2}\hat{\rho}_A \end{pmatrix} + \mathcal{O}(\epsilon), \end{aligned} \tag{2.84}$$

$$\mathbf{M}_2 = \begin{pmatrix} \frac{a^2}{\kappa^2}{\psi'_{\vec{k}}}^2 & -\frac{3a^2}{\kappa^2}({\psi'_{\vec{k}}}^2 + \frac{2}{3}\hat{\rho}_A\alpha'^2) - \frac{3}{2}z^2\alpha'^2 \\ -\frac{3a^2}{\kappa^2}({\psi'_{\vec{k}}}^2 + \frac{2}{3}\hat{\rho}_A\alpha'^2) - \frac{3}{2}z^2\alpha'^2 & \frac{9a^2}{\kappa^2}({\psi'_{\vec{k}}}^2 + \frac{2}{3}\hat{\rho}_A\alpha'^2) - \frac{\kappa^2 z^2}{a^2} + \frac{3z^2\alpha'^2}{2}(1 + \frac{2z'}{\alpha' z}) \end{pmatrix} + \frac{a^2k^2}{\kappa^2}\begin{pmatrix} 0 & -(1 - \frac{\Delta_{\vec{k}}\Sigma}{4}) \\ -(1 - \frac{\Delta_{\vec{k}}\Sigma}{4}) & (1 + \frac{\Delta_{\vec{k}}\Sigma}{2} - \frac{\kappa^2 z^2}{2a^2}) \end{pmatrix} + \mathcal{O}(\epsilon^2), \quad (2.85)$$

$$\mathbf{Q} = \begin{pmatrix} 0 & i\frac{a}{\sqrt{2}\kappa}\psi'_{\vec{k}} & 0 & \sqrt{2}\frac{a}{\kappa}{\psi'_{\vec{k}}}^2 & -i\frac{a}{\sqrt{2}\kappa}\psi'_{\vec{k}}\alpha' & 4\frac{a^2}{\kappa^2 z}{\psi'_{\vec{k}}}^2 \\ 0 & 0 & 0 & -3\sqrt{2}\frac{a}{\kappa}{\psi'_{\vec{k}}}^2 + \frac{ak^2\Sigma}{4\sqrt{2}\kappa}(\Delta_{\vec{k}} - 4) & 0 & \frac{1}{2}k^2 z - 12\frac{a^2}{\kappa^2 z}{\psi'_{\vec{k}}}^2 \end{pmatrix} + \mathcal{O}(\epsilon^{3/2}), \quad (2.86)$$

and $\psi'_{\vec{k}}$ is as in (2.44). Note here the identity

$$\alpha'^2(\Delta_{\vec{k}} - 4)\hat{\rho}_A = -4{\psi'_{\vec{k}}}^2. \quad (2.87)$$

Solving the (constraint) equations of motion derived by varying the action with respect to Φ and Ψ and plugging the constraint equations back into the action leads to the action in terms of the three dynamical fields:

$$S^{\text{even}} = \int d\eta \int \frac{d^3k}{(2\pi)^3}\left[\mathbf{H}^\dagger\left(\mathbf{M}_1 - \mathbf{Q}^\dagger\mathbf{M}_2^{-1}\mathbf{Q}\right)\mathbf{H}\right]. \quad (2.88)$$

Keep in mind that $\psi'_{\vec{k}}$ is a direction-dependent quantity that varies from zero to plus or minus $\sqrt{\hat{\rho}_A}$, depending on the orientation of the wave vector with respect to the preferred direction. The bottom right element of $\mathbf{M}_1$, representing (minus) the effective mass for $\hat{r}$, is $\frac{1}{2}(\frac{z''}{z} - k^2)$ in the isotropic limit. So if, for example, $\hat{\rho}_A$ is order $\frac{\kappa^2 z^2}{a^2} = \mathcal{O}(\epsilon)$ then we should expect a very dramatic direction-dependent effect on the curvature perturbation power spectrum, because the direction-dependent term would be on the same order as the normal, isotropic term (at least in the long-wavelength

limit). In fact, assuming that taking into account the $\mathbf{Q}^\dagger\mathbf{M}_2^{-1}\mathbf{Q}$ correction to $\mathbf{M}_1$ and properly diagonalizing the kinetic term in the action would not weaken the direction-dependent effect on the power spectrum, we can get a rough limit on the average value of $\hat{\rho}_A/(\kappa^2 z^2/a^2)$ during inflation, after horizon crossing. Based on the argument of section 2.3.5, we may take a 30% direction-dependent contribution to curvature perturbation power spectrum to be an upper limit. Noting that $\frac{z''}{z} = \alpha'^2(2+\mathcal{O}(\epsilon,\delta))$, the 30% limit translates roughly to[14]

$$\frac{\hat{\rho}_A a^2}{\kappa^2 z^2}\Big|_{\text{average}} \approx \frac{\hat{\rho}_A}{2\epsilon}\Big|_{\text{average}} < 10^{-2} \qquad \text{(approximate)}. \tag{2.89}$$

Given phenomenological constraints, it is therefore most interesting to consider scenarios in which $\hat{\rho}_A \ll \epsilon$. Taking

$$\hat{\rho}_A \sim (9/2)\Sigma \ll \epsilon, \tag{2.90}$$

by inspection one can see that in the long-wavelength limit,

$$\mathbf{Q}^\dagger\mathbf{M}_2^{-1}\mathbf{Q} = \mathcal{O}(\hat{\rho}_A/\epsilon), \tag{2.91}$$

and

$$\mathbf{M}_1 = \begin{pmatrix} \frac{1}{2} & 0 & 0 & 0 & 0 & 0 \\ 0 & \frac{1}{2} & 0 & 0 & 0 & -i2\sqrt{2}\frac{a}{\kappa z}\psi'_{\vec{k}} \\ 0 & 0 & \frac{1}{2} & 0 & 0 & 0 \\ 0 & 0 & 0 & \alpha'^2 - \frac{k^2}{2} & 0 & 0 \\ 0 & 0 & 0 & 0 & \alpha'^2 - \frac{k^2}{2} & -i4\sqrt{2}\frac{a\alpha'}{\kappa z}\psi'_{\vec{k}} \\ 0 & i2\sqrt{2}\frac{a}{\kappa z}\psi'_{\vec{k}} & 0 & 0 & i4\sqrt{2}\frac{a\alpha'}{\kappa z}\psi'_{\vec{k}} & \frac{1}{2}\frac{z''}{z} - \frac{k^2}{2} \end{pmatrix} + \mathcal{O}(\epsilon, \hat{\rho}_A/\epsilon). \tag{2.92}$$

[14] The first equality can be seen from equations (2.16) and (2.37), given that $\hat{\rho}_A$ must be small compared to $\kappa^2 z^2/a^2$.

We will find, with a careful analysis in the $\hat{\rho}_A \ll \epsilon$ limit, that the actual constraint on $\hat{\rho}_A$ is much stronger than the approximate constraint in (2.89). Thus the $\hat{\rho}_A \ll \epsilon$ approximation is valid.

2.5.1 Diagonalizing the Action

Once again, the resulting kinetic terms are not diagonalized and canonical quantization cannot proceed. In the $\hat{\rho}_A \ll \epsilon \ll 1$ limit, the kinetic terms can be diagonalized by performing a time-dependent unitary rotation

$$\begin{pmatrix} \hat{r} \\ \hat{A}^+ \end{pmatrix} = \begin{pmatrix} \cos\theta_{\vec{k}}(\eta) & -i\sin\theta_{\vec{k}}(\eta) \\ -i\sin\theta_{\vec{k}}(\eta) & \cos\theta_{\vec{k}}(\eta) \end{pmatrix} \begin{pmatrix} U_1 \\ U_2 \end{pmatrix}, \tag{2.93}$$

where

$$\theta'_{\vec{k}}(\eta) \equiv -2\sqrt{2}\frac{a}{\kappa z}\psi'_{\vec{k}} = -2\sqrt{2}\frac{a}{\kappa z}\left(\frac{k_2 e^{-\beta}}{\sqrt{k^2}}\sqrt{\hat{\rho}_A}\alpha'\right), \tag{2.94}$$

and where $\psi'_{\vec{k}}$ is the rotation angle in the odd sector, given by (2.44). The rotation of $\hat{r}$ and $\hat{A}^+$ occurs on a much faster timescale than that of $\hat{h}^\times$ and $\hat{A}^-$ since $\psi'_{\vec{k}} = \mathcal{O}(\sqrt{\hat{\rho}_A})$ and $\theta'_{\vec{k}} = \mathcal{O}(\sqrt{\hat{\rho}_A/\epsilon})$.

In terms of these rotated fields the even action takes the form

$$S^{\text{even}} = \int d\eta \int \frac{d^3k}{(2\pi)^3}\Big[\frac{1}{2}\hat{h}^{+\prime}\hat{h}^{+*\prime} - \frac{1}{2}\left(k^2 - 2\alpha'^2\right)\hat{h}^+\hat{h}^{+*} + \frac{1}{2}\begin{pmatrix} U'_1 \\ U'_2 \end{pmatrix}^\dagger \begin{pmatrix} U'_1 \\ U'_2 \end{pmatrix} - \frac{1}{2}\begin{pmatrix} U_1 \\ U_2 \end{pmatrix}^\dagger M \begin{pmatrix} U_1 \\ U_2 \end{pmatrix} + \dots\Big], \tag{2.95}$$

where the Hermitian matrix M is defined

$$M \equiv \left(k^2 - 2\alpha'^2\right)\mathbb{I} + \left[\sin(2\theta_{\vec{k}})\sigma_3 - \cos(2\theta_{\vec{k}})\sigma_2\right]\left(3\frac{\theta'_{\vec{k}}}{\alpha'}\right)\alpha'^2 \tag{2.96}$$

up to corrections of order ϵ, δ, and $\hat{\rho}_A/\epsilon$.[15] We have used the same convention for Pauli matrices as in Eq. (2.49) and, again, $\mathbb{I}$ is the 2×2 identity matrix.

[15] Recall that, e.g., $z''/2z = \alpha'^2 + \mathcal{O}(\epsilon, \delta)$ and $z'/z = \alpha' + \mathcal{O}(\epsilon, \delta)$.

2.5.2 Correlations Using Perturbation Theory

The analysis of correlations of dynamical fields in this sector will be very similar to that of the odd sector, up to minus signs and replacing $\psi_{\vec{k}}$ with $\theta_{\vec{k}}$. It should be noted that the largest direction-dependent corrections to correlations in the odd sector are order $\sqrt{\hat{\rho}_A}$, whereas here we are working to order $\sqrt{\hat{\rho}_A/\epsilon}$ assuming $\hat{\rho}_A \ll \epsilon$. It therefore should be unsurprising that the autocorrelation of the gravitational wave amplitude, $\hat{h}^+$, has no anisotropic contribution at $\mathcal{O}(\sqrt{\hat{\rho}_A/\epsilon})$. The same can be said of the cross-correlation between $\hat{h}^+$ and $\hat{A}^+$.

Considering now only terms up to order $\sqrt{\hat{\rho}_A/\epsilon}$ given $\hat{\rho}_A \ll \epsilon$, we choose as our free Hamiltonian,

$$H_0^{\text{even}} \equiv \int \frac{d^3k}{(2\pi)^3}\Big[\frac{1}{2}\hat{h}^{+\prime}\hat{h}^{+*\prime} + \frac{1}{2}\left(\gamma^{ij}(\eta_0)k_ik_j - \frac{2}{\eta^2}\right)\hat{h}^+\hat{h}^{+*} + \frac{1}{2}\begin{pmatrix}U_1'\\U_2'\end{pmatrix}^\dagger\begin{pmatrix}U_1'\\U_2'\end{pmatrix} + \frac{1}{2}\begin{pmatrix}U_1\\U_2\end{pmatrix}^\dagger M^{(0)}\begin{pmatrix}U_1\\U_2\end{pmatrix}\Big], \quad (2.97)$$

where

$$M^{(0)} \equiv \left(\gamma^{ij}(\eta_0)k_ik_j - \frac{2}{\eta^2}\right)\mathbb{I}. \quad (2.98)$$

The interaction-picture fields then obey the following equations,

$$\frac{d^2U_i^I}{d\eta^2} + \left(\gamma^{ij}(\eta_0)k_ik_j - \frac{2}{\eta^2}\right)U_i^I = 0. \quad (2.99)$$

As in section 2.4, the fields can be expanded into appropriately normalized mode functions and time-independent creation and annihilation operators. Dropping terms of order ϵ, $\hat{\rho}_A/\epsilon$, δ or higher (including terms with coefficients $(\gamma^{ij}(\eta) - \gamma^{ij}(\eta_0))k_ik_j$) the interaction-picture Hamiltonian takes the form

$$H_I(\eta) = \int \frac{d^3k}{(2\pi)^3}\left(\frac{1}{2}\begin{pmatrix}U_1^I\\U_2^I\end{pmatrix}^\dagger M^{(1)}\begin{pmatrix}U_1^I\\U_2^I\end{pmatrix}\right), \quad (2.100)$$

where

$$M^{(1)} = M - M^{(0)} = 3\left[\sin(2\theta_{\vec{k}})\sigma_3 - \cos(2\theta_{\vec{k}})\sigma_2\right]\left(\frac{\theta'_{\vec{k}}}{\alpha'}\right)\alpha'^2. \tag{2.101}$$

After computing correlations of the rotated variables using the "in-in" formalism, we can find the correlations of the unrotated variables using the equations analogous to equations (2.70) through (2.72).

The correlations are approximately given by

$$P_{\hat{r}}(\vec{p},\eta) \approx |\chi^{(0)}(p,\eta)|^2 + p^{-2}\left(\int^{\eta} \sin\left(2\theta_{\vec{p}}(\eta') - 2\theta_{\vec{p}}(\eta)\right)\, 3\frac{\theta'_{\vec{p}}(\eta')}{\alpha'(\eta')}\alpha'^2(\eta')\,\tilde{I}(p\eta', p\eta)d\eta'\right), \tag{2.102}$$

$$P_{\hat{A}^+}(\vec{p},\eta) \approx |\chi^{(0)}(p,\eta)|^2 - p^{-2}\left(\int^{\eta} \sin\left(2\theta_{\vec{p}}(\eta') - 2\theta_{\vec{p}}(\eta)\right)\, 3\frac{\theta'_{\vec{p}}(\eta')}{\alpha'(\eta')}\alpha'^2(\eta')\,\tilde{I}(p\eta', p\eta)d\eta'\right), \tag{2.103}$$

$$C_{\hat{r}\hat{A}^+}(\vec{p},\eta) \approx ip^{-2}\left\{\int^{\eta} \cos\left(2\theta_{\vec{p}}(\eta') - 2\theta_{\vec{p}}(\eta)\right)\, 3\frac{\theta'_{\vec{p}}(\eta')}{\alpha'(\eta')}\alpha'^2(\eta')\,\tilde{I}(p\eta', p\eta)d\eta'\right\} \tag{2.104}$$
$$= -C_{\hat{A}^+\hat{r}}(\vec{p},\eta),$$

where $\tilde{I}$ is defined in (2.69).

Assuming $\hat{\rho}_A$ and $\frac{\kappa\phi'}{\alpha'} = \frac{z}{\kappa a}$ are nearly constant during inflation, as in the scenarios we described in section 2.2, then

$$\theta_{\vec{p}}(\eta) \approx \frac{\theta'_{\vec{p}}}{\alpha'}\,\alpha(\eta), \tag{2.105}$$

and we may estimate the relevant integral as in appendix A.4. Then we see that

$$P_{\hat{r}}(\vec{p},\eta) \approx \frac{(aH)^2}{2p^3}\left(1 - 2\left(\cos\left(\left(2\frac{\theta'_{\vec{p}}}{\alpha'}\right)\log(aH/p)\right) - 1\right)\right), \tag{2.106}$$

$$P_{\hat{A}^+}(\vec{p},\eta) \approx \frac{(aH)^2}{2p^3}\left(1 + 2\left(\cos\left(\left(2\frac{\theta'_{\vec{p}}}{\alpha'}\right)\log(aH/p)\right) - 1\right),\right) \tag{2.107}$$

$$C_{\hat{r}\hat{A}^+}(\vec{p},\eta) \approx i\frac{(aH)^2}{p^3}\sin\left(\left(2\frac{\theta'_{\vec{p}}}{\alpha'}\right)\log(aH/p)\right) = -C_{\hat{A}^+\hat{r}}(\vec{p},\eta), \tag{2.108}$$

where $\frac{\theta'_{\vec{p}}}{\alpha'}$ should be taken as the average value after horizon crossing.

Now g_*, the parameter that characterizes the effect of a preferred direction on the CMB power spectrum, is roughly given by

$$|g_*| \approx -2 \left(\cos \left(\left(2 \frac{\theta'_{\vec{p}}}{\alpha'} \right) \log(aH/p) \right) - 1 \right) \Big|_{\max}. \tag{2.109}$$

The maximal value of $\frac{\theta'_{\vec{p}}}{\alpha'}$ for a given wave vector is approximately $2\sqrt{\frac{\hat{\rho}_A}{\epsilon}}$. So even if $\hat{\rho}_A/\epsilon$ is, say, order 10^{-4}, the argument of the cosine in (2.109) could be significant for modes of astrophysical interest because for such modes $\log(aH/p) \approx 60$. It is then clear that $|g_*|$ could be order one even for very small values of Σ and $\hat{\rho}_A$.

Let us suppose that $\hat{\rho}_A$ is small enough to satisfy the $|g_*| < 0.3$ bound of section 2.3.5. Then the cosine in (2.106) can be expanded in a Taylor series to give

$$P_{\hat{r}}(\vec{p}, \eta) \approx \frac{(aH)^2}{2p^3} \left(1 + 16 \frac{\hat{\rho}_A}{\epsilon} (\log(aH/p))^2 (1 - (\hat{n} \cdot \hat{p})^2) \right), \tag{2.110}$$

where $\hat{n}$ is the preferred direction, and therefore

$$g_* \approx -16 \frac{\hat{\rho}_A}{\epsilon} \left(\log \left(\frac{aH}{p} \right) \right)^2 \approx -72 \frac{\Sigma}{\epsilon} \left(\log \left(\frac{aH}{p} \right) \right)^2. \tag{2.111}$$

Note that g_* is negative, as is $g_{*\mathrm{grav}}$ (see equation (2.80)). A negative g_* means that, for a given scale, power is minimized in the preferred direction. We can understand this general feature in the following way: the pressure contributed by the background electric field slows the expansion of the direction along which the electric field points. In other words, expansion is slower along the preferred direction. Generically the power in primordial perturbations increases in proportion to the Hubble parameter squared; the faster the expansion, the more quickly quantum fluctuations are stretched into "classical" perturbations. Since the power of primordial perturbations increases with the Hubble parameter, squared, and since in our scenario the space-time is expanding most slowly in the preferred direction, we might expect that the power of perturbations with wave vectors parallel to the preferred direction will

be smaller than the power of perturbations with wave vectors in any other direction. We predict that, generically, models in which a preferred direction expands more rapidly/slowly than other directions will lead to positive/negative values of g_*.

The limit $|g_*| < 0.3$ translates into a limit on the average value of $\frac{\hat{\rho}_A}{\epsilon}$ during inflation (after horizon-crossing) for modes of astrophysical interest:

$$\frac{\hat{\rho}_A}{\epsilon}\Big|_{\text{average after horizon crossing}} < \frac{3}{160\,(60)^2}. \tag{2.112}$$

Since $\hat{\rho}_A$ is assumed to be essentially constant during inflation (as is $\hat{\rho}_\phi$), the limit can be written,

$$\frac{\hat{\rho}_A}{\hat{\rho}_\phi \epsilon}\Big|_{\text{average after horizon crossing}} \lesssim 10^{-6}. \tag{2.113}$$

The measurement of g_* puts a very stringent constraint on the ratio of vector field energy density to the inflaton energy density. At the same time, we see that even a very small $U(1)$ gauge field energy density during inflation could lead to a significant direction-dependent effect on the curvature perturbation power spectrum.

Supposing that $\hat{\rho}_A \ll \epsilon$, as we've just seen must be the case in order to comply with observation, the ratio of the gravitational wave power spectrum (P_T) to the scalar power spectrum (P_S) is approximately[16,17]

$$\frac{P_T}{P_S} = 4\frac{P_{E^+} + P_{E^\times}}{P_r} \approx \frac{8P_{\hat{h}^\times}}{P_{\hat{r}}}\left(\frac{\kappa^2 z^2}{a^2}\right) \approx 16\epsilon \tag{2.114}$$

This fact, in conjuction with (2.80) and (2.111), leads to the prediction

$$\frac{g_{*\text{grav}}}{g_*} \approx \frac{1}{64}\frac{P_T}{P_S}. \tag{2.115}$$

[16]In the last equality we used equations (2.16) and (2.37), given that $\hat{\rho}_A$ must be small compared to $\kappa^2 z^2/a^2$.

[17]What are identified as tensor perturbations are the amplitudes of the transverse, traceless (TT) part of $\delta g_{ij}/a^2$. We defined $\delta g_{ij,TT}/a^2 = 2E_{ij}$, thus the extra factor of 4.

The direction-dependent effects of a small persistent anisotropy during inflation on the tensor power spectrum are suppressed with respect to the direction-dependent effects on the scalar power spectrum by a number of order the tensor-to-scalar ratio. This is a consistency condition for the model, given the constraint from observation, $\hat{\rho}_A \ll \epsilon$.

2.6 Conclusions

In this paper, we considered gauge-invariant perturbations in a class of models with a persistent background anisotropy. After determining the quadratic action in terms of the dynamical fields, we computed the dominant direction-dependent effects of the background anisotropy on primordial power spectra.

We showed that even a very small persistent anisotropy (with the anisotropy parameter much smaller than the slow-roll parameter ϵ) can give rise to a dramatic direction-dependent effect on the primordial power spectra of dynamical fields. In an anisotropic background, the coupling between what reduce to the spin-1 and the spin-0 and spin-2 degrees of freedom in the isotropic case is extremely important. We showed that such couplings give rise to the dominant direction-dependent contributions to the primordial power spectra of tensor and scalar perturbations.

There has been a fair amount of work on vector fields with time-dependent couplings that are put in by hand, assuming exponential expansion. We found that the amount of anisotropy in power spectra are quite sensitive to the details of how nonexponential the expansion is, and how long the expansion lasts. Perhaps this sensitivity is unsurprising in light of the no-hair theorem.

We found that for a given scale $|\vec{k}|$, the curvature power, $P(\vec{k})$, is minimized when $\vec{k}$ points along the preferred direction.[18] We attribute this feature to the fact that, in the class of models we considered, the preferred direction is expanding more slowly

[18] In other words, we found that g_* is negative.

than other directions.

We showed that anisotropic effects are more pronounced in the scalar power spectrum than in the tensor power spectra. In fact, we showed that the direction-dependent effects on the tensor power spectrum are suppressed with respect to the direction-dependent effects on the scalar power spectrum by a number of order the tensor-to-scalar ratio. A priori one might have expected that the tensor power spectra and the scalar power spectrum would develop fractional direction dependence of the same magnitude. We find that this is not the case.

Finally, upon examination of the quadratic action for all dynamical degrees of freedom, we find no indication of instabilities in this model. This should not be surprising since the matter stress-energy satisfies the dominant energy condition.

We did not calculate the cross correlation between tensor and scalar perturbations. But one can see from the form of the quadratic action[19] that such a nonzero, direction-dependent correlation should exist. The cross-correlation effect will be small compared to the direction-dependent effect on the curvature power spectrum, but it could be interesting.

[19]See equations (2.84) through (2.88).

Chapter 3

Dark Matter, Baryon Asymmetry, and Spontaneous B and L Breaking

We investigate the dark matter and the cosmological baryon asymmetry in a simple theory where baryon (B) and lepton (L) number are local gauge symmetries that are spontaneously broken. In this model, the cold dark matter candidate is the lightest new field with baryon number, and its stability is an automatic consequence of the gauge symmetry. Dark matter annihilation is either through a leptophobic gauge boson whose mass must be below a TeV or through the Higgs boson. Since the mass of the leptophobic gauge boson has to be below the TeV scale one finds that in the first scenario there is a lower bound on the elastic cross section of about 5×10^{-46} cm^2. Even though baryon number is gauged and not spontaneously broken until the weak scale, a cosmologically acceptable baryon excess is possible. There can be a tension between achieving both the measured baryon excess and the dark matter density.

The contents of this chapter were written in collaboration with Pavel F. Perez and Mark B. Wise and have been published in [2].

3.1 Introduction

In the LHC era, we hope to either verify the standard model or discover the theory that describes the physics of the weak scale. One of the open issues in the standard model (SM) is the origin of the accidental global symmetries, $U(1)_B$ and $U(1)_L$, where B stands for baryon number and L for the total lepton number. At the non-

renormalizable level in the SM one can find operators that violate baryon number and lepton number. For example, $QQQl/\Lambda_B^2$ and $llHH/\Lambda_L$, where Λ_B and Λ_L are the scales where B and L are respectively broken [36]. Since the $QQQl/\Lambda_B^2$ operator gives rise to proton decay [37] the cutoff of the theory has to be very large, $\Lambda_B > 10^{15}$ GeV. There is no other reason that the cutoff of the SM has to be that large, and so it is worth thinking about the possibility that both B and L are local gauge symmetries that are spontaneously broken [38] at a much lower scale (e.g., the weak scale) and it is these gauge symmetries that prevent proton decay.

Recently, two simple models (denoted model (1) and model (2)) where B and L are local gauge symmetries have been proposed [38]. In these models all anomalies are cancelled by adding a single new fermionic generation. One of the theories (model (1)) has an interesting realization of the seesaw mechanism [39, 40, 41] for neutrino masses and they both have a natural suppression of tree-level flavor changing neutral currents in the quark and leptonic sectors due to the gauge symmetries and particle content. In model (2), the neutrinos have Dirac masses. In addition, for model (2), the lightest new field with baryon number is a candidate for the cold dark matter and its stability is an automatic consequence of the gauge symmetry. It has been shown in Ref. [38] that B and L can be broken at the weak scale and one does not generate dangerous operators mediating proton decay. We show how a dark matter candidate can arise in model (1).

In this chapter we investigate the properties of the cold dark matter candidates in the models proposed in Ref. [38] and study the implications of spontaneous B and L breaking at the weak scale for the baryon asymmetry in the Universe. In model (2), the dark matter candidate, X, which has baryon number $-2/3$ can either annihilate through the leptophobic Z_B present in the theory or through the Higgs boson. We study the constraints from the relic density and the predictions for the elastic cross section relevant for direct detection experiments. We discuss the implications of the gauging of B and L for baryogenesis. In model (2), there is a potential conflict between the measured baryon excess and dark matter density.

For model (1), we discuss the generation of a baryon excess. We introduce a limit

of the theory where L is broken at a high scale but B is spontaneously broken at the weak scale. In this limit standard leptogenesis plus a primordial excess in the field responsible for baryon number breaking can give rise to an acceptable baryon excess and dark matter density even though the baryon number gauge symmetry is not broken until the weak scale.

This chapter is organized as follows: In Section 3.2 we discuss the main features of the model. In Section 3.3 we discuss, for model (2), the properties of the dark matter candidate in the theory, constraints from the relic density and the predictions for the elastic cross section relevant for direct detection experiments. The properties of the dark matter candidate in model (1) are similar to cases already discussed in the literature (see for example [42] and [43]). In Section 3.4 we discuss the implications of the breaking of B and L at the weak scale for baryogenesis. We summarize the main results in Section 3.5.

3.2 Spontaneous B and L Breaking

The theory proposed in Ref. [38] is based on the gauge group

$$SU(3)_C \bigotimes SU(2)_L \bigotimes U(1)_Y \bigotimes U(1)_B \bigotimes U(1)_L.$$

To fix notation, the particle content of the SM is summarized in Table 3.1. The superscript index (i) on standard model fermion fields labels the generation. We have added three generations of right-handed neutrinos to the minimal standard model.

When gauging B and L, one can have two different scenarios:

3.2.1 Model (1)

In this model the baryonic anomalies are cancelled by adding the new quarks $Q_L^{'}$, $u_R^{'}$ and $d_R^{'}$ that transform under the SM gauge group in the same way as the SM quarks but have baryon number $B = -1$. At the same time the leptonic anomalies are cancelled if one adds new leptons $l_L^{'}$, $\nu_R^{'}$ and $e_R^{'}$ with lepton number, $L = -3$.

Table 3.1: Standard model particle content

Field	$SU(3)$	$SU(2)$	$U(1)_Y$	$U(1)_B$	$U(1)_L$
$Q_L^{(i)} = \begin{pmatrix} u_L^{(i)} \\ d_L^{(i)} \end{pmatrix}$	**3**	**2**	$\frac{1}{6}$	$\frac{1}{3}$	0
$u_R^{(i)}$	**3**	**1**	$\frac{2}{3}$	$\frac{1}{3}$	0
$d_R^{(i)}$	**3**	**1**	$-\frac{1}{3}$	$\frac{1}{3}$	0
$l_L^{(i)} = \begin{pmatrix} \nu_L^{(i)} \\ e_L^{(i)} \end{pmatrix}$	**1**	**2**	$-\frac{1}{2}$	0	1
$\nu_R^{(i)}$	**1**	**1**	0	0	1
$e_R^{(i)}$	**1**	**1**	-1	0	1
$H = \begin{pmatrix} H^+ \\ H^0 \end{pmatrix}$	**1**	**2**	$\frac{1}{2}$	0	0

All anomalies in the SM gauge group are cancelled since we have added one full new family. The particle content of model (1), beyond that of the SM, is summarized in the Table 3.2.

Let us discuss the main features of this scenario.

- *Quark Sector*

  In this model the masses for the new quarks are generated through the terms,

$$-\Delta\mathcal{L}^{(1)}_{q'\text{mass}} \;=\; Y'_U\;\overline{Q'_L}\;\tilde{H}\;u'_R \;+\; Y'_D\;\overline{Q'_L}\;H\;d'_R \;+\; \text{h.c.}. \tag{3.1}$$

  Here $\tilde{H} = i\sigma_2 H^*$. In order to avoid a stable colored quark, the scalar doublet ϕ has been added to mediate the decays of the fourth generation of quarks. The following terms occur in the Lagrange density

$$-\Delta\mathcal{L}^{(1)}_{DM} \;=\; Y_1\;\overline{Q'_L}\;\tilde{\phi}\;u_R \;+\; Y_2\;\overline{Q_L}\;\phi\;d'_R \;+\; \text{h.c.}. \tag{3.2}$$

  Here flavor indices on the Yukawa couplings Y_i, and the standard model quark

Table 3.2: Particle content beyond the SM in model (1)

Field	$SU(3)$	$SU(2)$	$U(1)_Y$	$U(1)_B$	$U(1)_L$
$Q'_L = \begin{pmatrix} u'_L \\ d'_L \end{pmatrix}$	**3**	**2**	$\frac{1}{6}$	-1	0
u'_R	**3**	**1**	$\frac{2}{3}$	-1	0
d'_R	**3**	**1**	$-\frac{1}{3}$	-1	0
$l'_L = \begin{pmatrix} \nu'_L \\ e'_L \end{pmatrix}$	**1**	**2**	$-\frac{1}{2}$	0	-3
ν'_R	**1**	**1**	0	0	-3
e'_R	**1**	**1**	-1	0	-3
S_B	**1**	**1**	0	$-\frac{8}{3}$	0
S_L	**1**	**1**	0	0	2
S	**1**	**1**	0	$-\frac{4}{3}$	0
$\phi = \begin{pmatrix} \phi^+ \\ \phi^0_R + i\phi^0_I \end{pmatrix}$	**1**	**2**	$\frac{1}{2}$	$\frac{4}{3}$	0

fields have been suppressed. The field ϕ does not get a vacuum expectation value (VEV), and so there is no mass mixing between the new exotic generation of quarks and their SM counterparts. When the real or imaginary component of ϕ is the lightest new particle with baryon number, it is stable. The field ϕ has flavor-changing couplings that cause transitions between quarks with baryon number -1 and the usual quarks with baryon number 1/3. However, since there is no mass mixing between these two types of quarks, integrating out the ϕ does not generate any tree-level flavor changing neutral currents for the ordinary quarks.

These effects first occur at one loop. For example, there are one loop box diagrams (see Fig. 3.1) that give a contribution to $K - \bar{K}$ mixing.

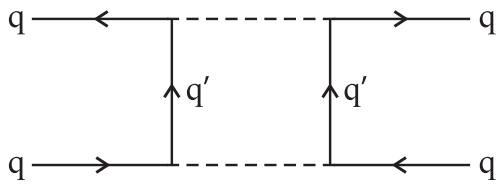

Figure 3.1: Box diagram leading to a contribution to $K - \bar{K}$ mixing.

We estimate this mixing to be of order

$$\Delta m_K \sim \left(\frac{f_K^2 m_K Y^4}{16\pi^2 M^2} \right), \tag{3.3}$$

where Y^4 is a shorthand for something quartic in the Yukawa couplings Y_1, Y_2. For $M = 400$ GeV and Yukawas of about 10^{-2}, this mass difference is on the order of 10^{-15} MeV which is much smaller than the measured value. A detailed study of the model's flavor sector is beyond the scope of this work and will be reserved for a future publication.

- *Leptonic Sector*

  The interactions that generate masses for the new charged leptons are

$$-\Delta\mathcal{L}_l^{(1)} \;=\; Y_E^{'}\, \overline{l_L^{'}}\, H\, e_R^{'} \;+\; \text{h.c.}, \tag{3.4}$$

  while for the neutrinos they are

$$\begin{aligned} -\Delta\mathcal{L}_\nu^{(1)} \;&=\; Y_\nu\, lH\nu^C \;+\; Y_\nu^{'}\, l^{'} HN \;+ \\ &+\; \frac{\lambda_a}{2}\, \nu^C\, S_L\, \nu^C \;+\; \lambda_b\, \nu^C\, S_L^\dagger\, N \;+\; \text{h.c.}, \end{aligned} \tag{3.5}$$

  where $S_L \sim (1, 1, 0, 0, 2)$ is the Higgs that breaks $U(1)_L$, generating masses for the right-handed neutrinos and the quark-phobic $Z_L^{'}$. We introduce the notation $\nu^C = (\nu_R)^C$ and $N = (\nu_R^{'})^C$. After symmetry breaking the mass matrix for neutrinos in the left-handed basis, $(\nu, \nu^{'}, N, \nu^C)$, is given by the eight by eight

matrix,

$$\mathcal{M}_N = \begin{pmatrix} 0 & 0 & 0 & M_D \\ 0 & 0 & M_D^{'} & 0 \\ 0 & (M_D^{'})^T & 0 & M_b \\ M_D^T & 0 & M_b^T & M_a \end{pmatrix}. \tag{3.6}$$

Here, $M_D = Y_\nu v_H/\sqrt{2}$ and $M_a = \lambda_a v_L/\sqrt{2}$ are 3×3 matrices, $M_b = \lambda_b v_L^*/\sqrt{2}$ is a 1×3 matrix, $M_D^{'} = Y_\nu^{'} v_H/\sqrt{2}$ is a number and $\langle S_L\rangle = v_L/\sqrt{2}$. Let us assume that the three right-handed neutrinos ν^C are the heaviest. Then, integrating them out generates the following mass matrix for the three light neutrinos:

$$\mathcal{M}_\nu = M_D\ M_a^{-1}\ M_D^T. \tag{3.7}$$

In addition, a Majorana mass M' for the fourth-generation right-handed neutrino N,

$$M^{'} = M_b M_a^{-1} M_b^T, \tag{3.8}$$

is generated. Furthermore, suppose that $M^{'} << M_D^{'}$, then the new fourth generation neutrinos $\nu^{'}$ and N are quasi-Dirac with a mass equal to $M_D^{'}$. Of course we need this mass to be greater than $M_Z/2$ to be consistent with the measured Z-boson width. In this model we have a consistent mechanism for neutrino masses which is a particular combination of Type I seesaw.

- *Higgs Sector*

  The minimal Higgs sector needed to have a realistic theory where B and L are both gauged, and have a DM candidate is composed of the SM Higgs, H, S_L, $S \sim (1,1,0,-4/3,0)$, S_B and ϕ. S_B and S_L are the scalars field whose vacuum expectation values break $U(1)_B$ and $U(1)_L$, respectively, generating masses for the gauge bosons coupling to baryon number and lepton number. Here one introduces the scalar field S in order to have a viable cold dark matter

candidate. In this case the scalar potential of the model must contain the terms

$$\mu_1 \ \left(H^\dagger \phi\right) \ S \ + \ \mu_2 \ S_B^\dagger \ S^2 \ + \ \text{h.c.}, \tag{3.9}$$

in order to generate the effective interaction: $c\ (H^\dagger\phi)^2 S_B \ +$ h.c., which breaks the degeneration between the ϕ_R^0 and ϕ_I^0. Here S does not get the VEV. Then, one of them can be a dark matter candidate and the mass splitting is given by

$$M^2_{\phi_R^0} - M^2_{\phi_I^0} = \sqrt{2}\frac{v_H^2 v_B \mu_1^2 \mu_2}{M_S^4}. \tag{3.10}$$

By adjusting the phases of the fields S and ϕ, the parameters $\mu_{1,2}$ can be made real and positive. In this case, the imaginary part of the neutral component of ϕ, denoted ϕ_I^0 is the dark matter candidate. Notice, that this DM scenario is quite similar to the case of the Inert Higgs Doublet Model since we do not have annihilation through the Z_B in the non-degerate case. It is well-known that if the real and imaginary parts are degenerate in mass one cannot satisfy the bounds coming from direct detection, therefore one needs a mass splitting. This dark matter candidate is very similar to that of the Inert Doublet Model (see, for example, [42] and [43]).

Before concluding the discussion of model (1) one should mention that in this model local $U(1)_B$ and $U(1)_L$ are broken by the Higgs mechanism, as explained before, and one gets that in the quark sector a global symmetry (baryonic) is conserved, while in the leptonic sector the total lepton number is broken.

3.2.2 Model (2)

In this model, the baryonic anomalies are cancelled by adding the new quarks Q'_R, u'_L and d'_L which transform under the SM gauge group the same way as the SM quarks but have opposite chirality and baryon number $B = 1$. At the same time the leptonic anomalies are cancelled if one adds new leptons l'_R, ν'_L and e'_L with opposite chirality of their SM counterparts and with lepton number, $L = 3$. The particle content of

model (2), beyond that of the SM, is summarized in the Table 3.3.

Table 3.3: Particle content beyond the SM in model (2)

Field	$SU(3)$	$SU(2)$	$U(1)_Y$	$U(1)_B$	$U(1)_L$
$Q'_R = \begin{pmatrix} u'_R \\ d'_R \end{pmatrix}$	**3**	**2**	$\frac{1}{6}$	1	0
u'_L	**3**	**1**	$\frac{2}{3}$	1	0
d'_L	**3**	**1**	$-\frac{1}{3}$	1	0
$l'_R = \begin{pmatrix} \nu'_R \\ e'_R \end{pmatrix}$	**1**	**2**	$-\frac{1}{2}$	0	3
ν'_L	**1**	**1**	0	0	3
e'_L	**1**	**1**	-1	0	3
S_B	**1**	**1**	0	n_B	0
S_L	**1**	**1**	0	0	2
S'_L	**1**	**1**	0	0	n_L
X	**1**	**1**	0	$-\frac{2}{3}$	0

- *Quark Sector*

  In this model the masses for the new quarks are generated through the terms,

$$-\Delta\mathcal{L}^{(2)}_{q'\text{mass}} \;=\; Y'_U\;\overline{Q'_R}\;\tilde{H}\;u'_L \;+\; Y'_D\;\overline{Q'_R}\;H\;d'_L \;+\; \text{h.c.}. \tag{3.11}$$

  As in the previous model, one has to avoid a stable colored quark. For this reason, we add the scalar field X to mediate the decays of the fourth generation of quarks. The following terms occur in the Lagrange density

$$\begin{aligned} -\Delta\mathcal{L}^{(2)}_{DM} \;&=\; \lambda_Q\;X\;\overline{Q_L}\;Q'_R \;+\; \lambda_U\;X\;\overline{u_R}\;u'_L \\ &+\quad \lambda_D\;X\;\overline{d_R}\;d'_L \;+\; \text{h.c.}. \end{aligned} \tag{3.12}$$

Here flavor indices on the Yukawa couplings Y, λ and the standard model quark fields have been suppressed. The field X does not get a vacuum expectation value (VEV) and so there is no mass mixing between the new exotic generation of quarks and their SM counterparts. When X is the lightest new particle with baryon number, it is stable. This occurs because the model has a global $U(1)$ symmetry where the Q'_R, u'_L, d'_L and X get multiplied by a phase. This $U(1)$ symmetry is an automatic consequence of the gauge symmetry and the particle content. Notice that the new fermions have $V + A$ interactions with the W-bosons.

The field X has flavor-changing couplings that cause transitions between quarks with baryon number 1 and the usual quarks with baryon number 1/3. However, since there is no mass mixing between these two types of quarks, integrating out the X does not generate any tree-level flavor-changing neutral currents for the ordinary quarks. Those first occur at the one loop level (see the discussion concerning such flavor changing effects in model (1)).

- *Leptonic Sector*

The interactions for the new leptons are

$$\begin{aligned} -\Delta\mathcal{L}_l^{(2)} &= Y'_E\ \overline{l'_R}\ H\ e'_L\ +\ \lambda_e\ \bar{e}_R\ S_L^{\dagger} e'_L\ + \\ &+\ Y_\nu\ \overline{l_L}\ \tilde{H}\ \nu_R\ +\ Y'_\nu\ \overline{l'_R}\ \tilde{H}\ \nu'_L\ +\ \frac{\lambda_a}{2}\ \nu_R^T\ C\ S_L^{\dagger}\ \nu_R \\ &+\ \ \lambda_b\ \overline{\nu_R}\ S_L^{\dagger}\ \nu'_L\ +\ \lambda_l\ \overline{l'_R}\ S_L\ l_L\ + \text{h.c.}. \end{aligned} \tag{3.13}$$

The neutrinos are Dirac fermions with masses proportional to the vacuum expectation value of the SM Higgs boson. Here S_L must be introduced to evade the experimental constraints on heavy stable Dirac neutrino from dark matter direct detection and collider bounds. In order to avoid flavor violation in the leptonic sector we assume that S_L does not get a vacuum expectation value.

- *Higgs Sector*

  The minimal Higgs sector needed to have a realistic theory where B and L are both gauged, and have a DM candidate is composed of the SM Higgs, H, S_L, S'_L, S_B and X. S_B and S'_L are the scalars field whose vacuum expectation values break $U(1)_B$ and $U(1)_L$, respectively, generating masses for the gauge bosons coupling to baryon number and lepton number. The scalar potential of the model is given by

$$V_{BL}^{(2)} = \sum_{\Phi_i=H,S_L,S'_L,S_B,X} M_{\Phi_i}^2 \Phi_i^\dagger \Phi_i + \sum_{\Phi_i\Phi_j} \lambda_{\Phi_i\Phi_j} \left(\Phi_i^\dagger \Phi_i\right)\left(\Phi_j^\dagger \Phi_j\right). \quad (3.14)$$

  In this theory one has five physical CP-even neutral Higgses $\{H^0, S_L^0, S_L^{\prime\,0}, S_B^0, X_R^0\}$, and two CP-odd neutral Higgses X_I^0 and S_I^0. Here, X_R^0 and X_I^0 have the same mass and they are cold dark matter candidates.

In this model one should notice that the local symmetries $U(1)_B$ and $U(1)_L$ are broken, and after symmetry breaking one has a baryonic and leptonic global symmetries. Therefore, the proton is stable and the neutrinos are Dirac fermions.

These are the main features of the two models that are needed to investigate the implications and/or constraints coming from cosmological observations.

3.3 X as a Candidate for the Cold Dark Matter in Model (2)

As we have mentioned before, the lightest new field with baryon number, X, is a cold dark matter candidate in model (2). In this section we study in detail the possible cosmological constraints and the predictions for elastic dark matter-nucleon cross section relevant for direct searches of dark matter. Some of this material is standard and has been discussed in the literature in the context of other dark matter candidates; however, we include it for completeness.

3.3.1 Constraints from the Relic Density

There are two main scenarios for the study of the relic density. In the first case X annihilates through the leptophobic Z_B gauge boson, while in the second case X annihilates through the SM Higgs. The properties of a SM singlet scalar dark matter candidate that annihilates through the Higgs have been investigated in many previous studies [44, 45, 46, 47, 48]; however, the case of annihilation through the Z_B is more specific to the model we are currently examining.

- $XX^\dagger \to Z_B^* \to q\bar{q}$:

  We begin by studying the case where X annihilation through the baryon number gauge boson Z_B, i.e., $XX^\dagger \to Z_B^* \to q\bar{q}$, dominates the annihilation cross section. Here we include all the quarks that are kinematically allowed. Of course the heavy fourth-generation quarks must be heavier than the X so that they do not occur in the final state. This also limits the upper range of X masses since the theory is not perturbatively unitary if the fourth-generation Yukawa's are too large.

  The annihilation cross section through intermediate Z_B in the non-relativistic limit with a quark-antiquark pair in the final state is given by

$$\sigma_{Z_B} v = \frac{2}{81\pi}\frac{g_B^4}{M_{Z_B}^4}\frac{M_X^2}{\left(1-4\frac{M_X^2}{M_{Z_B}^2}\right)^2+\frac{\Gamma_{Z_B}^2}{M_{Z_B}^2}}\frac{v^2}{} \times \sum_q \Theta\left(1-\frac{m_q}{M_X}\right)\left(1+\left(\frac{m_q^2}{2M_X^2}\right)\right)\sqrt{1-\frac{m_q^2}{M_X^2}} \quad (3.15)$$

  where Θ is the unit step function and Γ_{Z_B} is the width of the Z_B. The width of the leptophobic gauge boson is given by

$$\Gamma_{Z_B} = \sum_q \frac{g_B^2 M_{Z_B}}{36\pi}\left(1-2\frac{m_q^2}{M_{Z_B}^2}\right)\left(1-4\frac{m_q^2}{M_{Z_B}^2}\right)^{1/2}\Theta\left(1-4\frac{m_q^2}{M_{Z_B}^2}\right). \quad (3.16)$$

- $XX^\dagger \to H^* \to SMSM$:

  In the case where X annihilates into massive SM fields, through an intermediate H, we find that the annihilation cross section (in the non-relativistic limit) is

$$\begin{aligned}
\sigma_H v \;&= \sum_f \left(\frac{\lambda_1^2 N_c^f}{4\pi M_H^2}\right)\left(\frac{m_f}{M_H}\right)^2 \frac{\Theta\left(1-\frac{m_f}{M_X}\right)\left(1-\left(\frac{m_f}{M_X}\right)^2\right)^{3/2}}{\left(1-4\frac{M_X^2}{M_H^2}\right)^2+\frac{\Gamma_H^2}{M_H^2}} \\
&+ \left(\frac{\lambda_1^2}{64\pi M_X^2}\right)\left(1-\left(\frac{M_H}{M_X}\right)^2\right)^{1/2}\Theta\left(1-\frac{M_H}{M_X}\right)\left|1+\frac{3}{\left(\frac{4M_X^2}{M_H^2}-1\right)+i\frac{\Gamma_H}{M_H}}\right|^2 \\
&+ \left(\frac{\lambda_1^2}{2\pi M_H^2}\right)\frac{\Theta\left(1-\frac{M_W}{M_X}\right)\left(1-\left(\frac{M_W}{M_X}\right)^2\right)^{1/2}}{\left(1-4\frac{M_X^2}{M_H^2}\right)^2+\frac{\Gamma_H^2}{M_H^2}}\left(1+\frac{3M_W^4}{4M_X^4}-\frac{M_W^2}{M_X^2}\right) \\
&+ \left(\frac{\lambda_1^2}{4\pi M_H^2}\right)\frac{\Theta\left(1-\frac{M_Z}{M_X}\right)\left(1-\left(\frac{M_Z}{M_X}\right)^2\right)^{1/2}}{\left(1-4\frac{M_X^2}{M_H^2}\right)^2+\frac{\Gamma_H^2}{M_H^2}}\left(1+\frac{3M_Z^4}{4M_X^4}-\frac{M_Z^2}{M_X^2}\right), \qquad (3.17)
\end{aligned}$$

  where N_c^f is the number of colors of the particular species of fermion, $M_{W,Z}$ are the W and Z boson masses. Included in the width, where kinematically allowed, is the invisible decay to dark matter. We have ignored corrections to this formula that come from annihilation into two standard model massless gauge bosons. For previous studies of this type of scenario see [44, 45, 46, 47, 48].

Using these results, we are ready to compute the approximate freeze-out temperature $x_f = M_X/T_f$ assuming that one of the two annihilation channels dominates the annihilation of the dark matter. Writing the thermally averaged annihilation cross section as $\langle\sigma v\rangle = \sigma_0 (T/M_X)^n$, then the freeze-out temperature is given by,

$$\begin{aligned}
x_f \;&= \ln\left[0.038(n+1)\left(\frac{g}{\sqrt{g_*}}\right)\; M_{Pl} M_X \sigma_0\right] \\
&- \left(n+\frac{1}{2}\right)\ln\left[\ln\left[0.038(n+1)\left(\frac{g}{\sqrt{g_*}}\right)\; M_{Pl}\; M_X\sigma_0\right]\right], \qquad (3.18)
\end{aligned}$$

where M_{Pl} is the Planck mass, g is the number of internal degrees of freedom and g_* is the effective number of relativistic degrees of freedom evaluated around the freeze-out temperature.[1]

The present day energy density of the relic dark matter particles X is given by

$$\Omega_X h^2 = \frac{1.07 \times 10^9}{\text{GeV}} \left(\frac{(n+1)x_f^{n+1}}{\sqrt{g_*}\sigma_0 M_{Pl}} \right) \tag{3.19}$$

where we have used the fact that $g_{*,S}(T) = g_*(T)$ in our case (all particle species have a common temperature). The WMAP team recently gave a seven-year fit [7] and found the present-day dark matter energy density to be $\Omega_{DM}h^2 = 0.1109 \pm 0.0056$.

Using the experimental constraints on the relic density of the cold dark matter and the annihilation cross sections calculated above, we plot in Figure 3.2 (left panel) the allowed values for the gauge coupling g_B and the mass of X when the annihilation occurs through an intermediate Z_B boson. Here we use as input parameter the mass of Z_B, $M_{Z_B} = 500$ GeV. In order to understand the behavior of the numerical solutions close to resonance, we show the results in Figure 3.2 (right panel), where the mass region $M_X \approx M_{Z_B}/2$ is focussed on. In the second scenario when the annihilation takes place through the SM Higgs boson one can display similar results. Assuming only annihilation at tree level into SM fermions and gauge bosons for simplicity, we show in Figure 3.3 the allowed parameter space after imposing the constraints on the relic density when $M_H = 120$ GeV.

It is important to note that using the perturbative limit on the Yukawa couplings for the new fermions, $|Y'| < 2\sqrt{\pi}$, the masses of the new quarks, $M_{q'} = Y' v_H/\sqrt{2}$, are smaller than 500 GeV (since the VEV of the SM Higgs, v_H, is 246 GeV). In order to achieve the right value for the relic density, M_X has to be close to the $M_{Z_B}/2$. Hence, in the first scenario M_{Z_B} must be below a TeV if X annihilates primarily through the Z_B and is the dark matter. This is an acceptable kinematic range for discovery at the LHC. Next, we study the constraints coming from the direct detection experiments

[1] See, for example, [4].

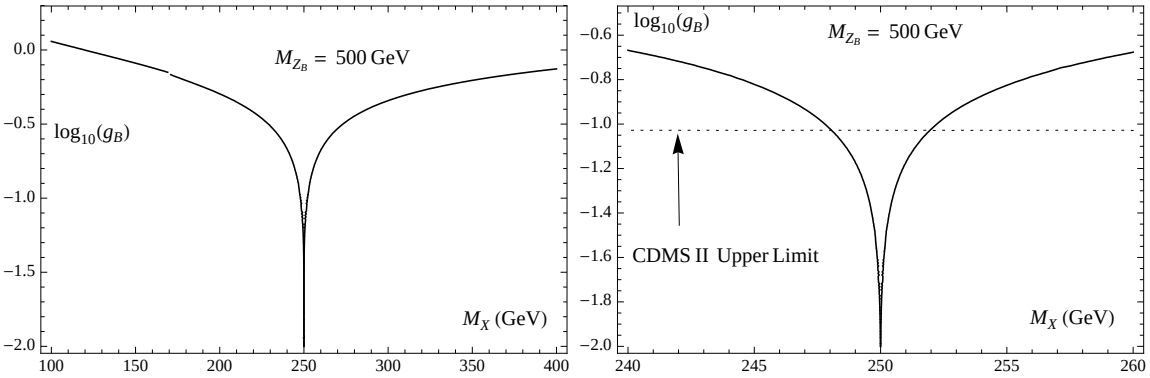

Figure 3.2: In these figures, we plot the values of the (logarithm of the) coupling g_B and dark matter mass M_X that lead to the value of the dark matter relic abundance measured by WMAP assuming annihilation through intermediate Z_B is dominant. We use $M_{Z_B} = 500$ GeV for these plots. The plot on the right is an enlarged version of the left plot around the region near the resonance. For dark matter masses around 250 GeV, CDMS II excludes dark matter-nucleon elastic scattering cross sections larger than $6 \times 10^{-44}\text{cm}^2$. The region below the dashed line is allowed by CDMS II [49].

(which have already been used in the right panels of Figures 3.2 and 3.3).

A more precise calculation of the dark matter relic density is required when annihilation proceeds near resonance. This is because the expansion of the annihilation cross section in terms of a polynomial in the temperature breaks down near the resonance [50]. Generalizing Eq. (3.15) and Eq. (3.17) for general relative velocities, we determine the relic abundance near the resonance using the more precise calculation described below. The freeze-out temperature can be determined iteratively from the following equation,

$$x_f = \ln\left[\frac{0.038 g M_X M_{Pl} \langle\sigma v\rangle}{\sqrt{g_* x_f}}\right], \tag{3.20}$$

where the thermally averaged annihilation cross section is determined numerically by

$$\langle\sigma v\rangle = \frac{x^{3/2}}{2\pi^{1/2}} \int_0^\infty v^2 (\sigma v) e^{-xv^2/4} dv. \tag{3.21}$$

The relic density is then given by

$$\Omega h^2 = \frac{1.07 \times 10^9}{\text{GeV}} \left(\frac{1}{J\sqrt{g_*} M_{Pl}}\right), \tag{3.22}$$

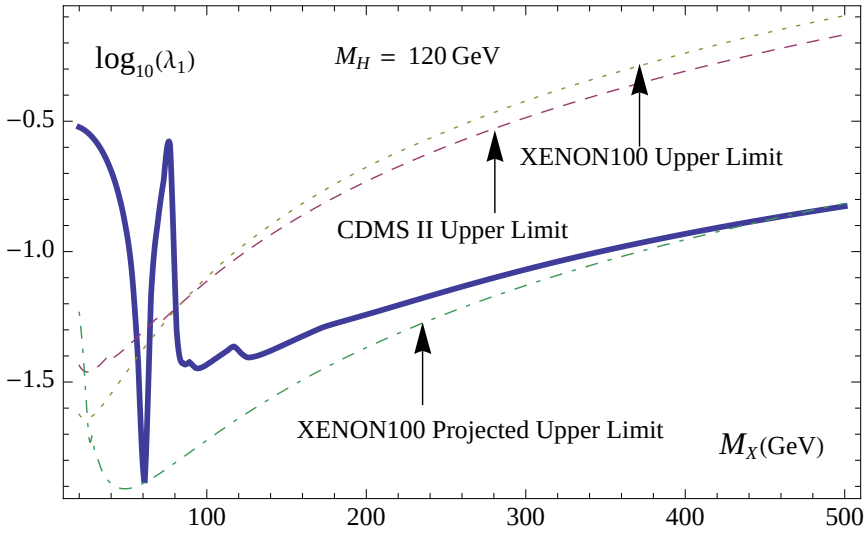

Figure 3.3: In these figures, we plot the values of the (logarithm of the) coupling λ_1 and dark matter mass M_X that lead to the value of the dark matter relic abundance measured by WMAP assuming annihilation through intermediate Higgs is dominant. We use $M_H = 120$ GeV for this plots.

where

$$J = \int_{x_f}^{\infty} \frac{\langle \sigma v \rangle}{x^2} dx, \tag{3.23}$$

takes into account the annihilations that continue to occur, but become less effective, after the freeze-out temperature.

In Fig. 3.4, we show the contour that leads to the observed relic abundance of dark matter assuming annihilation through an intermediate Z_B with mass of 500 GeV is dominant. After comparing this plot to the right panel in Fig. 3.2, it is clear that one needs to take into account the precise thermal averaging when annihilation proceeds near resonance. The thermal averaging works to widen the contour and move the minimum below $M_{Z_B}/2$. This is because at finite temperatures the effective mass of the dark matter candidate is higher and therefore the minimum of the contour is shifted to lower dark matter masses.

Similarly, in Fig. 3.5, we show the contour that leads to the observed relic abundance of dark matter assuming annihilation through an intermediate Higgs with mass of 120 GeV is dominant.

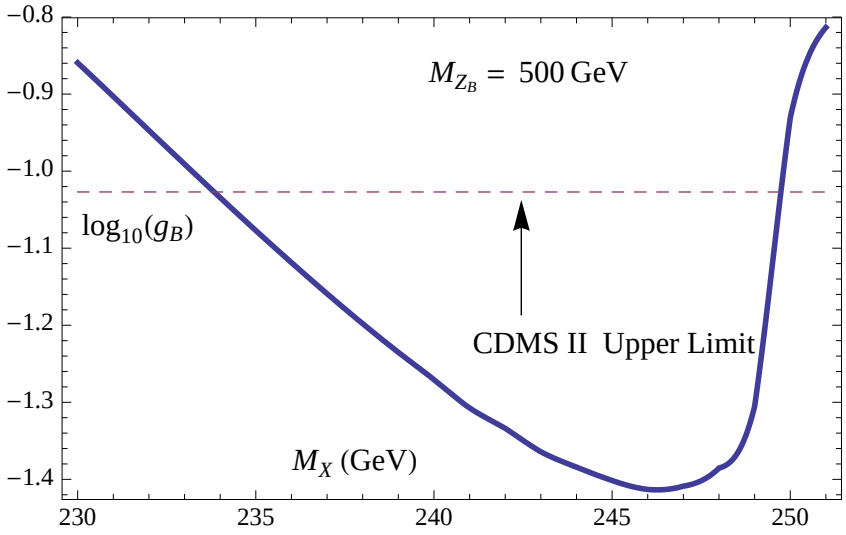

Figure 3.4: In this figure, we plot the results of the numerical relic abundance calculation with the correct thermal averaging around the resonance. The contour plotted shows the values of the (logarithm of the) coupling g_B and dark matter mass M_X that lead to the value of the dark matter relic abundance measured by WMAP assuming annihilation through an intermediate Z_B is dominant. We use $M_{Z_B} = 500$ GeV for this plot.

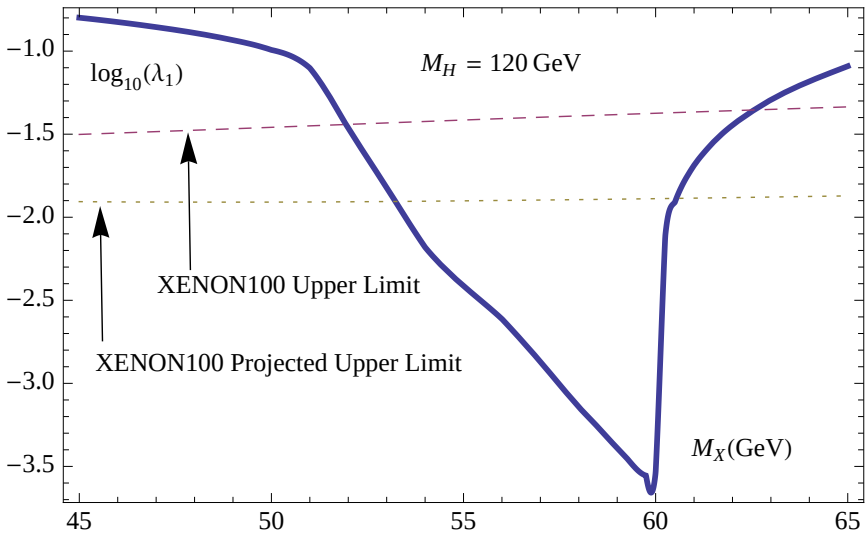

Figure 3.5: In this figure, we plot the results of the numerical relic abundance calculation with the correct thermal averaging around the resonance. The contour plotted shows the values of the (logarithm of the) coupling λ_1 and dark matter mass M_X that lead to the value of the dark matter relic abundance measured by WMAP assuming annihilation through an intermediate Higgs is dominant and taking $M_H = 120$ GeV.

3.3.2 Constraints from Direct Detection

In this section we present the cross sections for elastic scattering of our dark matter candidate off of nucleons. These cross sections are very tightly constrained by the Cryogenic Dark Matter Search (CDMS) for dark matter masses in above approximately 100 GeV and XENON100 for dark matter masses below approximately 100 GeV [49, 51].

In the first scenario discussed above we need the constraints coming from direct detection when the scattering is through the $U(1)_B$ gauge boson. In the non-relativistic limit, the cross section for elastic scattering of dark matter off of nucleons through an intermediate Z_B is given by

$$\sigma_{SI}^B = \frac{4g_B^4}{9\pi}\left(\frac{\mu^2}{M_{Z_B}^4}\right), \tag{3.24}$$

where $\mu = M_N M_X/(M_N + M_X)$ is the reduced mass of the dark matter-nucleon final state and M_N is the nucleon mass. Putting in the numbers, this cross section can be written as

$$\sigma_{SI}^B = (8.8 \times 10^{-40}\text{cm}^2) g_B^4 \left(\frac{500\text{ GeV}}{M_{Z_B}}\right)^4 \left(\frac{\mu}{1\text{ GeV}}\right)^2. \tag{3.25}$$

From the CDMS II upper limits on the spin-independent cross section in [49], one can conclude that if we want the correct relic abundance then 235 GeV $\lesssim M_X \lesssim$ 250 GeV and $g_B \lesssim 10^{-1}$, for $M_{Z_B} \approx 500$ GeV. For the relevant region of parameter space, see Figure 3.4.

If M_{Z_B} is near its 1 TeV upper bound, the direct detection limits on the coupling g_B are the weakest and the required range is $0.06 \lesssim g_B \lesssim 0.2$. Using the plot in Fig. 3.4 and Eq. (3.25), we set a lower limit on the dark matter-nucleon scattering cross section of about $\sigma_{SI}^B \gtrsim 5 \times 10^{-46}$ cm^2.

For the second case when the elastic scattering of the dark matter off of nucleons is via the Higgs exchange, we need the effective coupling of the Higgs to nucleons. For this purpose, we follow [52] and we find this effective coupling appropriate for at

rest nucleon matrix element to be

$$\mathcal{L} = -\frac{h}{v}\left(\sum_l m_l \bar{q}_l q_l + \sum_h m_h \bar{q}_h q_h\right) \to -\frac{h}{v}\left(\frac{10}{27} + \frac{17}{27}\hat{\chi}_+\right) M_N \left(\bar{p}p + \bar{n}n\right). \quad (3.26)$$

Using the leading order chiral perturbation theory result in the appendix of [52] and the $\Sigma_{\pi N}$ term from [53] we obtain $\hat{\chi}_+ = 0.55 \pm 0.18$ where the errors are indicative of a 30% violation of $SU(3)$ flavor symmetry. This value of $\hat{\chi}_+$ gives

$$\mathcal{L} = -\frac{h}{v}\left(0.72\right) M_N \left(\bar{p}p + \bar{n}n\right). \quad (3.27)$$

With the three generations of the SM, one would have expected a number $2/9 + 7/9(0.55) = 0.65$ instead of 0.72. This is consistent with the 0.56 ± 0.11 number quoted in references [54] and [55].

One can use this result to compute the elastic scattering cross section,

$$\sigma_{SI}^H = \frac{\lambda_1^2}{4\pi}\left(\frac{10}{27} + \frac{17}{27}\hat{\chi}_+\right)^2 \left(\frac{\mu^2 M_N^2}{M_X^2 M_H^4}\right). \quad (3.28)$$

Plugging in the numbers, this cross section can be written as (using $\hat{\chi}_+ = 0.55$)

$$\sigma_{SI}^H = (3.0 \times 10^{-41}\text{cm}^2)\lambda_1^2 \left(\frac{120\text{ GeV}}{M_H}\right)^4 \left(\frac{\mu}{1\text{ GeV}}\right)^2 \left(\frac{50\text{ GeV}}{M_X}\right)^2. \quad (3.29)$$

In order to satisfy the direct detection bounds from XENON100 [51] for elastic scattering of dark matter off of nucleons, 51 GeV $\lesssim M_X \lesssim$ 63 GeV with $\lambda_1 \lesssim 10^{-1.5}$, for a 120 GeV Higgs. This gives us a narrow region of parameter space that is not yet ruled out by the XENON100 experiment and that also leads to the correct dark matter relic abundance. See Figure 3.5 for a plot of the allowed region. For a 120 GeV Higgs, the dark matter-nucleon elastic cross section has a lower bound of about $\sigma_{SI}^H \gtrsim 10^{-48}$ cm^2.

One can see from Figure 3.3 that if XENON100 reaches its projected sensitivity without detecting DM, the scenario where annihilation proceeds through the Higgs will be all but ruled out. The only region that will be allowed from this future

experiment will be the region in Figure 3.5. For dark matter masses at the lower end of this region, the decay of the SM Higgs is dominated by the invisible decay into dark matter.

In a more generic context, this model is different from the literature in that the dark matter mass has an upper bound (since it facilitates the decay of the fourth generation quarks and these quarks should have mass below about 500 GeV if perturbative unitarity holds). Most models of scalar dark matter do not have an upper limit on the dark matter mass, and therefore a wider region of masses are allowed at the TeV scale.

We need to also consider the limits direct detection experiments place on dark matter scattering off of nucleons from the interactions $\lambda X \bar{q} q'$. To fix notation, the interactions in Eq. (3.12) are

$$\begin{aligned} -\Delta\mathcal{L}_{DM} &= \tilde{\lambda}_Q\ X\ \bar{u}\left(\frac{1+\gamma_5}{2}\right)u' \ +\ \tilde{\lambda}_U\ X\ \bar{u}\left(\frac{1-\gamma_5}{2}\right)u' \\ &+\ \lambda'_Q\ X\ \bar{d}\left(\frac{1+\gamma_5}{2}\right)d' \ +\ \lambda'_d\ X\ \bar{d}\left(\frac{1-\gamma_5}{2}\right)d' \ +\ \text{h.c.}, \end{aligned} \tag{3.30}$$

where $\{u, d\}$ ($\{u', d'\}$) are the Dirac spinors corresponding to the standard model (fourth-generation) quarks and $(\tilde{\lambda}_Q)_i = U^\dagger(u, L)_i{}^j(\lambda_Q)_j$ and $(\lambda'_Q)_i = U^\dagger(d, L)_i{}^j(\lambda_Q)_j$ are the coefficients in Eq. (3.12) after rotating to the mass eigenstate basis. We find the effective low energy interaction of the dark matter with the standard model quarks by integrating out the heavy fourth generation quarks. Then, the effective interactions for non-relativistic X is given by

$$\begin{aligned} -\mathcal{L}_{eff} &= \left(\frac{X^\dagger X M_X}{2M_{u'}^2}\right)\left(|(\tilde{\lambda}_Q)_i|^2 + |(\tilde{\lambda}_u)_i|^2\right)(u^\dagger)^i u_i \\ &+\ \left(\frac{X^\dagger X}{2M_{u'}}\right)\left((\tilde{\lambda}_Q)_i\ (\tilde{\lambda}_u^*)^i\ +\ (\tilde{\lambda}_Q^*)_i\ (\tilde{\lambda}_u)^i\right)\bar{u}^i u_i \\ &+\ \left(\frac{X^\dagger X M_X}{2M_{d'}^2}\right)\left(|(\lambda'_Q)_i|^2 + |(\lambda'_d)_i|^2\right)(d^\dagger)^i d_i \\ &+\ \left(\frac{X^\dagger X}{2M_{d'}}\right)\left((\lambda'_Q)_i\ (\lambda'^*_d)^i\ +\ (\lambda'^*_Q)_i\ (\lambda'_d)^i\right)\bar{d}^i d_i, \end{aligned} \tag{3.31}$$

where the flavor index i should be summed over. To get the effective interaction with nucleons, we need the nucleon matrix elements $< N|q^\dagger q|N >$ and $< N|\bar{q}q|N >$ when $q = u, d$. We truncate the sum over flavors to the light up and down flavors. The former simply counts the number of individual valence quarks in the nucleon, and the latter matrix element is related by the coefficients f_{Tq} to the former matrix elements. This gives the effective interactions appropriate for the nucleon matrix elements,

$$\begin{aligned}
-\mathcal{L}_{eff} \;\rightarrow\; & \left(\frac{X^\dagger X M_X}{2M_{u'}^2}\right)\left(|(\tilde{\lambda}_Q)_1|^2 + |(\tilde{\lambda}_u)_1|^2\right)(2\bar{p}p + \bar{n}n) \\
+ \; & \left(\frac{X^\dagger X}{2M_{u'}}\right)\left((\tilde{\lambda}_Q)_1\ (\tilde{\lambda}_u^*)^1 \;+\; (\tilde{\lambda}_Q^*)_1\ (\tilde{\lambda}_u)^1\right) f_{Tu}(2\bar{p}p + \bar{n}n) \\
+ \; & \left(\frac{X^\dagger X M_X}{2M_{d'}^2}\right)\left(|(\lambda'_Q)_1|^2 + |(\lambda'_d)_1|^2\right)(\bar{p}p + 2\bar{n}n) \\
+ \; & \left(\frac{X^\dagger X}{2M_{d'}}\right)\left((\lambda'_Q)_1\ (\lambda'^*_d)^1 \;+\; (\lambda'^*_Q)_1\ (\lambda'_d)^1\right) f_{Td}(\bar{p}p + 2\bar{n}n). \qquad (3.32)
\end{aligned}$$

To get an order of magnitude estimate of the size of the couplings involved, we represent the various Yukawa couplings by λ assuming they are all the same order of magnitude. The cross section for DM scattering off of nucleons will be small enough to evade the direct detection bounds if the Yukawa couplings, λ are on the order of 10^{-1} assuming the masses of the fourth generation quarks are a few hundred GeV. Similar constraints hold for $Y_{1,2}$ in model (1) where ϕ_I^0 is the dark matter candidate.

3.4 Cosmological Baryon Number

It may be difficult to generate the observed cosmological baryon density since baryon and lepton number are gauge symmetries in the model we are considering. Here we study this issue following closely the approach of Harvey and Turner [56]. Assuming, $\mu \ll T$, one can write the excess of particle over antiparticle as

$$\frac{n_+ - n_-}{s} = \frac{15g}{2\pi^2 g_*}\frac{\mu}{T}, \qquad (3.33)$$

for bosons and in the case of fermions one has

$$\frac{n_+ - n_-}{s} = \frac{15g}{4\pi^2 g_*}\frac{\mu}{T}, \tag{3.34}$$

where μ is the chemical potential of the particle species, g counts the internal degrees of freedom, $s = 2\pi^2 g_* T^3/45$ is the entropy density, and g_* counts the total number of relativistic degree of freedom.

For each of the fields, we associate a chemical potential. Since the chemical potential of the gluons vanishes, all colors of quarks have the same chemical potential. Furthermore, we assume mixing between the quarks and amongst the leptons is efficient. This reduces the number of chemical potentials to a chemical potential for each chirality of usual leptons $\{\mu_{e_L},\ \mu_{e_R},\ \mu_{\nu_L},\ \mu_{\nu_R}\}$ and quarks $\{\mu_{u_L},\ \mu_{u_R},\ \mu_{d_L},\ \mu_{d_R}\}$ as well as the fourth-generation leptons $\{\mu_{e'_L},\ \mu_{e'_R},\ \mu_{\nu'_L},\ \mu_{\nu'_R}\}$ and fourth-generation quarks $\{\mu_{u'_L},\ \mu_{u'_R},\ \mu_{d'_L},\ \mu_{d'_R}\}$. We also have a chemical potential for each of the scalars S_L and S_B (denoted as μ_{S_L} and μ_{S_B}, respectively), a chemical potential for μ_- for the charged field in the Higgs doublet, μ_0 for the neutral Higgs field. At temperatures above the electroweak phase transition ($T \gtrsim 300$ GeV), we set the third component of the gauged weak isospin to zero. This condition implies that the chemical potential for the charged W bosons vanishes and leads to the conditions

$$\mu_{u_L} = \mu_{d_L}, \quad \text{and} \quad \mu_{e_L} = \mu_{\nu_L}, \tag{3.35}$$

for the SM quark and lepton fields and

$$\mu_{u'_{L(R)}} = \mu_{d'_{L(R)}}, \quad \text{and} \quad \mu_{e'_{L(R)}} = \mu_{\nu'_{L(R)}}, \tag{3.36}$$

in model 1 (2) for the fourth-generation quark and lepton fields.

3.4.1 Model (1)

In model (1), we also need a chemical potential for the scalar S, denoted μ_S, a chemical potential for the charged field in the doublet ϕ, denoted μ_{ϕ^+}, and a chemical potential for the neutral component of the ϕ doublet, denoted μ_ϕ. Again, since the chemical potential for the charged W bosons vanishes, $\mu_\phi = \mu_{\phi^+}$.

Before study the possibility to have a baryon asymmetry let us discuss the different conditions we must satisfy. Using Eqs. (3.1), (3.4), (3.5) and (3.9) one obtains

$$\mu_0 = \mu_{u'_R} - \mu_{u'_L}, \quad \mu_0 = \mu_{d'_L} - \mu_{d'_R}, \tag{3.37}$$

$$\mu_0 = \mu_{\nu_R} - \mu_{\nu_L}, \quad \mu_0 = \mu_{\nu'_R} - \mu_{\nu'_L}, \tag{3.38}$$

$$\mu_{S_L} = 2\mu_{\nu_R}, \quad \mu_0 = \mu_{e'_L} - \mu_{e'_R}, \tag{3.39}$$

$$\mu_0 = \mu_\phi + \mu_S, \quad \mu_{S_B} = 2\mu_S, \tag{3.40}$$

and

$$\mu_{S_L} = -\mu_{\nu_R} - \mu_{\nu'_R}. \tag{3.41}$$

Yukawa interactions with the Higgs boson in the SM imply the following relations,

$$\mu_0 = \mu_{u_R} - \mu_{u_L}, \qquad -\mu_0 = \mu_{d_R} - \mu_{d_L}, \tag{3.42}$$

$$-\mu_0 = \mu_{e_R} - \mu_{e_L}, \qquad \mu_0 = \mu_{\nu_R} - \mu_{\nu_L}. \tag{3.43}$$

Now, we using these relations to write the baryon number density (B), lepton number density (L) and electric charge density (Q). We find the following expressions for these

comoving number densities,

$$B^{(1)} \equiv \frac{n_B - n_{\bar{B}}}{s} = \frac{15}{4\pi^2 g_* T}\left(12\mu_{u_L} - 12\mu_{u'_L} - \frac{20}{3}\mu_{S_B} + \frac{16}{3}\mu_\phi \right), \quad (3.44)$$

$$L^{(1)} \equiv \frac{n_L - n_{\bar{L}}}{s} = \frac{15}{4\pi^2 g_* T}\left(20\mu_{\nu_L} - 12\mu_{\nu'_L} + 8\mu_\phi + 4\mu_{S_B} \right), \quad (3.45)$$

$$Q^{(1)} \equiv \frac{n_Q - n_{\bar{Q}}}{s} = \frac{15}{4\pi^2 g_* T} \times \left(20\mu_\phi + 9\mu_{S_B} + 6\mu_{u_L} + 2\mu_{u'_L} - 6\mu_{\nu_L} - 2\,\mu_{\nu'_L} \right). \quad (3.46)$$

See Tables 3.1 and 3.2 for the leptonic and baryonic charges. At high temperatures, each of the charge densities in Eqs. (3.44), (3.45) and (3.46) must vanish. These three conditions, along with the sphaleron condition

$$3(2\mu_{u_L} + \mu_{d_L} + \mu_{e_L}) + (2\mu_{u'_L} + \mu_{d'_L} + \mu_{e'_L}) = 9\mu_{u_L} + 3\mu_{\nu_L} + 3\mu_{u'_L} + \mu_{\nu'_L} = 0. \quad (3.47)$$

give us four equations. Unfortunately, in the general case we do not have a symmetry which guarantees the conservation of a given number density. We analyze the small λ_b limit.[2] In this limit, we have the following approximate global symmetries:

$(B-L)_1$: $(Q_L, u_R, d_R, \phi) \to e^{i\alpha/3}(Q_L, u_R, d_R, \phi)$, $(l_L, e_R, \nu_R) \to e^{-i\alpha}(l_L, e_R, \nu_R)$, $S_L \to e^{-2i\alpha} S_L$, $S \to e^{-i\alpha/3} S$, $S_B \to e^{-2i\alpha/3} S_B$,

and

$(B-L)_2$: $(Q'_L, u'_R, d'_R, S) \to e^{-i\alpha}(Q'_L, u'_R, d'_R, S)$, $(l'_L, e'_R, \nu'_R) \to e^{i3\alpha}(l'_L, e'_R, \nu'_R)$, $\phi \to e^{i\alpha}\phi$, $S_B \to e^{-2i\alpha} S_B$.

Both of these approximate global symmetries are anomaly free and not gauged.

[2] λ_b must be small enough so that the mixing between the ordinary right-handed neutrinos and the fourth generation right-handed neutrino can be neglected in the early Universe, but large enough so that the fourth generation right-handed neutrino can decay.

The corresponding charge densities are given by

$$(B-L)_1 = \frac{15}{4\pi^2 g_* T}\left(12\mu_{u_L} + \frac{4}{3}\mu_\phi - 12\mu_{\nu_L} - 4\mu_{S_L} - \frac{2}{3}\mu_S - \frac{4}{3}\mu_{S_B}\right), \tag{3.48}$$

and

$$(B-L)_2 = \frac{15}{4\pi^2 g_* T}\left(-12\mu_{u'_L} - 2\mu_S + 12\mu_{\nu'_L} + 2\mu_\phi - 4\mu_{S_B}\right). \tag{3.49}$$

The baryon number density at late times will include the contribution of the ordinary quarks and the contribution from the decay of the fourth generation quarks. In ordinary quarks we have

$$\frac{1}{3}(3)(3)\left(\mu_{u_L} + \mu_{u_R} + \mu_{d_L} + \mu_{d_R}\right) = 12\mu_{u_L}. \tag{3.50}$$

The contribution from the fourth-generation quarks ($Q' \to \phi + u_R$ and $d'_R \to \phi + Q_L$) gives

$$\frac{1}{3}(3)\left(\mu_{u'_L} + \mu_{d'_L} + 2\mu_{d'_R}\right) = 4\mu_{u'_L} - 2\mu_\phi - \mu_{S_B}. \tag{3.51}$$

Then,

$$\begin{aligned} B_f^{(1)} &= \frac{15}{4\pi^2 g_* T}\left(12\mu_{u_L} + 4\mu_{u'_L} - 2\mu_\phi - \mu_{S_B}\right) \\ &= \frac{269}{1143}(B-L)_1 - \frac{13}{381}(B-L)_2. \end{aligned} \tag{3.52}$$

Depending on the initial charge densities, it is possible to simultaneously explain the DM relic density and the baryon asymmetry in this scenario. Notice that one can have leptogenesis at the high scale if the symmetry breaking scale for $U(1)_L$ is much larger than the electroweak scale.

3.4.2 Model (2)

In model (2), we must introduce a chemical potential for the scalar S'_L, denoted $\mu_{S'_L}$, and a chemical potential for the dark matter candidate X, denoted μ_X.

The action is invariant under the transformations $S_B \to e^{i\alpha_B} S_B$ and $S'_L \to e^{i\alpha_L} S'_L$.

These automatic $U(1)$ symmetries are anomaly free, since no fermions transform under them. The symmetries are spontaneously broken by the vacuum expectation values of S_B and S'_L, respectively; however, at high temperatures the symmetry is restored. We begin by assuming that in the early Universe a non-zero S_B and S'_L asymmetry is generated. This could occur for example from the decay of the inflaton after inflation. We examine if this can lead to the observed baryon excess.

We assume that lepton number and baryon number are spontaneously broken at the weak scale. In this case we have the following relations, assuming that the coupling constants $\{\lambda_a, \lambda_b, \lambda_l, \lambda_e\}$ are large enough to preserve thermal equilibrium when $T \gtrsim 300$ GeV,

$$\mu_{S_L} = 2\mu_{\nu_R}, \tag{3.53}$$

$$\mu_{S_L} = \mu_{\nu'_L} - \mu_{\nu_R}, \tag{3.54}$$

$$\mu_{S_L} = \mu_{e'_R} - \mu_{e_L}, \tag{3.55}$$

$$\mu_{S_L} = \mu_{e'_L} - \mu_{e_R}. \tag{3.56}$$

Interactions with the Higgs boson imply the following relations,

$$\mu_0 = \mu_{u'_L} - \mu_{u'_R}, \qquad -\mu_0 = \mu_{d'_L} - \mu_{d'_R}, \tag{3.57}$$

$$-\mu_0 = \mu_{e'_L} - \mu_{e'_R}, \qquad \mu_0 = \mu_{\nu'_L} - \mu_{\nu'_R}. \tag{3.58}$$

We also have the following equations relating the chemical potentials of the fourth generation quarks, ordinary quarks and the dark matter

$$\mu_X = \mu_{u_L} - \mu_{u'_R}, \qquad \mu_X = \mu_{u_R} - \mu_{u'_L}, \tag{3.59}$$

$$\mu_X = \mu_{d_L} - \mu_{d'_R}, \qquad \mu_X = \mu_{d_R} - \mu_{d'_L}, \tag{3.60}$$

assuming the couplings in Eq. (3.12) are large enough that these interactions are in thermal equilibrium at high temperatures.

We use these relations to write the baryon number density (B), lepton number

density (L) and electric charge density (Q) in terms of $\{\mu_{u_L},\ \mu_0,\ \mu_{S_L},\ \mu_{S'_L},\ \mu_{S_B},\ \mu_X\}$. We find the following expressions for these comoving number densities,

$$B^{(2)} = \frac{15}{4\pi^2 g_* T}\left(\ 24\mu_{u_L}\ +\ 2n_B\mu_{S_B}\ -\ \frac{40}{3}\mu_X\right), \tag{3.61}$$

$$L^{(2)} = \frac{15}{4\pi^2 g_* T}\left(\ 28\mu_{S_L}\ -\ 24\mu_0 +\ 2n_L\mu_{S'_L}\right), \tag{3.62}$$

$$Q^{(2)} = \frac{15}{4\pi^2 g_* T}\left(\ 8\mu_{u_L}\ +\ 26\mu_0\ -\ 6\mu_{S_L}\ -\ 2\mu_X\right), \tag{3.63}$$

see Tables 3.1 and 3.3 for the leptonic and baryonic charges. At high temperatures, each of these charge densities in Eqs. ((3.61)), ((3.62)) and ((3.63)) must vanish. These three conditions, along with the sphaleron condition,

$$3(2\mu_{u_L} + \mu_{d_L} + \mu_{e_L}) - (2\mu_{u'_R} + \mu_{d'_R} + \mu_{e'_R}) = 6\mu_{u_L} - 2\mu_0 + 3\mu_X = 0, \tag{3.64}$$

give us four equations and six unknowns. We solve this system of equations in terms of the chemical potentials μ_{S_B} and $\mu_{S'_L}$ since these are the chemical potentials corresponding to the conserved charges in the transformation laws $S_B \to e^{i\alpha_B}S_B$ and $S'_L \to e^{i\alpha_L}S'_L$.

We find that in thermal equilibrium the following relations amongst the chemical potentials,

$$\begin{aligned}
\mu_0 &= \frac{9}{8630}\left(21n_B\mu_{S_B} - 19n_L\mu_{S'_L}\right),\\
\mu_{S_L} &= \frac{1}{8630}\left(162n_B\mu_{S_B} - 763n_L\mu_{S'_L}\right),\\
\mu_X &= \frac{3}{8630}\left(247n_B\mu_{S_B} - 18n_L\mu_{S'_L}\right),\\
\mu_{u_L} &= -\frac{3}{3452}\left(41n_B\mu_{S_B} + 4n_L\mu_{S'_L}\right).
\end{aligned} \tag{3.65}$$

Using these equilibrium relations, we find what is called the baryon number density at late times. The baryon number density at late times will include the contribution of the ordinary quarks and the contribution from the decay of the fourth-generation

quarks. In ordinary quarks we have

$$\frac{1}{3}(3)(3)\left(\mu_{u_L}+\mu_{u_R}+\mu_{d_L}+\mu_{d_R}\right)=12\mu_{u_L}. \tag{3.66}$$

The contribution from the fourth-generation quarks ($Q'\to X^\dagger+q$) gives

$$\frac{1}{3}(3)\left(\mu_{u'_L}+\mu_{u'_R}+\mu_{d'_L}+\mu_{d'_R}\right)=4\left(\mu_{u_L}-\mu_X\right). \tag{3.67}$$

The observed baryon excess is the sum of these two contributions and is given by

$$\begin{aligned} B_f^{(2)} &= \frac{15}{4\pi^2 g_* T}\left(12\mu_{u_L}+4\left(\mu_{u_L}-\mu_X\right)\right) && (3.68)\\ &= \frac{15}{4\pi^2 g_* T}\left(4\left(4\mu_{u_L}-\mu_X\right)\right)\\ &= -\frac{1971}{4315}\left(\frac{15n_B}{2\pi^2 g_*}\left(\frac{\mu_{S_B}}{T}\right)\right)-\frac{66}{4315}\left(\frac{15n_L}{2\pi^2 g_*}\left(\frac{\mu_{S'_L}}{T}\right)\right)\\ &\simeq -0.46\left(\frac{15n_B}{2\pi^2 g_*}\left(\frac{\mu_{S_B}}{T}\right)\right)-0.02\left(\frac{15n_L}{2\pi^2 g_*}\left(\frac{\mu_{S'_L}}{T}\right)\right). && (3.69)\end{aligned}$$

Since X is the cold dark matter candidate in the theory one has to check the prediction for the ratio between the DM density and the baryon asymmetry. The DM asymmetry is given by

$$\begin{aligned} \frac{n_X-n_{\bar{X}}}{s} &= \frac{15}{2\pi^2 g_* T}\left(\mu_X-\frac{3}{2}\left(\mu_{u'_L}+\mu_{d'_L}+\mu_{u'_R}+\mu_{d'_R}\right)\right)\\ &= \frac{15}{2\pi^2 g_* T}\left(7\mu_X-6\mu_{u_L}\right). && (3.70)\end{aligned}$$

Therefore, in this case using Eq. (3.65) one finds

$$\frac{n_X-n_{\bar{X}}}{s} = \frac{15}{2\pi^2 g_* T}\left(\frac{3516}{4315}n_B\mu_{S_B}-\frac{99}{4315}n_L\mu_{S'_L}\right). \tag{3.71}$$

One can find an upper bound on M_X using the constraint $|n_X-n_{\bar{X}}|\le n_{DM}$. This gives the constraint

$$\frac{\Omega_{DM}/M_X}{\Omega_B/M_p}\ge\frac{\left|3516\Delta S_B-99\Delta S'_L\right|}{1971\Delta S_B+66\Delta S'_L}, \tag{3.72}$$

where $M_p \simeq 1$ GeV is the proton mass and the observed ratio $\Omega_{DM} \simeq 5\Omega_b$. So in this scenario the dark matter mass must be in the range,

$$M_X \leq M_p \left(\frac{\Omega_{DM}}{\Omega_B}\right) \frac{1971\Delta S_B + 66\Delta S'_L}{\left|3516\Delta S_B - 99\Delta S'_L\right|}. \tag{3.73}$$

The work in Section 3.3 shows that the dark matter mass must be at least 50 GeV to obtain the correct dark matter relic density while evading direct detection limits. Depending on the initial charge densities, it is possible to simultaneously explain the DM relic density and the baryon asymmetry in this scenario. Eq. (3.73) shows that this requires a somewhat awkward fine-tuning between the initial charge densities of the global symmetries $S_B \to e^{i\alpha_B} S_B$ and $S'_L \to e^{i\alpha_L} S'_L$.

In model (2) one can have a non-zero baryon asymmetry (even if B and L are broken at the low scale) if there is a primordial asymmetry in the scalar sector; however, we need physics beyond what is in model (2) to explain how this primordial asymmetry is generated.

3.5 Summary

We have investigated the cosmological aspects of two simple models, denoted (1) and (2), in which baryon number (B) and lepton number (L) are local gauge symmetries that are spontaneously broken around the weak scale. In these models, the stability of our scalar dark matter candidate is a consequence of the gauge symmetry.

In model (2), we studied the possible dark matter annihilation channels and found what values of the masses and couplings lead to the observed relic abundance of dark matter. In the case where the s-wave annihilation through an intermediate Higgs dominates, we find that, for $M_H = 120$ GeV, in order to evade the direct detection bounds the coupling between the Higgs and the dark matter must be less than $10^{-1.5}$ and 51 GeV $\lesssim \mathrm{M_X} \lesssim$ 63 GeV. In the case where the p-wave annihilation through an intermediate leptophobic gauge boson dominates, we find that the coupling between the leptophobic Z_B and the dark matter must be less than 0.1 and 235 GeV $\lesssim$

$M_X \lesssim 250$ GeV when $M_{Z_B} = 500$ GeV. In this case the leptophobic gauge boson has to be below the TeV scale and one finds a lower bound on the elastic cross section $\sigma^B_{SI} \gtrsim 5 \times 10^{-46}$ cm^2. In both cases, direct detection experiments constrain the annihilation to proceed close to resonance in order to evade direct detection and to produce the observed relic abundance of dark matter. We have shown that even though baryon number is gauged and spontaneously broken at the weak scale it is possible to generate a cosmological baryon excess. A modest fine-tuning is needed to achieve both the measured dark matter relic abundance and baryon excess.

In model (1), we introduced a simple mechanism to split the masses of the real of the imaginary part of the neutral component of the new scalar doublet to evade direct detection limits. We showed that one can simultaneously achieve both the observed baryon asymmetry of the Universe and the dark matter relic abundance. In particular, when L is broken at the high scale but B is spontaneously broken at the weak scale, standard leptogenesis can be applied.

Appendix A

Appendix

A.1 Parametrization of Perturbations

In the following we use many of the same conventions and notation as in [28]. Since the background space-time is homogeneous, we decompose our perturbations into Fourier modes,

$$\delta(x^i, \eta) = \int \frac{d^3k}{(2\pi)^3}\, e^{ik_j x^j} \delta(k_i, \eta). \tag{A.1}$$

For a given Fourier mode, characterized by the time-independent wave vector k_i, we form an orthonormal basis $\{e_i^1, e_i^2\}$ for the subspace perpendicular to the wave vector such that

$$\gamma^{ij} e_i^a e_j^b = \delta^{ab}, \quad \text{and} \quad \gamma^{ij} e_i^a k_j = 0. \tag{A.2}$$

Here γ_{ij} is the spatial metric defined in (2.4). Such an orthonormal basis for the spatial hypersurfaces is uniquely defined up to a spatial rotation about the wave vector k_i. To remain properly normalized with the above normalization condition, these basis vectors must be time dependent.

For definiteness, and without loss of generality, we will take wave vectors to be of the form $k_i = (k_1, k_2, 0)$. The basis vectors can then be written as

$$e_i^1 = \left(-\frac{e^{-3\beta} k_2}{\sqrt{k^2}},\ \frac{e^{3\beta} k_1}{\sqrt{k^2}},\ 0 \right) \quad \text{and} \quad e_j^2 = \left(0,\ 0,\ e^{\beta}\right), \tag{A.3}$$

where $\gamma^{ij} k_i k_j = k^2$.

It turns out that there always exists a choice of basis vectors e_i^1 and e_j^2 that results in the basis vectors having definite sign under what we will call

$$\text{k parity:} \quad k_i \to -k_i. \tag{A.4}$$

Our basis (A.3) is such that under k parity, $e_i^a \to (-1)^a e_i^a$. Such a choice of basis is now unique up to discrete spatial rotations around the k_i-axis by multiples of $\pi/2$.

We parametrize the most general perturbations about the background Bianchi I metric (2.4) in the standard way,

$$ds^2 = -a(\eta)^2 \left[(1+2A)d\eta^2 + 2B_i dx^i dt + (\gamma_{ij}(\eta) + h_{ij}) dx^i dx^j\right]. \tag{A.5}$$

Following [28],

$$B_i = \partial_i B + \bar{B}_i, \tag{A.6}$$

$$h_{ij} = 2C\left(\gamma_{ij} + \frac{\sigma_{ij}}{\mathcal{H}}\right) + 2\partial_i\partial_j E + 2\partial_{(i}E_{j)} + 2E_{ij}, \tag{A.7}$$

where $\sigma_{ij} = \frac{1}{2}\gamma'_{ij}$ and $\mathcal{H} = \alpha'$ and also,

$$\gamma^{ij}\partial_i \bar{B}_j = 0, \quad \gamma^{ij}\partial_i E_j = 0, \quad \gamma^{ij}\partial_i E_{jk} = 0, \quad \text{and} \quad \gamma^{ij}E_{ij} = 0. \tag{A.8}$$

We parametrize perturbations of the inflaton field and the electromagnetic field by $\delta\phi$ and $\delta F_{\mu\nu}$, respectively.

One can show that the following are $U(1)$ gauge and diffeomorphism-invariant

variables,

$$\Phi(k) = A + \frac{1}{a(\eta)}\left(a\left(B - \frac{(k^2E)'}{k^2}\right)\right)', \tag{A.9}$$

$$\Psi(k) = -C - \frac{a'(\eta)}{a(\eta)}\left[B - \frac{(k^2E)'}{k^2}\right], \tag{A.10}$$

$$\Phi^i(k) = \bar{B}^i - (E^i)', \tag{A.11}$$

$$E_{ij}, \tag{A.12}$$

$$\chi(k) = \delta\phi + \phi'(\eta)\left[B - \frac{(k^2E)'}{k^2}\right], \tag{A.13}$$

$$\Phi^F_{ij}(k) = \delta F_{ij} + 2\bar{F}_{\eta[i}ik_{j]}\left[B - \frac{(k^2E)'}{k^2}\right], \tag{A.14}$$

$$\Phi^F_i(k) = \delta F_{\eta i} - \gamma^{jk}\bar{F}_{\eta j}ik_i(ik_kE + E_k) + \left(\bar{F}_{\eta i}\left[B - \frac{(k^2E)'}{k^2}\right]\right)'. \tag{A.15}$$

The perturbation in the gauge field can be decomposed along directions transverse and parallel to the spatial wave vector:

$$\delta A_i = (i\delta A^{(\perp,+)}(k,\eta))e^1_i + (\delta A^{(\perp,-)}(k,\eta))e^2_i + (i\delta A^{\parallel}(k,\eta)))\hat{k}_i, \tag{A.16}$$

where the amplitudes $\delta A^{(\perp,\pm)}(k,\eta)$ are $U(1)$ gauge invariant.[1] In $A_0 = E = B = B_i = 0$ gauge the electromagnetic gauge fields $\delta A^{(\perp,\pm)}(k,\eta)$ are simply related to the gauge-invariant magnetic and electric field perturbations. In particular we may define

$$\delta A^+(k,\eta) \equiv \frac{i(e^1)^ik^j\Phi^F_{ij}}{k^2}, \qquad \text{and} \qquad \delta A^-(k,\eta) \equiv -\frac{(e^2)^ik^j\Phi^F_{ij}}{k^2}, \tag{A.17}$$

where $\gamma^{ij}k_ik_j = k^2$ and where spatial indices are understood to be raised and lowered with the spatial metric, γ_{ij}. The dynamical, gauge-invariant dynamical electromagnetic variables are $\delta A^{\pm}(k,\eta)$ as defined above and are equal to $\delta A^{(\perp,\pm)}(k,\eta)$ as defined in (A.16) in $A_0 = E = B = B_i = 0$ gauge (a modified Newtonian gauge).

The tensor perturbations, E_{ij} are gauge-invariant by construction. We will further decompose the tensor perturbations by constructing the two independent symmetric

[1]The factors of i accompanying some perturbations is to ensure that the relation $\delta^*(k,\eta) = \delta(-k,\eta)$ holds for all Fourier amplitudes.

traceless tensors that are transverse to the wave vector k_i. We again follow [28] and define these tensors as

$$E_{ij} = E^{+}\epsilon^{+}_{ij} + iE^{\times}\epsilon^{\times}_{ij}, \tag{A.18}$$

$$\epsilon^{+}_{ij} = \frac{e^1_i e^1_j - e^2_i e^2_j}{\sqrt{2}}, \tag{A.19}$$

$$\epsilon^{\times}_{ij} = \frac{e^1_i e^2_j + e^2_i e^1_j}{\sqrt{2}}. \tag{A.20}$$

We have chosen this normalization since,

$$\gamma^{ik}\gamma^{jl}\epsilon^{\lambda}_{ij}\epsilon^{\lambda'}_{kl} = \delta^{\lambda\lambda'}. \tag{A.21}$$

Because we have chosen a basis with the property that, under k-parity, $e^a_i \to (-1)^a e^a_i$ these tensors have k-parity transformations $\epsilon^{+}_{ij} \to +\epsilon^{+}_{ij}$ and $\epsilon^{\times}_{ij} \to -\epsilon^{\times}_{ij}$.

We will take the Mukhanov-Sasaki scalar variable (which is conserved outside the horizon in the isotropic limit) to be

$$r \equiv \frac{\alpha'}{\bar{\phi}'}\chi + \Psi. \tag{A.22}$$

In a gauge with spatially flat slicing, this variable corresponds to minus the curvature perturbation, $-\zeta$, as defined, e.g., in [32].

Some of the variables listed are not dynamical and must be removed from the action using constraint equations. There are a total of five dynamical variables in the theory. In the isotropic limit, these variables correspond to two electromagnetic perturbations, two tensor perturbations and one scalar perturbation. Furthermore, the action separates into uncoupled parts according to the transformation of fields under k parity: a piece including E^{+}, δA^{+} and r and one including $E^{\times}$ and δA^{-}.

A.2 Quadratic Action and Einstein's Equations

Given a metric $g_{\mu\nu} = \bar{g}_{\mu\nu} + \delta g_{\mu\nu}$, the Einstein-Hilbert action to quadratic order in $\delta g_{\mu\nu}$ can be written as

$$\begin{aligned}
\delta^{(2)} S_{EH} &= \int d^4x \sqrt{-\bar{g}} \Big\{ \frac{1}{4\kappa^2} \bar{g}^{\mu\nu} (\bar{\nabla}^\alpha \delta g_{\beta\mu})(\bar{\nabla}^\beta \delta g_{\alpha\nu}) - \frac{1}{4\kappa^2} \bar{g}^{\mu\nu} (\bar{\nabla}^\alpha \delta g_{\mu\nu})(\bar{\nabla}^\beta \delta g_{\alpha\beta}) \\
&+ \frac{1}{8\kappa^2} \bar{g}^{\mu\nu} \bar{g}^{\rho\sigma} (\bar{\nabla}^\alpha \delta g_{\mu\nu})(\bar{\nabla}_\alpha \delta g_{\rho\sigma}) - \frac{1}{8\kappa^2} \bar{g}^{\mu\nu} \bar{g}^{\rho\sigma} (\bar{\nabla}^\alpha \delta g_{\mu\rho})(\bar{\nabla}_\alpha \delta g_{\nu\sigma}) \\
&+ \frac{1}{2\kappa^2} \bar{R}^{\mu\nu} \bar{g}^{\rho\sigma} (\delta g_{\mu\rho})(\delta g_{\nu\sigma}) - \frac{1}{4\kappa^2} \bar{R}^{\mu\nu} \bar{g}^{\rho\sigma} (\delta g_{\mu\nu})(\delta g_{\rho\sigma}) \\
&+ \frac{1}{8\kappa^2} \bar{R} \, (\bar{g}^{\mu\nu} \delta g_{\mu\nu})^2 - \frac{1}{8\kappa^2} \bar{R} \, \bar{g}^{\mu\nu} \bar{g}^{\rho\sigma} (\delta g_{\mu\rho} \delta g_{\nu\sigma}) \Big\}
\end{aligned} \tag{A.23}$$

after dropping boundary terms. In the above equation, the covariant derivatives ($\bar{\nabla}$) are compatible with the background metric

$$\bar{\nabla}_\alpha \bar{g}_{\mu\nu} = 0. \tag{A.24}$$

We used this form of the action and our parameterization to compute Einstein's equations. In particular, the first-order change in the components Einstein tensor can

be written in the following way (in Newtonian gauge, where $E = B = B_i = 0$),

$$
\begin{aligned}
a^2\delta G^\eta_\eta &= -2\Delta\Psi + 6\mathcal{H}\Psi' - \left(\frac{\Psi}{\mathcal{H}}\right)'\sigma^2 + \frac{\sigma^{ij}}{\mathcal{H}}\partial_i\partial_j\Psi - \sigma^i_j\partial_i\Phi^j \\
&+ (E^i_j)'\sigma^j_i + (6\mathcal{H}^2 - \sigma^2)\Phi - \frac{1}{2}(\sigma^2)'\frac{\Psi}{\mathcal{H}}, \qquad \text{(A.25)} \\
a^2\delta G^\eta_i &= -\sigma^2\frac{\partial_i\Psi}{\mathcal{H}} + \sigma^j_i\partial_j\left(\Phi + \left(\frac{\Psi}{\mathcal{H}}\right)'\right) - 2\partial_i(\Psi' + \mathcal{H}\Phi) + \frac{1}{2}\Delta\gamma_{ij}\Phi^j \\
&- 2\sigma^j_k\partial_j E^k_i + \sigma^k_j\partial_i E^j_k + 3\sigma^j_i\partial_j\Psi + \frac{(\sigma^j_i)'}{\mathcal{H}}\partial_j\Psi, \qquad \text{(A.26)} \\
a^2\delta G^i_j &= \delta^i_j\left[2\Psi'' + (2\mathcal{H}^2 + 4\mathcal{H}')\Phi + \Delta(\Phi - \Psi) + 2\mathcal{H}\Phi' + 4\mathcal{H}\Psi'\right] - \partial^i\partial_j(\Phi - \Psi) \\
&- 2\frac{\sigma^{(i}_k}{\mathcal{H}}\partial_{j)}\partial^k\Psi + \sigma^i_j\left[-\mathcal{H}\left(\frac{\Psi'}{\mathcal{H}^2}\right)' + \left(\frac{\mathcal{H}'}{\mathcal{H}^2}\right)'\Psi + \frac{\Delta\Psi}{\mathcal{H}} - \Phi'\right] \\
&+ \delta^i_j\left[\sigma^2(\Phi + (\Psi/\mathcal{H})') + \frac{\sigma^{kl}}{\mathcal{H}}\partial_k\partial_l\Psi\right] + (E^i_j)'' - \Delta E^i_j + 2\mathcal{H}(E^i_j)' - \sigma^l_k(E^k_l)'\delta^i_j \\
&+ \delta^i_j(\sigma^k_l\partial_k\Phi^l) - 2\mathcal{H}\gamma^{ik}\partial_{(k}\Phi_{j)} - \gamma^{ik}\left[\partial_{(k}\Phi'_{j)} - 2\sigma^l_{(k}\partial_{|l|}\Phi_{j)}\right] \\
&+ (\sigma^i_j)'\left[2\frac{\mathcal{H}'}{\mathcal{H}^2}\Psi - 2\frac{\Psi'}{\mathcal{H}} - 2(\Phi + \Psi)\right] + \sigma^i_j\left[2\frac{\mathcal{H}'}{\mathcal{H}}\Psi - 4\mathcal{H}\Phi\right] + \frac{1}{2}\delta^i_j\frac{\sigma^{2\prime}}{\mathcal{H}}\Psi \\
&- \frac{(\sigma^i_j)''}{\mathcal{H}}\Psi + 4\mathcal{H}\left[\sigma^i_k E^k_j - \sigma^k_j E^i_k\right] + 2\left[\sigma^i_k E^k_j - \sigma^k_j E^i_k\right]' - 5\sigma^i_j\Psi' \\
&+ 2\mathcal{H}\left[\sigma^i_k\partial_j E^k - \sigma^k_j\partial_k E^i\right] + \left[(\sigma^i_k)'\partial_j E^k - (\sigma^k_j)'\partial_k E^i\right], \qquad \text{(A.27)}
\end{aligned}
$$

where $'$ denotes derivatives with respect to conformal time and

$$
\mathcal{H} = \frac{a'}{a}, \quad \sigma_{ij} = \frac{1}{2}\gamma'_{ij}. \qquad \text{(A.28)}
$$

In these equations, spatial indices are raised and lowered with γ_{ij}.

Our expressions (A.25) through (A.27) match those of [28] up to factors of the anisotropic stress, $\sigma^{i\prime}_j + 2\mathcal{H}\sigma^i_j$, which in [28] was set to zero. Note that the Einstein tensor is gauge covariant rather than gauge invariant.

A.3 Diagonalizing a Kinetic Term

Suppose a kinetic term takes the form

$$K = \frac{1}{2}X^{\dagger\prime}X' + X^{\dagger\prime}MX + X^{\dagger}M^{\dagger}X', \tag{A.29}$$

where X is a vector of fields and M is a time-dependent matrix. Diagonalizing the kinetic term requires a change of variables,

$$X \longrightarrow VY, \tag{A.30}$$

where V is a time-dependent unitary matrix, such that

$$K \longrightarrow \frac{1}{2}Y^{\dagger\prime}Y' + \text{total derivative} + Y^{\dagger}QY, \tag{A.31}$$

where Q is some Hermitian matrix. We can calculate directly that

$$K = \frac{1}{2}Y^{\dagger\prime}Y' + Y^{\dagger}\Big(V^{\dagger\prime}V + V^{\dagger}(M^{\dagger} - M)V\Big)Y' + \text{total derivative} + Y^{\dagger}QY. \tag{A.32}$$

The kinetic term is diagonalized by a unitary matrix V that satisfies

$$V^{\dagger\prime}V = -V^{\dagger}(M^{\dagger} - M)V, \qquad \text{or equivalently} \qquad VV^{\dagger\prime} = M - M^{\dagger}. \tag{A.33}$$

If M were a time-independent matrix, then the kinetic term would be diagonalized by a constant unitary matrix V such that

$$V^{\dagger}(M - M^{\dagger})V = D, \tag{A.34}$$

where D is a constant diagonal matrix.

A.4 Estimates of Integrals

In order to get a quantitative estimate of the effect of the anisotropic background on power spectra, we must estimate the integrals in (2.74) through (2.76). We may take $\hat{\rho}_A$, Σ, and the slow-roll parameters to be nearly constant. Then the relevant integrals are

$$\begin{aligned} & p^{-2}\int^{\eta}\sin\left(2\psi_{\vec{p}}(\eta')-2\psi_{\vec{p}}(\eta)\right)\,\alpha'(\eta')^2\,\tilde{I}(p\eta',p\eta)d\eta', \\ & p^{-2}\int^{\eta}\cos\left(2\psi_{\vec{p}}(\eta')-2\psi_{\vec{p}}(\eta)\right)\,\alpha'(\eta')^2\,\tilde{I}(p\eta',p\eta)d\eta', \qquad \text{(A.35)} \\ & \int^{\eta}(e^{2n\beta(\eta')}-e^{2n\beta(\eta_0)})\,\tilde{I}(p\eta',p\eta)d\eta', \\ & \text{and} \qquad p^{-2}\int^{\eta}\alpha'(\eta')^2\,\tilde{I}(p\eta',p\eta)d\eta' \qquad \text{(A.36)} \end{aligned}$$

where $\tilde{I}(x,y)$ was defined in (2.69) as

$$\begin{aligned} \tilde{I}(x,y) &= \left(\frac{1}{2x^2y^2}-\frac{1}{2x^2}+\frac{2}{xy}-\frac{1}{2y^2}+\frac{1}{2}\right)\sin(2x-2y) \\ &+ \left(\frac{1}{x^2y}-\frac{1}{xy^2}+\frac{1}{x}-\frac{1}{y}\right)\cos(2x-2y). \qquad \text{(A.37)} \end{aligned}$$

During slow-roll inflation,

$$\alpha'(\eta)=e^{\alpha(\eta)}H(\eta)\approx-\frac{1}{\eta} \qquad \text{(A.38)}$$

$$\psi_{\vec{p}}(\eta')-\psi_{\vec{p}}(\eta)\approx(\alpha(\eta')-\alpha(\eta))\,\frac{k_2e^{-\beta_0}}{k_0}\sqrt{\hat{\rho}_A} \qquad \text{(A.39)}$$

$$(e^{2n\beta(\eta')}-e^{2n\beta(\eta_0)})\approx 2n\Sigma\left(\alpha(\eta')-\alpha(\eta_0)\right). \qquad \text{(A.40)}$$

Let us define a new variable z by[2]

$$-p\eta=e^{-z}. \qquad \text{(A.41)}$$

[2]This is just a convenient dimensionless variable and is not equal to $a\phi'/\alpha'$ as in (2.37).

From (A.38) it is clear that

$$e^z \approx \frac{aH}{p} \qquad \text{and so} \qquad z \approx \log(H/p) + \alpha. \tag{A.42}$$

We may thus rewrite the integrals (A.35) and (A.36) in terms of the variable z:

$$\begin{aligned} I_s &\equiv p^{-1} \int^{z_*} \sin\left(2\frac{\psi'_{\vec{p}}}{\alpha'}(z - z_*)\right) \tilde{I}(-e^{-z}, -e^{-z_*})e^z dz, \\ I_c &\equiv p^{-1} \int^{z_*} \cos\left(2\frac{\psi'_{\vec{p}}}{\alpha'}(z - z_*)\right) \tilde{I}(-e^{-z}, -e^{-z_*})e^z dz, \end{aligned} \tag{A.43}$$

$$I_1 \equiv p^{-1} \int^{z_*} (z - z_0)\, \tilde{I}(-e^{-z}, -e^{-z_*})e^{-z} dz,$$

$$\text{and} \quad I_2 \equiv p^{-1} \int^{z_*} \tilde{I}(-e^{-z}, -e^{-z_*})e^z dz, \tag{A.44}$$

where z_* is the value of z at the end of inflation and

$$\frac{\psi'_{\vec{p}}}{\alpha'} \equiv \frac{p_2 e^{-\beta_0}}{p}\sqrt{\hat{\rho}_A}. \tag{A.45}$$

The function

$$\tilde{I}(-e^{-z}, -e^{-z_*})e^z \tag{A.46}$$

oscillates rapidly with growing amplitude for $z < 0$. See Fig. A.1. For $z > 0$ and values of z_* on the order of tens, the function is well approximated by a constant

$$\tilde{I}(-e^{-z}, -e^{-z_*})e^z \approx -\frac{2}{3}e^{2z_*}, \qquad 0 < z < z_*. \tag{A.47}$$

The constant can be found by expanding the function about $z_* = \infty$ and then about $z = \infty$.

The contribution of terms that go like I_1 will be subdominant compared to contributions from terms proportional to the other integrals,[3] so we will not bother to

[3] The contribution from I_1 can be important if inflation lasts a very long time—on the order of 10^3 e-folds.

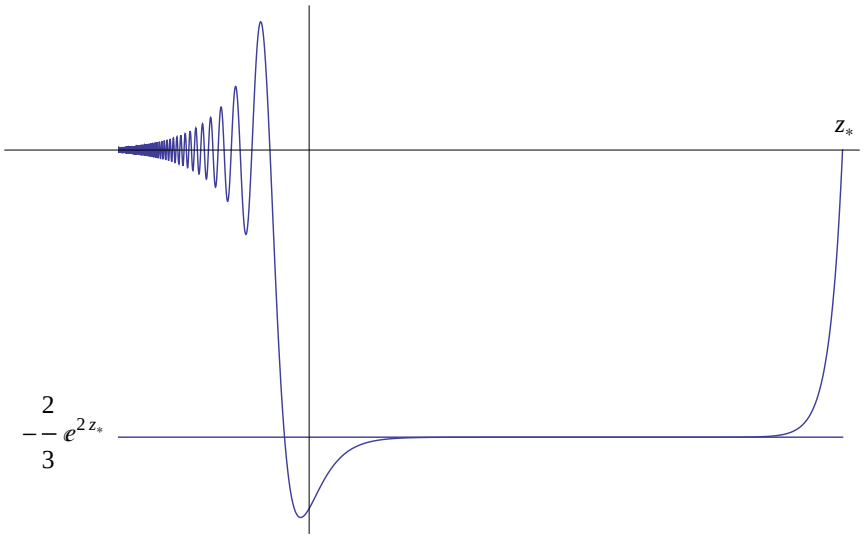

Figure A.1: The function $e^z \tilde{I}(-e^z, -e^{-z_*})$ on a linear scale. The axes cross at the point $\{0, 0\}$. For $0 < z < z_*$ the function is well approximated by $-\frac{2}{3}e^{2z_*}$. The frequency of oscillation for $z < 0$ does not vary much as z_* increases—only the amplitude changes. The plot above was generated using $z_* = 15$.

calculate I_1. Since the dominant contribution to the other integrals will occur when $z > 0$ (which corresponds to after horizon crossing) we may approximate the integrals by

$$\begin{aligned} I_s &\approx -\frac{2}{3}e^{2z_*}p^{-1}\int_0^{z_*}\sin\left(2\frac{\psi'_{\vec{p}}}{\alpha'}(z-z_*)\right)dz \\ &= -\frac{2}{3}e^{2z_*}p^{-1}\left(\frac{2\psi'_{\vec{p}}}{\alpha'}\right)^{-1}\left(\cos\left(\frac{2\psi'_{\vec{p}}}{\alpha'}z_*\right)-1\right), \qquad \text{(A.48)} \\ I_c &\approx -\frac{2}{3}e^{2z_*}p^{-1}\int_0^{z_*}\cos\left(2\frac{\psi'_{\vec{p}}}{\alpha'}(z-z_*)\right)dz, \\ &= -\frac{2}{3}e^{2z_*}p^{-1}\left(\frac{2\psi'_{\vec{p}}}{\alpha'}\right)^{-1}\left(-\sin\left(\frac{2\psi'_{\vec{p}}}{\alpha'}z_*\right)\right) \qquad \text{(A.49)} \\ I_2 &= p^{-1}\int^{z_*}\tilde{I}(-e^{-z}, -e^{-z_*})e^z dz \approx -\frac{2}{3}e^{2z_*}p^{-1}z_*. \qquad \text{(A.50)} \end{aligned}$$

Modes of astrophysical interest crossed the horizon about 60 e-folds—plus or minus a few—before the end of inflation. Such modes of astrophysical interest therefore correspond to $z_* \approx 60$.

Bibliography

[1] T. R. Dulaney and M. I. Gresham. Primordial power spectra from anisotropic inflation. *Phys. Rev.*, D81:103532, 2010.

[2] T. R. Dulaney, P. F. Perez, and M. B. Wise. Dark matter, baryon asymmetry, and spontaneous B and L breaking. *Phys. Rev.*, D83:023520, 2011.

[3] S. Weinberg. *Cosmology*. Oxford, UK: Oxford Univ. Pr. (2008) 593 p.

[4] E. W. Kolb and M. S. Turner. *The Early Universe*. Addison-Wesley, Redwood City, USA, 1988.

[5] L. Ackerman, S. M. Carroll, and M. B. Wise. Imprints of a Primordial Preferred Direction on the Microwave Background. *Phys. Rev.*, D75:083502, 2007.

[6] M. Watanabe, S. Kanno, and J. Soda. Inflationary Universe with Anisotropic Hair. *Phys. Rev. Lett.*, 102:191302, 2009.

[7] D. et al. Larson. Seven-Year Wilkinson Microwave Anisotropy Probe (WMAP) Observations: Power Spectra and WMAP-Derived Parameters. 2010.

[8] R. W. Wald. Asymptotic behavior of homogeneous cosmological models in the presence of a positive cosmological constant. *Phys. Rev.*, D28:2118–2120, 1983.

[9] T. R. Dulaney, M. I. Gresham, and M. B. Wise. Classical stability of a homogeneous, anisotropic inflating space-time. *Phys. Rev.*, D77:083510, 2008.

[10] B. Himmetoglu, C. R. Contaldi, and M. Peloso. Instability of the ACW model, and problems with massive vectors during inflation. *Phys. Rev.*, D79:063517, 2009.

[11] S. M. Carroll, T. R. Dulaney, M. I. Gresham, and H. Tam. Instabilities in the Aether. *Phys. Rev.*, D79:065011, 2009.

[12] L. Parker. Particle creation in expanding universes. *Phys. Rev. Lett.*, 21:562–564, 1968.

[13] M. S. Turner and L. M. Widrow. Inflation Produced, Large Scale Magnetic Fields. *Phys. Rev.*, D37:2743, 1988.

[14] B. Ratra. Cosmological 'seed' magnetic field from inflation. *Astrophys. J.*, 391:L1–L4, 1992.

[15] V. Demozzi, V. Mukhanov, and H. Rubinstein. Magnetic fields from inflation? *JCAP*, 0908:025, 2009.

[16] K. Bamba, N. Ohta, and S. Tsujikawa. Generic estimates for magnetic fields generated during inflation including Dirac-Born-Infeld theories. *Phys. Rev.*, D78:043524, 2008.

[17] S. Kanno, J. Soda, and M.-a. Watanabe. Cosmological Magnetic Fields from Inflation and Backreaction. *JCAP*, 0912:009, 2009.

[18] D. Grasso and H. R. Rubinstein. Magnetic fields in the early universe. *Phys. Rept.*, 348:163–266, 2001.

[19] K. Dimopoulos, M. Karciauskas, and J. M. Wagstaff. Vector Curvaton without Instabilities. *Phys. Lett.*, B683:298–301, 2010.

[20] S. Yokoyama and J. Soda. Primordial statistical anisotropy generated at the end of inflation. *JCAP*, 0808:005, 2008.

[21] E. A. Lim. Can we see Lorentz-violating vector fields in the CMB? *Phys. Rev.*, D71:063504, 2005.

[22] T. S. Koivisto and D. F. Mota. Vector Field Models of Inflation and Dark Energy. *JCAP*, 0808:021, 2008.

[23] A. Golovnev and V. Vanchurin. Cosmological perturbations from vector inflation. *Phys. Rev.*, D79:103524, 2009.

[24] K. Dimopoulos, M. Karciauskas, D. H. Lyth, and Y. Rodriguez. Statistical anisotropy of the curvature perturbation from vector field perturbations. *JCAP*, 0905:013, 2009.

[25] C. A. Valenzuela-Toledo, Y. Rodriguez, and D. H. Lyth. Non-gaussianity at tree- and one-loop levels from vector field perturbations. *Phys. Rev.*, D80:103519, 2009.

[26] C. A. Valenzuela-Toledo and Y. Rodriguez. Non-gaussianity from the trispectrum and vector field perturbations. *Phys. Lett.*, B685:120–127, 2010.

[27] B. Himmetoglu. Spectrum of Perturbations in Anisotropic Inflationary Universe with Vector Hair. *JCAP*, 1003:023, 2010.

[28] T. S. Pereira, C. Pitrou, and J.-P. Uzan. Theory of cosmological perturbations in an anisotropic universe. *JCAP*, 0709:006, 2007.

[29] V. F. Mukhanov, H. A. Feldman, and R. H. Brandenberger. Theory of cosmological perturbations. Part 1. Classical perturbations. Part 2. Quantum theory of perturbations. Part 3. Extensions. *Phys. Rept.*, 215:203–333, 1992.

[30] S. Weinberg. Quantum contributions to cosmological correlations. *Phys. Rev.*, D72:043514, 2005.

[31] P. Adshead, R. Easther, and E. A. Lim. Cosmology With Many Light Scalar Fields: Stochastic Inflation and Loop Corrections. *Phys. Rev.*, D79:063504, 2009.

[32] S. Dodelson. *Modern Cosmology*. 2003. Amsterdam, Netherlands: Academic Pr. (2003) 440 p.

[33] N. E. Groeneboom, L. Ackerman, I. K. Wehus, and H. K. Eriksen. Bayesian analysis of an anisotropic universe model: systematics and polarization. 2009.

[34] D. Hanson and A. Lewis. Estimators for CMB Statistical Anisotropy. *Phys. Rev.*, D80:063004, 2009.

[35] A. R. Pullen and M. Kamionkowski. Cosmic Microwave Background Statistics for a Direction-Dependent Primordial Power Spectrum. *Phys. Rev.*, D76:103529, 2007.

[36] S. Weinberg. Baryon and lepton nonconserving processes. *Phys. Rev. Lett.*, 43:1566–1570, 1979.

[37] P. Nath and P. F. Perez. Proton stability in grand unified theories, in strings, and in branes. *Phys. Rept.*, 441:191–317, 2007.

[38] P. F. Perez and M. B. Wise. Baryon and Lepton Number as Local Gauge Symmetries. *Phys. Rev.*, D82:011901, 2010.

[39] P. Minkowski. mu $\rightarrow$ e gamma at a Rate of One Out of 1-Billion Muon Decays? *Phys. Lett.*, B67:421, 1977.

[40] M. Gell-Mann, P. Ramond, and R. Slansky. *in Supergravity.* North-Holland, Amsterdam, 1979.

[41] R. N. Mohapatra and G. Senjanovic. Neutrino mass and spontaneous parity nonconservation. *Phys. Rev. Lett.*, 44:912, 1980.

[42] L. Lopez Honorez, E. Nezri, J. F. Oliver, and M. H. G. Tytgat. The inert doublet model: An archetype for dark matter. *JCAP*, 0702:028, 2007.

[43] E. M. Dolle and S. Su. The Inert Dark Matter. *Phys. Rev.*, D80:055012, 2009.

[44] J. McDonald. Gauge Singlet Scalars as Cold Dark Matter. *Phys. Rev.*, D50:3637–3649, 1994.

[45] C. P. Burgess, M. Pospelov, and T. ter Veldhuis. The minimal model of non-baryonic dark matter: A singlet scalar. *Nucl. Phys.*, B619:709–728, 2001.

[46] S. Andreas, T. Hambye, and M. H. G. Tytgat. WIMP dark matter, Higgs exchange and DAMA. *JCAP*, 0810:034, 2008.

[47] V. Barger, P. Langacker, M. McCaskey, M. J. Ramsey-Musolf, and G. Shaughnessy. LHC Phenomenology of an Extended Standard Model with a Real Scalar Singlet. *Phys. Rev.*, D77:035005, 2008.

[48] X.-G. He, T. Li, X.-Q. Li, J. Tandean, and H.-C. Tsai. Constraints on Scalar Dark Matter from Direct Experimental Searches. *Phys. Rev.*, D79:023521, 2009.

[49] Z. et al. Ahmed. Results from the Final Exposure of the CDMS II Experiment. 2009.

[50] K. Griest and D. Seckel. Three exceptions in the calculation of relic abundances. *Phys. Rev.*, D43:3191–3203, 1991.

[51] E. Aprile et al. First Dark Matter Results from the XENON100 Experiment. *Phys. Rev. Lett.*, 105:131302, 2010.

[52] D. B. Kaplan and M. B. Wise. Couplings of a light dilaton and violations of the equivalence principle. *JHEP*, 08:037, 2000.

[53] M. M. Pavan, I. I. Strakovsky, R. L. Workman, and R. A. Arndt. The pion nucleon Sigma term is definitely large: Results from a GWU analysis of pi N scattering data. *PiN Newslett.*, 16:110–115, 2002.

[54] J. R. Ellis, K. A. Olive, and C. Savage. Hadronic Uncertainties in the Elastic Scattering of Supersymmetric Dark Matter. *Phys. Rev.*, D77:065026, 2008.

[55] M. Farina, D. Pappadopulo, and A. Strumia. CDMS stands for Constrained Dark Matter Singlet. 2009.

[56] J. A. Harvey and M. S. Turner. Cosmological baryon and lepton number in the presence of electroweak fermion-number violation. *Phys. Rev. D*, 42(10):3344–3349, Nov 1990.